

Received by CDTI

OCT 09 1990

IS-T--1450

DE91 000611

Electrocatalysis of Anodic and Cathodic Oxygen-Transfer
Reactions

by

Wels, Brian

PHD Thesis submitted to Iowa State University

Ames Laboratory, U.S. DOE

Iowa State University

Ames, Iowa 50011

Date Transmitted: September 21, 1990

PREPARED FOR THE U.S. DEPARTMENT OF ENERGY

UNDER CONTRACT NO. W-7405-Eng-82.

MASTER
DISTRIBUTION OF THIS DOCUMENT IS UNLIMITED

DISCLAIMER

This report was prepared as an account of work sponsored by an agency of the United States Government. Neither the United States Government nor any agency thereof, nor any of their employees, makes any warranty, express or implied, or assumes any legal liability or responsibility for the accuracy, completeness or usefulness of any information, apparatus, product, or process disclosed, or represents that its use would not infringe privately owned rights. Reference herein to any specific commercial product, process, or service by trade name, trademark, manufacturer, or otherwise, does not necessarily constitute or imply its endorsement, recommendation, or favoring by the United States Government or any agency thereof. The views and opinions of authors expressed herein do not necessarily state or reflect those of the United States Government or any agency thereof.

Electrocatalysis of anodic and cathodic
oxygen-transfer reactions¹

Brian Reid Wels

Under the supervision of Dennis C. Johnson
From the Department of Chemistry
Iowa State University

The electrocatalysis of oxygen-transfer reactions is discussed in two parts. In Part I, the reduction of iodate (IO_3^-) is examined as an example of cathodic oxygen transfer. On oxide-covered Pt electrodes (PtO), a large cathodic current is observed in the presence of IO_3^- to coincide with the reduction of PtO . The total cathodic charge exceeds the amount required for reduction of PtO and IO_3^- to produce an adsorbed product. An electrocatalytic link between reduction of IO_3^- and reduction of PtO is indicated.

In addition, on oxide-free Pt electrodes, the reduction of IO_3^- is determined to be sensitive to surface treatment. The results are consistent with a mechanism involving the adsorption of IO_3^- onto I° -covered Pt sites ($\text{Pt}(\text{I}_{\text{ads}}^\circ)$). Previous researchers have relied on chemical steps in the mechanism of IO_3^- reduction to account for their results.

¹DOE Report IS-T 1450. This work was performed under contract No. W-7405-eng-82 with the U.S. Department of Energy.

The electrocatalytic oxidation of CN^- is presented as an example of anodic oxygen transfer in Part II. The electrocatalytic oxidation of CN^- is considered to be an important process for the treatment of industrial and laboratory wastes. Present electrode materials are unsuitable for CN^- oxidation for reasons of low current efficiency and high attrition rates. The voltammetric response of CN^- is virtually nonexistent at PbO_2 electrodes. Whereas the response is not improved by doping PbO_2 with Bi, the response is significantly improved by doping PbO_2 with Cu. Cyanide is also oxidized effectively at CuO-film electrodes. Copper is concluded to serve as an adsorption site for CN^- . It is proposed that an oxygen tunneling mechanism comparable to electron tunneling does not occur at the electrode-solution interface. The adsorption of CN^- is therefore considered to be a necessary prerequisite for oxygen transfer.

Electrocatalysis of anodic and cathodic
oxygen-transfer reactions

by

Brian Reid Wels

A Dissertation Submitted to the
Graduate Faculty in Partial Fulfillment of the
Requirements for the Degree of
DOCTOR OF PHILOSOPHY

Department: Chemistry
Major: Analytical Chemistry

Approved:

In Charge of Major Work

For the Major Department

For the Graduate College

Iowa State University
Ames, Iowa

1990

TABLE OF CONTENTS

	Page
LIST OF SYMBOLS AND ABBREVIATIONS	vi
INTRODUCTION	1
REFERENCES	5
LITERATURE REVIEW	6
REFERENCES	21
PART I. ELECTROCATALYTIC REDUCTION OF IODATE	27a
INTRODUCTION	27b
EXPERIMENTAL	29
RESULTS AND DISCUSSION	31
CONCLUSIONS	54
REFERENCES	60
PART II. ELECTROCATALYTIC OXIDATION OF CYANIDE	62a
INTRODUCTION	62b
EXPERIMENTAL	66
RESULTS AND DISCUSSION	70
CONCLUSIONS	95
SUMMARY	100
SUGGESTIONS FOR FUTURE RESEARCH	102
REFERENCES	103
ACKNOWLEDGMENTS	105
APPENDIX	106

LIST OF FIGURES

	Page
Figure I-1. Current-potential curves for IO_3^- at a Pt RDE by cyclic voltammetry in 0.50 M H_2SO_4	32
Figure I-2. Current-potential curves for 0.50 mM IO_3^- at a Pt RRDE by cyclic voltammetry in 0.50 M H_2SO_4	35
Figure I-3. Current-potential curves for IO_3^- at a Pt RDE by cyclic voltammetry in 0.50 M H_2SO_4	39
Figure I-4. Current vs. $w^{1/2}$ data obtained from i-E curves recorded at 6.0 V min^{-1} scan rate	41
Figure I-5. Effect on i-E curves of changing the cathodic scan limit (E_-) for 0.50 mM IO_3^- at a Pt RDE in 0.50 M H_2SO_4	43
Figure I-6. Effect of changing anodic scan limit on current-potential curves for 0.50 mM IO_3^- at a Pt RDE in 0.50 M H_2SO_4	45
Figure I-7A. Effect of surface treatment on current-potential curves for 0.50 mM IO_3^- at a Pt RDE in 0.50 M H_2SO_4 . Electrode was polished with 0.50- μm alumina prior to treatment with H_2O and a cotton swab. Arrows indicate scan direction	48
Figure I-7B. Effect of surface treatment on current-potential curves for 0.50 mM IO_3^- at a Pt RDE in 0.50 M H_2SO_4 . Electrode was polished with 0.50- μm alumina prior to treatment with H_2O and a Kimwipe. Arrows indicate scan direction	49
Figure I-7C. Effect of surface treatment on current-potential curves for 0.50 mM IO_3^- at a Pt RDE in 0.50 M H_2SO_4 . Electrode was polished with 0.50- μm alumina prior to treatment with H_2O and a microcloth	50
Figure I-7D. Effect of surface treatment on current-potential curves for 0.50 mM IO_3^- at a Pt RDE in 0.50 M H_2SO_4 . Electrode was polished with 0.50- μm alumina prior to rinsing with H_2O	51

Figure II-1.	Current-potential curves for CN^- at a $\beta\text{-PbO}_2$ RDE in 0.1 M NaClO_4 , 10 mM NaOH	71
Figure II-2.	Current-potential curves for CN^- at a Bi-doped (30 mole % Bi) PbO_2 RDE in 0.1 M NaClO_4 , 10 mM NaOH	72
Figure II-3.	Current-potential curves for CN^- at an $\alpha\text{-PbO}_2$ RDE in 0.1 M NaClO_4 , 10 mM NaOH	73
Figure II-4.	Current-potential curves for CN^- at a Cu-doped PbO_2 RDE in 0.1 M NaClO_4 , 10 mM NaOH	75
Figure II-5.	X-ray diffraction spectra of Cu-doped PbO_2	76
Figure II-6.	Scanning electron micrograph of copper oxide films	78
Figure II-7.	X-ray diffraction spectra of copper oxide films from Figure II-6a	80
Figure II-8.	Voltammetric response of NaCN at a rotated, CuO-film, disk electrode as a function of concentration in 0.10 M Na_2SO_4 with 0.010 M NaOH	81
Figure II-9.	Amperometric response for NaCN at a rotated, CuO-film, disk electrode as a function of concentration in 0.10 M Na_2SO_4 with 0.010 M NaOH	82
Figure II-10.	Voltammetric response of a rotated, CuO-film, disk electrode as a function of film thickness in 0.10 M Na_2SO_4 with 0.010 M NaOH	85
Figure II-11.	Residual voltammetric response of a rotated, CuO-film, disk electrode in 0.10 M Na_2SO_4 with 0.010 M NaOH	87
Figure II-12.	Effect of pH on the voltammetric response for 1.0 mM NaCN at a rotated, CuO-film electrode at constant ionic strength	89
Figure II-13.	Koutecky-Levich plot for 1.0 mM NaCN at a rotated, CuO-film, disk electrode in 0.10 M Na_2SO_4 with 0.010 M NaOH	91

LIST OF TABLES

	Page
Table I-1. Examples of electrochemical oxygen-transfer reactions	3
Table II-1. Kinetic data for oxidation of 1.0 mM NaCN at the rotated, CuO-film, disk electrode	93

LIST OF SYMBOLS AND ABBREVIATIONS

A	- Area of electrode
α	- (alpha) Transfer coefficient
α_a	- Asymmetry constant
C_x^b	- Bulk concentration of species x
C_x^s	- Surface concentration of species x
D	- Diffusion coefficient
$E_{1/2}$	- Half-wave potential
E_d	- Disk potential
E_p	- Peak potential
E_r	- Ring potential
E°	- Standard potential
E_-	- Cathodic potential scan limit
E_+	- Anodic potential scan limit
F	- Faraday constant
i_d	- Disk current
i_{lim}	- Limiting current
i_p	- Peak current
i_r	- Ring current
k_{app}	- Apparent heterogeneous rate constant
k_o	- Heterogeneous rate constant
n	- Electrons per molecule oxidized or reduced
SS	- Stainless steel
η	- Overpotential
ν	- Kinematic viscosity

- σ^* - Antibonding orbital
- ϕ - Scan rate
- w - Rotational velocity

INTRODUCTION

Many electrochemical reactions occur only at very high overpotentials because of slow heterogeneous kinetics. The rate of electrochemical reactions can be altered by modification of such parameters as electrode material, surface morphology, and chemical composition of the double layer at the electrode/solution interface. The objective of electrocatalysis research is to find reaction pathways of lower activation energy in order to permit such reactions to occur at high current densities near the equilibrium potential. Therefore, the term "electrocatalysis" can apply to the acceleration of the rate of the electrochemical reaction by manipulation of one or all of these parameters. Bard and Faulkner (1) described electrocatalysis using the general example of dissociative adsorption of chemical species to produce reactive fragments. The search for electrocatalytic conditions for a specific reaction is still largely an empirical process. As recently as 1985, catalyst design was described as a goal for the future (2).

The study of electrocatalysis is of great importance in applied electrochemistry. The energy efficiency of any electrochemical cell is established in part by the overpotentials required at the electrodes. Suitable electrocatalysts for the oxidation of primary fuels (e.g., hydrocarbons, alcohols, and carbon monoxide) and for the

reduction of oxygen need to be found for the development of economical fuel cells (3). The development of new electrocatalysts has been partly responsible for recent significant advances in organic electrosynthesis (4). The use of electrochemical techniques for the detoxification of hazardous chemical wastes is a promising new area of research in electrocatalysis (5-7).

Certain oxidation-reduction reactions can be characterized by a change in the oxygen content of the reacting species (8). The oxidizing agent loses oxygen, in the process of being reduced, whereas the reducing agent gains oxygen in the process of being oxidized. For these types of reactions occurring in aqueous solution, it is possible that the oxygen appearing on the reducing agent is derived from water as in the oxidation of sulfite by nitrite (9).

Electrochemical oxygen-transfer reactions necessarily occur at electrode surfaces. Examples of electrochemical oxygen-transfer reactions are given in Table I. Anodic oxygen-transfer reactions can be schematically represented by the generic mechanism given in Equations 1-3.

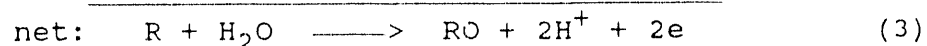
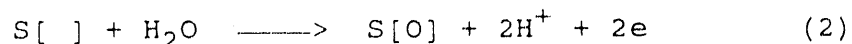
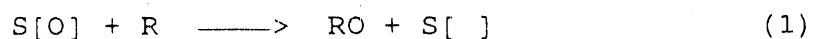

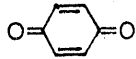
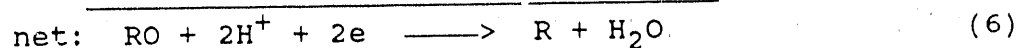
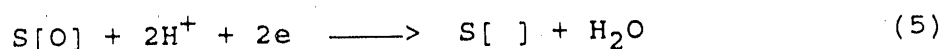
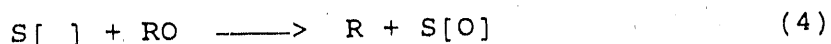


Table I-1. Examples of electrochemical oxygen-transfer reactions

Reactant		Product
Anodic processes:		
H_2O	→	O_2
I^-	→	IO_3^-
AsO_3^-	→	AsO_4^-
	→	
Me_2SO	→	Me_2SO_2
Mn^{+2}	→	MnO_4^-
Cathodic processes:		
O_2	→	H_2O
IO_3^-	→	I^-

In the equations above, S[O] represents labile surface-bound oxygen and S[] represents a vacant adsorption site. Similarly, cathodic oxygen-transfer reactions can be represented by the reaction sequence shown below.



According to these reaction schemes, the electrode surface can act as a catalyst (or electrocatalyst) for the oxygen-transfer reaction. It should be noted that, although these schemes imply the possibility of electrochemical reversibility, that property is rarely observed.

The research described in this dissertation has been divided into two parts:

Part I. Electrocatalytic reduction of IO_3^-

Part II. Electrocatalytic oxidation of CN^-

Part I is concerned with the discovery of a cathodic oxygen-transfer pathway analogous to Equations 4-6. Iodate was investigated because of previous reports of catalytic reduction on Pt electrodes. Part II is concerned with the search for a suitable electrode material which will exhibit high current densities for the anodic oxidation of cyanide (CN^-).

REFERENCES

1. Bard, A. J.; Faulkner, L. R. Electrochemical Methods; John Wiley: New York, 1980; p 515.
2. Instrumental Methods in Electrochemistry; Kemp, T. J., Ed.; John Wiley: New York, 1985; Chapter 7.
3. Kordesch, K.; Reindl, M. in Electrochemical Reactors; Ismail, M. I., Ed.; Elsevier: New York, 1989; Chapter 15.
4. Jansson, R. Chem. Eng. News 1984, 62(47), 43.
5. Feng, J.; Johnson, D. C. J. Electrochem. Soc. 1990, 137, 507.
6. Wels, B.; Johnson, D. C. J. Electrochem. Soc. 1990, 137, 2785.
7. Kaba, L.; Hitchens, G. D.; Bockris, J. O'M. J. Electrochem. Soc. 1990, 137, 1341.
8. Halperin, J.; Taube, H. J. Am. Chem. Soc. 1950, 72, 3319.
9. Rutenberg, A. C.; Halperin, J.; Taube, H. J. Am. Chem. Soc. 1951, 73, 4487.

LITERATURE REVIEW

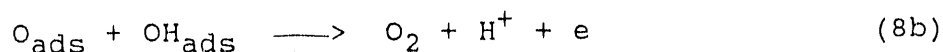
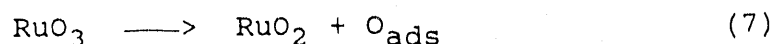
Nature of the surface-bound oxygen intermediate

The postulated mechanism of electrochemical oxygen transfer involves a surface-bound oxygen intermediate (i.e., $S[O]$ in Equations 1,2,4,5). The identity of the oxygen species is speculative. A brief review of the literature is included here to summarize present knowledge surrounding the identity of surface oxygen species involved in anodic processes.

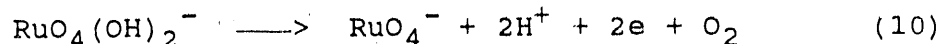
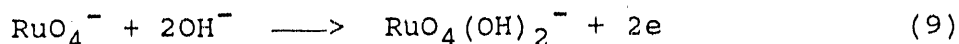
One of the most intensely investigated reactions listed in Table I-1 is the oxidation of water to produce dioxygen. The electrolysis of water plays a key role in energy storage systems based on hydrogen (1). The evolution of oxygen is also a side reaction in many anodic processes as well as the counter electrode reaction in such cathodic processes as electroplating, organic synthesis, and metal electrowinning. The activation overpotential of the oxygen evolution reaction at the anode is the primary source of lost energy efficiency in water electrolysis. Under conditions of oxygen evolution, metal surfaces always contain an oxide film. Therefore, much of the recent work in the electrocatalysis of oxygen evolution has focused on a variety of single and mixed oxides (2-13). The mechanism for oxygen evolution is difficult to determine because of the large number of possible pathways. Differences in

electrode preparation and variable or unknown intrinsic surface areas make comparisons of results difficult.

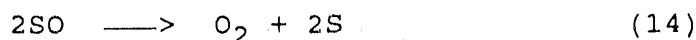
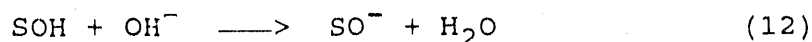
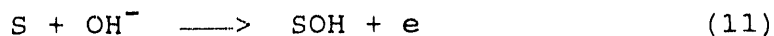
RuO_2 exhibits the highest catalytic activity (*i.e.*, lowest activation barrier) for oxygen evolution in short term tests (2-7). Burke *et al.* (2) correlated the anodic and cathodic charge passed during cyclic potential scans with true electrode surface areas. The evidence strongly suggested that redox processes occurring at the hydrated oxide surface could account for the observed voltammetric charging. The redox couples $\text{OH}_{\text{ads}}/\text{H}_2\text{O}$ and $\text{O}_{\text{ads}}/\text{OH}_{\text{ads}}$ among others were proposed. Decomposition of electrogenerated RuO_3 in acid was proposed according to Equation 7. The final step could occur by several paths. Equations 8a and 8b were suggested possibilities. Notice that the process



in Equation 8a does not contribute to the faradaic current. Under alkaline conditions, oxygen evolution was proposed to occur via decomposition of an electrogenerated peroxide species according to Equations 9 and 10. This scheme was supported by the conclusion of Carrington and Symons (14) that coordination of hydroxide to RuO_4^- was an important factor in the homogeneous decomposition of RuO_4^- .



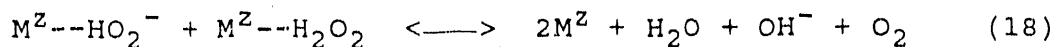
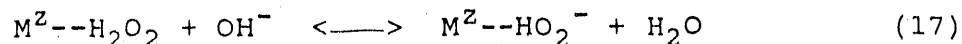
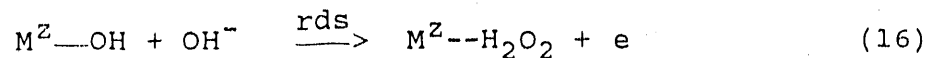
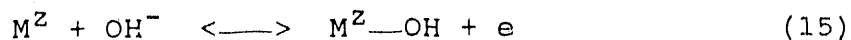
Perovskite oxides have received considerable attention as catalysts for oxygen electrode reactions (8-13). The general formula for these oxides is ABO_3 where A is typically a lanthanide and B is a transition metal. Mixed oxides with dissimilar lanthanides or transition metals (i.e., $\text{A}_{1-x}\text{A}'_x\text{BO}_3$ or $\text{AB}_{1-x}\text{B}'_x\text{O}_3$) can be prepared which may affect their catalytic activity. Matsumoto *et al.* (8-11) investigated the catalytic properties of several perovskite oxides: SrFeO_3 (8), $\text{La}_{1-x}\text{Sr}_x\text{MnO}_3$ (9), $\text{La}_{1-x}\text{Sr}_x\text{CoO}_3$ (10) and $\text{La}_{1-x}\text{Sr}_x\text{Fe}_{1-y}\text{Co}_y\text{O}_3$ (11). The general mechanism given by Equations 11-14 was proposed, where S represents the



transition metal ion on the electrode surface. The catalytic activity of these oxides was correlated with σ^* band formation in the oxide. Overlap between an e_g orbital of the transition metal with an sp orbital of oxygen is responsible for σ^* band formation. As x was increased in $\text{La}_{1-x}\text{Sr}_x\text{MnO}_3$ (9), for example, the degree of overlap between e_g and sp orbitals in the oxide was concluded to

increase. Hence, the rate of electron transfer in the primary discharge step (Equation 11) would be enhanced. Increased substitution (i.e., x in $\text{La}_{1-x}\text{Sr}_x\text{CoO}_3$) enhanced the rate of Equation 12 by increasing the positive charge density on the transition metal cation (10).

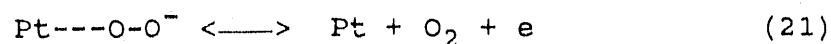
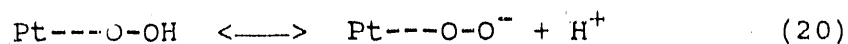
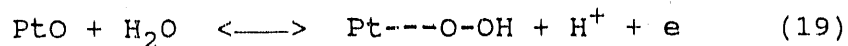
A systematic study of the catalytic activity of perovskite oxides for oxygen evolution was conducted by Bockris and Otagawa (13). The proposed mechanism is given by Equations 15-18 and involves H_2O_2 as an intermediate. A reasonably linear correlation was obtained for current



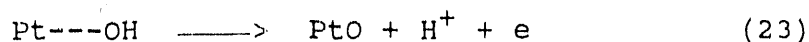
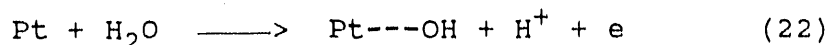
density vs. M-OH bond strengths for $\text{M}(\text{III})(\text{OH})_3$ hydroxides. The electrocatalytic activity for oxygen evolution was observed to decrease as M-OH bond strength increased. Thus, breaking the M-OH bond (Equation 16) was concluded to be the rate determining step.

Oxygen evolution on Pt has been studied in conjunction with the growth of oxide films (15-18). The production of OH radicals was postulated as the first step of oxide formation on Pt (19-21). The participation of the oxide film in oxygen evolution has been suggested by Damjanovic and Jovanovic (15). These authors suggested that oxygen

evolution on PtO involves adsorption of OH following discharge of water according to Equations 19-21.



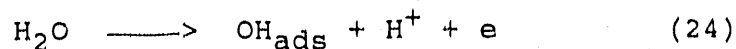
The oxide is reformed via discharge of water on Pt and also involves adsorbed OH intermediates (Equations 22-23).



Results of oxygen-18 tracer experiments (22,23) support this mechanism. The presence of adsorbed OH on Pt has been used to account for the observed electrocatalytic oxidation of I^- (24,25) and AsO_3^{-3} (26).

Oxygen evolution on PbO_2 electrodes in H_2SO_4 has been extensively investigated (27-30). A mechanism proposed by Krasil'shchikov (27) involves decomposition of a higher oxide (28). It has been established, however, that an oxide of lead having stoichiometry higher than that of PbO_2 does not exist (29). Therefore, PbO_2 is concluded to behave as an inert electrode and mechanisms proposed for oxygen evolution on PbO_2 are analogous to those proposed for noble metals (Equations 24-26).

The presence of OH_{ads} on PbO_2 during oxygen evolution has been confirmed (30).



An atom of oxygen adsorbed on an oxide surface (MO_x) is expected to simulate the formation of the higher oxide (MO_{x+1}). The strength of the oxide-oxygen interaction is generally regarded as the primary factor governing catalytic activity. Trasatti (31) correlated the enthalpy of transition (ΔH_f^\ddagger) of metal oxides from a lower to a higher oxidation state with electrochemical activity (i.e., overpotential) for oxygen evolution. The overpotential for oxygen evolution changed with ΔH_f^\ddagger of the oxide according to a volcano-shaped curve. Thus, oxides characterized by strong oxide-oxygen interaction (i.e., large ΔH_f^\ddagger) were concluded to be poor catalysts; desorption of reaction products was considered to be the rate limiting step. Similarly, oxides characterized by weak oxide-oxygen interaction (i.e., small ΔH_f^\ddagger) were concluded to be poor catalysts; water discharge was considered to be the rate limiting step. Highest activity was associated with oxides characterized by moderate oxide-oxygen interactions.

Reduction of iodate

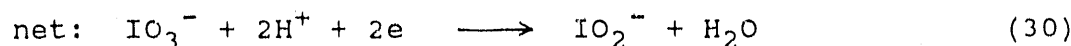
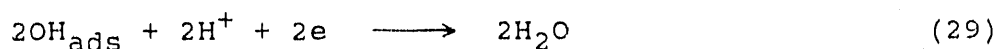
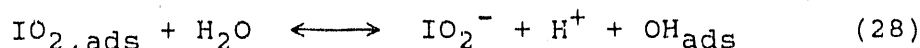
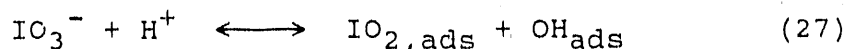
Anson (32) attributed the cathodic reduction of IO_3^- to $\text{I}_{2,\text{aq}}$ at a pre-oxidized Pt surface to an electrocatalytic

mechanism coupled to the oxide-reduction process. A rapid decrease in cathodic current for IO_3^- reduction was observed as the surface oxide was cathodically removed from the electrode surface. When oxide removal was complete, no current was observed for IO_3^- until the overpotential was sufficiently large to cause direct reduction of IO_3^- to I^- at the reduced Pt surface. When the potential of a pre-oxidized Pt electrode was stepped to a constant value in the region of IO_3^- reduction, the rate of current decay below the transport-limited value increased with increasingly negative potential values. In contrast, no decrease in current with time was observed for reactions such as the reductions of Fe(III) and $\text{I}_{2,\text{aq}}$ which do not involve mechanisms coupled to reduction of surface oxide. Anson (32) also observed that the voltammetric peak for IO_3^- reduction shifted to more negative values with increased pH in the range 1 to 6 in accord with the shift observed for reduction of the oxide film in the absence of IO_3^- . Based on these observations, Anson concluded that reduction of the oxide layer is essential for the IO_3^- reduction at values of overpotential (η) below 750 mV (32).

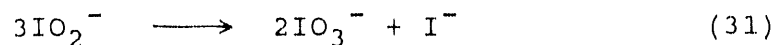
Davis (33) also concluded that IO_3^- reduction at Pt electrodes is facilitated by the simultaneous reduction of surface oxide (33). Current densities measured at 0.45 V vs. SCE were observed to increase as the potential for prior anodic polarization was increased. Furthermore, Davis (33)

observed an abrupt decrease in the kinetic term \underline{na} when the electrode had been reduced at $E < 0.25$ V; \underline{a} is the transfer coefficient characteristic of the symmetry of the activation barrier. Therefore, Davis (33) concluded that reduction of IO_3^- occurs via a different mechanism on a reduced Pt surface than on a pre-oxidized surface. No mechanisms were proposed, however.

Muller (34) proposed the mechanism given by Equations 27-30 for reduction of IO_3^- . This mechanism involves



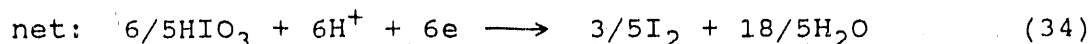
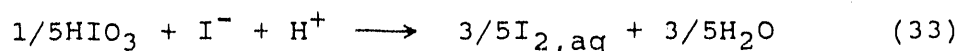
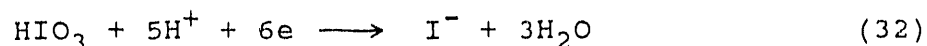
dissociative adsorption as the initial step (Equation 27) to produce adsorbed hydroxyl radicals (OH_{ads}) that are subsequently reduced to H_2O (Equation 29). The adsorbed iodite reacts further with H_2O to produce IO_2^- and another OH_{ads} (Equation 28) to be reduced to H_2O (Equation 29). The IO_2^- produced in Equation 28 disproportionates rapidly to give IO_3^- and I^- as shown by Equation 31.



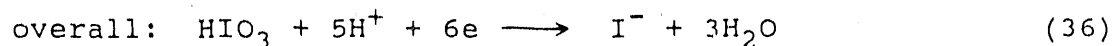
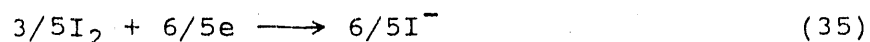
According to this mechanism, faradaic current originates solely from reduction of OH_{ads} (Equation 29). Muller

concluded that the adsorption step (Equation 27) is accelerated on the oxide film.

Desideri (35) discussed two mechanisms for reduction of IO_3^- at oxide-free Pt electrodes, as described by Equations 32-36. The direct reduction of HIO_3 to I^- (Equation 32) is very slow, according to this mechanism. However, the I^- produced diffuses from the Pt surface and reacts rapidly with IO_3^- in the diffusion layer to give $\text{I}_{2,\text{aq}}$ (Equation 33).



The $\text{I}_{2,\text{aq}}$ in turn, can then be rapidly reduced to I^- at the electrode (Equation 35) with the net result of 6 equivalents of charge per mole of IO_3^- (Equation 36).



This mechanism was supported by observations that IO_3^- reduction at oxide-free Pt appeared to be catalyzed by addition of traces of $\text{I}_{2,\text{aq}}$ (35-39).

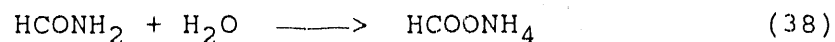
Beran and Bruckenstein (37) examined the chronoamperometric response for IO_3^- reduction following a potential step from 0.8 V to 0.2 V vs. SCE in the absence and presence of added $\text{I}_{2,\text{aq}}$. In the absence of $\text{I}_{2,\text{aq}}$, a steady-state current was not attained until ca. 5 sec

elapsed following the potential step. The delay was only 2 sec after addition of 10^{-5} M $I_{2,aq}$ and virtually zero for 5×10^{-5} M $I_{2,aq}$.

Oxidation of cyanide

Cyanide is a metabolic poison. Its lethality is derived from its inhibition of cytochrome oxidase in the mitochondrial respiratory chain (40). In order to place cyanide in a proper biochemical perspective, it should be noted that cyanide is a microconstituent of our "unpolluted" environment and a metabolic product of many species (41).

Complete books dating back to the early 1900s have been written about cyanide and cyanide compounds, their manufacture, properties, and determination (42-44). Cyanide is known to form complexes with nearly all of the transition metals. The hydrolysis of HCN according to Equations 37 and 38 is catalyzed by the presence of mineral acids (45,46). Interestingly, in the case of HCl, the rate increases in the



same order as the activity of molecular HCl. Kriebel *et al.* (47) noted a 600-fold increase in the rate of hydrolysis of HCN in 75% acetic acid containing HCl. The chemistry of cyanide as a ligand has been reviewed (48,49).

In the early 1900s, catalysts were sought for the

oxidation of gaseous HCN to NO (50,51). Initial efforts were directed at Pt (50), but later other oxides and mixtures of oxides were investigated (51). The oxide catalysts were heated (300-900°C) in a stream of HCN in air. The effect of temperature on the extent of HCN oxidation was determined by analyzing the reactor effluent. Cyanic acid (HCNO) was identified as an intermediate product in the oxidation of HCN to NO and CO or CO₂. Of the oxides studied, Fe₂O₃ mixed with Bi₂O₃, Co₂O₃, Co₂O₃ mixed with Bi₂O₃, and MnO₂ mixed with CuO were found to be almost as effective as Pt.

Reports of environmental concern over cyanide began to appear in the literature in the 1930s (52-54). Early methods of treating cyanide wastes included the lagooning of acidified waste (55), reaction with FeSO₄ to produce Prussian blue (56), and air scouring of acidified wastes (57). The use of sodium hypochlorite (NaClO) for eliminating cyanide from industrial wastes was first reported in 1941 (58). The process of alkaline chlorination of cyanide-bearing wastes has been described by Dobson (59). Metals present in waste are usually precipitated as hydroxides under these alkaline conditions. Chlorine demand can be increased substantially by other components of the waste stream (e.g., sulfites, degreasers).

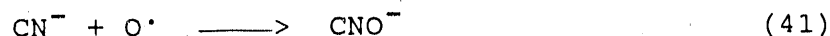
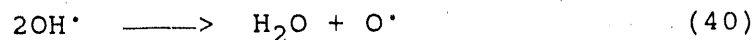
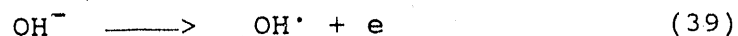
The Kastone process (60) was developed by Du Pont as an alternative to alkaline chlorination. Kastone is a

proprietary H_2O_2 formulation which oxidizes CN^- to CNO^- and favors the formation of metal oxides over hydroxides making filtration easier.

Carbonaceous materials have been demonstrated to catalyze the oxidation of CN^- to CNO^- by dissolved oxygen (61,62). According to Bernardin (63), the catalytic oxidation of CN^- on granular activated carbon is accelerated by the presence of Cu^{+2} . It was possible to impregnate the copper onto the activated carbon or feed it continuously into the flowing stream. The latter approach was observed to increase hydrolysis of cyanate, as well. Other metals (Cd, Fe, Zn, Ni) were found to be ineffective and, in fact, interfered with the function of Cu when present in the waste stream. Proper pre-treatment of the waste included removal of oils and tars which would foul the carbon surface. A similar approach was used to treat a CuCN effluent (64).

Electrolytic methods (65-67) of treating cyanide wastes have been investigated since the late 1940s. Sperry and Caldwell (65) used electrolysis at elevated temperatures ($>120^\circ\text{F}$) to treat copper cyanide solutions. While zero total cyanide was achieved after 35 hours in a 700 gallon plant trial, the carbon-steel anodes were rapidly attacked toward the end of the experiment. Dart *et al.* (66) described a method for electrolytic destruction of solid NaCN on a laboratory scale. Solid Na_2CO_3 was recovered by crystallization from the product mixture. Other products

included NH_3 , CO_2 , and H_2 . The anodic reactions were formulated as given by Equations 39-41.

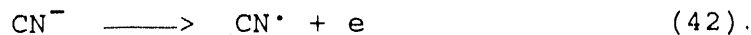


The advocates of electrolytic treatment generally agree on the advantages of the method:

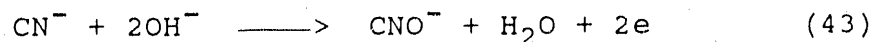
1. Cyanide is destroyed without formation of other toxic compounds;
2. Metals can be reclaimed easily;
3. No sludge disposal problem is created.

However, according to Easton (67), electrolytic decomposition is not practical for the treatment of dilute cyanide wastes.

The electrochemical oxidation of cyanide has been studied on Pt (68-72), graphite (73), and PbO_2 (74). Sawyer and Day (68) determined that only free CN^- was oxidized at Pt and they concluded from chronopotentiometric experiments that oxidation occurred via a one-electron step as shown by Equation 42. Tamura et al. (69) proposed instead the



reaction in Equation 43 based on a reported value of $\bar{n} = 2$

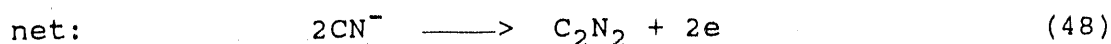
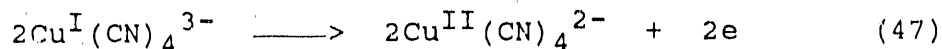
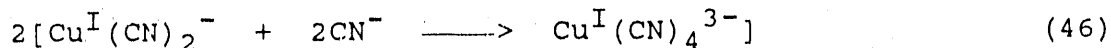
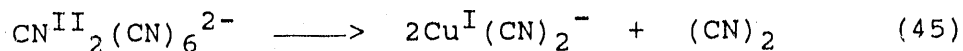
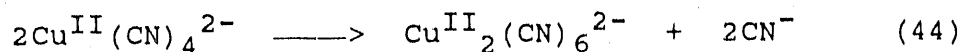


determined by controlled-potential coulometry. Equation 43 was supported by the work of Kitamura et al. (70,71) who

determined the presence of CNO^- on the Pt surface using Polarization Modulated Infrared Reflection Absorption Spectroscopy (PM IRRAS). Cyanogen was not detected as had been proposed by Sawyer and Day (68). Oxidation of cyanide in methanol failed to produce cyanate. Further oxidation of CNO^- above 0.8 V vs. Ag/AgCl was indicated by spectroscopic measurements (71).

Hine et al. (74) also proposed Equation 43 as the overall reaction of CN^- on PbO_2 electrodes. Discharge of CN^- by Equation 42 was concluded to be the rate determining step. Cyanogen was determined to be an intermediate product at low C_{OH^-} . The effect of coexistent metal ions (Cu, Cd, Zn, Fe) on the oxidation of cyanide was also determined by Hine et al. (74). Generally, these ions lowered current efficiency as a result of complex formation; however, cuprous ion was observed to promote cyanide oxidation. The Tafel slope for the oxidation of CN^- on PbO_2 was reported to be 300-350 mV decade⁻¹ in the absence of Cu^+ and 70-110 mV decade⁻¹ in the presence of Cu^+ . Katagiri et al. (72) considered the possibility that copper functioned as a mediator for CN^- oxidation according to Equations 44-48.

The anodic oxidation of cyanide on graphite electrodes was studied by Arikado et al. (73). The reaction was found to be first order in cyanide concentration and zero order in hydroxide. Controlled-potential coulometry indicated $\bar{n} = 2$ at high OH^- concentration (C_{OH^-}) but \bar{n} approached one at low



C_{OH}^- . Whereas CNO^- was detected in the product mixture at high and low C_{OH}^- , Arikado *et al.* (73) concluded that oxidation of CN^- proceeded through a CN^\cdot intermediate state on graphite.

Reports of cyanide waste treatment in the recent literature include electrolytic oxidation (75,76), biodegradation (77), photooxidation (78), and ozonation (79). In addition to treatment, waste minimization (80) and cyanide recycling techniques (81-85) have been investigated. Recent patent applications for cyanide waste treatment techniques include precipitation (86,87), biodegradation (88,89), hydrolysis (90-93) and a modification of alkaline chlorination (94). An overview of cyanide treatment technology prior to 1975 has been published by Patterson (95).

REFERENCES

1. Bockris, J. O'M.; Nagy, Z. Electrochemistry for Ecologists; Plenum: New York, 1974; Chapter 11.
2. Burke, L. D.; Murphy, O. J.; O'Neill, J. F.; Venkatesan, S. J. Chem. Soc. Faraday Trans. 1 1977, 73, 1659.
3. Kotz, R.; Lewerenz, H. J.; Bruesch, P.; Stucki, S. J. Electroanal. Chem. 1983, 150, 209.
4. Kotz, R.; Lewerenz, H. J.; Stucki, S. J. Electrochem. Soc. 1983, 130, 825.
5. Kotz, R.; Stucki, S.; Scherson, D.; Kolb, D. M. J. Electroanal. Chem. 1984, 172, 211.
6. Burke, L. D.; McCarthy, M. Electrochim. Acta 1984, 29, 211.
7. Doblhofer, K.; Metikos, M.; Ogumi, Z.; Gerischer, H. Ber. Bunsenges. Phys. Chem. 1978, 82, 1046.
8. Matsumoto, Y.; Kurimoto, J.; Sato, E. J. Electroanal. Chem. 1979, 102, 77.
9. Matsumoto, Y.; Sato, E. Electrochim. Acta 1979, 24, 421.
10. Matsumoto, Y.; Manabe, H.; Sato, E. J. Electrochem. Soc. 1980, 127, 811.
11. Matsumoto, Y.; Yamada, S.; Nishida, T.; Sato, E. J. Electrochem. Soc. 1980, 127, 2360.
12. Kobussen, A. B. C.; Willems, H.; Broers, G. H. J. J. Electroanal. Chem. 1982, 142, 67.
13. Bockris, J. O'M.; Otagawa, T. J. Electrochem. Soc. 1984, 131, 290.
14. Carrington, A.; Symons, M. C. R. J. Chem. Soc. 1960, 284.
15. Damjanovic, A.; Jovanovic, B. J. Electrochem. Soc. 1976, 123, 374.

16. Birss, V. I.; Damjanovic, A. J. Electrochem. Soc. 1983, 130, 1688.
17. Birss, V. I.; Damjanovic, A. J. Electrochem. Soc. 1983, 130, 1694.
18. Birss, V. I.; Damjanovic, A.; Hudson, P. G. J. Electrochem. Soc. 1986, 133, 1621.
19. Angerstein-Kozlowska, H.; Conway, B. E.; Sharp, W. B. A. J. Electroanal. Chem. 1973, 43, 9.
20. Conway, B. E.; Gottesfeld, S. J. Chem. Soc. Faraday Trans. 1 1973, 69, 1090.
21. Tilak, B. V.; Conway, B. E.; Angerstein-Kozlowska, H. J. Electroanal. Chem. 1973, 48, 1.
22. Rozenhal, K. I.; Veselovski, V. I. Dokl. Akad. Nauk USSR 1956, 111, 637; Chem. Abstr. 1957, 51, 12699b.
23. Churchill, C. R.; Hibbert, D. B. J. Chem. Soc. Faraday Trans. 1 1982, 78, 2937.
24. Austin, D. S.; Johnson, D. C.; Hines, T. G.; Berti, E. T. Anal. Chem. 1983, 55, 2222.
25. Austin, D. S. Ph.D. Dissertation, Iowa State University, 1984.
26. Cabelka, T. D.; Austin, D. S.; Johnson, D. C. J. Electrochem. Soc. 1984, 131, 1595.
27. Krasil'shchikov, A. J. Zh. Fiz. Khim. 1963, 37, 531; Chem. Abstr. 1963, 59, 1279g.
28. Glasstone, S. J. Chem. Soc. 1922, 121, 2091.
29. Amlie, R. G.; Ockerman, J. B.; Ruetschi, P. J. Electrochem. Soc. 1961, 108, 377.
30. Kokarev, G. A.; Bakhchisarait's'yan, N. G.; Medvedev, G. J. Katal. Reakts. Zhidk. Faze, Tr. Vses. Konf., 2nd, 1966, 1967, 405; Chem. Abstr. 1968, 68, 74586w.
31. Trasatti, S. J. Electroanal. Chem. 1980, 111, 125.
32. Anson, F. C. J. Am. Chem. Soc. 1959, 81, 1554.
33. Davis, D. G. Talanta 1960, 3, 335.

34. Muller, L. J. Electroanal. Chem. 1968, 16, 67.
35. Desideri, P. G. J. Electroanal. Chem. 1965, 9, 218.
36. Desideri, P. G. J. Electroanal. Chem. 1965, 9, 229.
37. Beran, P.; Bruckenstein, S. Anal. Chem. 1968, 40, 1044.
38. Beran, P.; Bruckenstein, S. J. Phys. Chem. 1968, 72, 3630.
39. Vallat, A.; Person, M.; Laviron, E. Electrochim. Acta 1982, 27, 657.
40. Solomonson, L. P. In Cyanide in Biology; Vennesland, B.; Conn, E. E.; Knowles, C. J.; Westley, J.; Wissing, F., Eds.; Academic Press: New York, 1981; pp. 11-29.
41. Cyanide in Biology; Vennesland, B.; Conn, E. E.; Knowles, C. J.; Westley, J.; Wissing, F., Eds.; Academic Press: New York, 1981; pp. 11-29.
42. Robine, R.; Lenglen, M. The Cyanide Industry; John Wiley: New York, 1906.
43. Migrdichian, V. The Chemistry of Organic Cyanogen Compounds; Reinhold Publishing: New York, 1947.
44. Williams, H. E. Cyanogen Compounds; Edward Arnold: London, 1948.
45. Krieble, V. K.; McNally, J. G. J. Am. Chem. Soc. 1929, 51, 3368.
46. Krieble, V. K.; Peiker, A. L. J. Am. Chem. Soc. 1933, 55, 2326.
47. Krieble, V. K.; Duennebier, F. C.; Colton, E. J. Am. Chem. Soc. 1943, 65, 1479.
48. Griffith, W. P. Quarterly Rev. 1962, 16, 188.
49. Sharpe, A. G. The Chemistry of Cyano Complexes of the Transition Metals; Academic Press: New York, 1976.
50. Hara, R.; Sinozaki, H. Technology Reports of the Tohoku University 1925, 5, 71.
51. Hara, R.; Sinozaki, H. Technology Reports of the Tohoku University 1926, 6, 95.

52. Schout, C. J. Am. Water Works Assoc. 1939, 31, 771.
53. Harsten, A. Black Hill Eng. 1934, 22, 145.
54. Smith, R. T. Science 1938, 87, 552.
55. Clevenger, G. H.; Morgan, H. Mining Science Press 1916, 113, 413.
56. Moir, J.; Gray, J. J. Chem. Metall. Soc. South Africa 1909, 10, 433.
57. Klempt, W. U.S. Patent 2 008 253, 1935; Chem. Abstr. 1935, 29, 6000².
58. Bezzubets, M. K.; Vozhdayera, U. N. J. Gen. Chem. Ind. USSR 1941, 18(14), 17; Chem. Abstr. 1944, 38, 2777².
59. Dobson, J. G. Metal Finishing 1947, 45(2), 78.
60. "New Process Detoxifies Cyanide Wastes," Environ. Sci. Technol. 1971, 5, 496.
61. Honda, S.; Kondo, G. Osaka Kogyo Gijutsu Shikensho Koho 1967, 18, 367; Chem. Abstr. 1968, 69, 45870z.
62. Bucksteag, W.; Thiele, H. German Patent 1 140 963, 1969; Chem. Abstr. 1969, 70, 80720t.
63. Bernardin, F. E. J. Water Poll. Control Fed. 1973, 45, 221.
64. Zhang, S.; Tian, B.; Li, M.; Li, X. Zhejiang Gongxueyuan Xuebao 1989, 44, 27; Chem. Abstr. 1990, 112, 222696b.
65. Sperry, L. B.; Caldwell, M. R. Plating 1949, 36, 343.
66. Dart, M. C.; Gentles, J. D.; Renton, D. G. J. Appl. Chem. 1963, 13, 55.
67. Easton, J. K. J. Water Poll. Control Fed. 1967, 39, 1621.
68. Sawyer, D. T.; Day, R. J. J. Electroanal. Chem. 1963, 5, 195.
69. Tamura, H.; Arikado, T.; Yoneyama, H.; Matsuda, Y. Electrochim. Acta 1974, 19, 273.

70. Kitamura, F.; Takahashi, M.; Ito, M. Chem. Phys. Lett. 1986, 130, 181.
71. Kitamura, F.; Takahashi, M.; Ito, M. Chem. Phys. Lett. 1987, 136, 62.
72. Katagiri, A.; Yoshimura, S.; Deguchi, Y.; Yoshizawa, S. Proceedings of the Symposium on Electrocatalysis; O'Grady, W. E.; Ross, P. N.; Will, F. G., Eds.; The Electrochemical Society: Pennington, NJ, 1982; pp 336-346.
73. Arikado, T.; Iwakura, C.; Yoneyama, H.; Tamura, H. Electrochim. Acta 1976, 21, 1021.
74. Hine, F.; Yasuda, M.; Iida, T.; Ogata, Y. Electrochim. Acta 1986, 31, 1389.
75. Wiaux, J. P.; Nguyen, T. Oberflaeche-Surf. 1990, 31, 20; Chem. Abstr. 1990, 112, 187736r.
76. Ochmann, R.; Kastening, B. Chem.-Ing.-Tech. 1989, 61, 830; Chem. Abstr. 1990, 112, 11430x.
77. Whitlock, J. Journal of Occupational Medicine 1989, 41(12), 36; Chem. Abstr. 1990, 112, 222630a.
78. Yazawa, T.; Nakamichi, H.; Eguchi, K.; Tanaka, H. Japan Patent 63 248 443, 1987; Chem. Abstr. 1989, 110, 102632.
79. Veresinina, E. E.; Preis, S.; Siirde, E. Khim. Tekhnol. Vody 1989, 11, 979; Chem. Abstr. 1990, 112, 185189.
80. Hanlon, D.; Callahan, M.; Le Thuy Land Disposal, Rem. Action, Incineration Treat. Hazard., Waste; U.S. Environmental Protection Agency, U.S. Government Printing Office: Washington, DC, 1988; EPA-600/9-88/021.
81. Semmens, M. J.; Chang, Y. Y. Proc. 43rd Ind. Waste Conf. 1988, 1989, 711.
82. Semmens, M. J.; Chang, Y. Y. Int. Conf. Physiochemical Biol. Detoxif. Hazard. Wastes 1988, 1989, 212.
83. Slawski, K.; Mromlinska, Z.; Wedzicha, L.; Waligora, A. Metalloberflaeche 1990, 44, 13; Chem. Abstr. 1990, 112, 167859e.

84. Huang, P.; Zhang, X. Huanan Ligong Daxue Xuebao, Ziran Kewueban 1988, 16, 55; Chem. Abstr. 1990, 112, 185199.
85. Qian, X.; Ma, X.; Shi, Y. Water Treatment 1989, 4, 99.
86. Odaka, T.; Toyoshima, T. Japan Patent 01 224 091, 1988; Chem. Abstr. 1990, 112, 83505y.
87. Schmidt, J.; Bamberg W. East German Patent 270 322, 1983; Chem. Abstr. 1990, 112, 81489x.
88. Winkler, M.; Dietel, S.; Patecki, H.; Richter, M.; Kranz, R.; Scheil, H. D. East German Patent 269 376, 1988; Chem. Abstr. 1990, 112, 83463h.
89. Kubota, T. Japan Patent 01 293 195, 1988; Chem. Abstr. 1990, 112, 164433a.
90. Faith, L. E.; Turner, L. H.; Martin, G. Q. European Patent 349 035, 1990; Chem. Abstr. 1990, 112, 102004c.
91. Yoshikawa, M.; Tonomoto, M.; Higuchi, S. Japan Patent 01 115 490, 1987; Chem. Abstr. 1990, 112, 164469s.
92. Yoshikawa, M.; Tonomoto, M.; Higuchi, S. Japan Patent 01 123 686, 1987; Chem. Abstr. 1990, 112, 164440a.
93. Yoshikawa, M.; Tonomoto, M.; Higuchi, S. Japan Patent 01 123 687, 1987; Chem. Abstr. 1990, 112, 164441b.
94. Tanno, F.; Edo, N.; Ichikawa, Y. Japan Patent 01 215 393, 1989; Chem. Abstr. 1990, 112, 83484r.
95. Patterson, J. W. Wastewater Treatment Technology; Ann Arbor Science: Ann Arbor, 1975; Chapter 9.

PART I. ELECTROCATALYTIC REDUCTION OF IODATE

INTRODUCTION

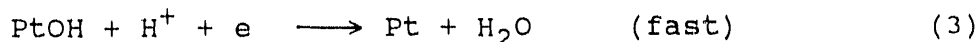
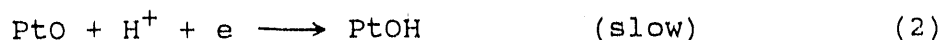
The anodic and cathodic behavior of Pt surfaces in aqueous media has been studied extensively over a large pH range. The following general conclusions have been drawn:

- i) Adsorbed hydroxyl radicals on Pt (PtOH) are formed as the initial product in the anodic generation of surface oxide.
- ii) The PtOH can readily participate in anodic O-transfer reactions.
- iii) Place exchange of OH and Pt can occur to produce a species depicted as OHPt (1).
- iv) The anodic conversion of PtOH and OHPt to a more stable oxide (PtO) inhibits anodic O-transfer processes (2).
- v) The electrochemical evolution of O_2 involves generation of adsorbed OH on the surface oxide (3) and, thereby, can have a catalytic effect on simultaneous anodic O-transfer reactions (4,5).

The electrocatalytic behavior exhibited by noble metal electrodes for anodic transfer of oxygen from H_2O to oxidation products has been attributed to hydroxyl radicals adsorbed on the electrode (4-13). Examples include the oxidations of $As(OH)_3$ to $OAs(OH)_3$ (4,6,7) and I^- to IO_3^- (5,8,9) on Pt; $As(OH)_3$ to $OAs(OH)_3$ (10) and NO_2^- to NO_3^- (11,12) on Au; and oxidation of methanol on Ru-doped Pt electrodes (13).

Studies of the cathodic behavior of previously anodized Pt electrodes indicate that the reduction of the oxides PtO

and OHPt also occurs with PtOH as an intermediate state (14) (Equations 1 and 2) followed by rapid reduction of PtOH to Pt (Equation 3).



Previous workers have noted that the reductions of O_2 (15), H_2O_2 (16), and IO_3^- (17-23) can occur more readily on pre-oxidized Pt surfaces simultaneously with reduction of the surface oxide.

A discussion of previous research surrounding the cathodic reduction of iodate was presented in the Literature Review section, earlier. Cyclic voltammetry at rotated disk electrodes was applied to a study of the electrocatalytic reduction of IO_3^- at Pt electrodes in 0.5 M H_2SO_4 . Results reported here support prior conclusions that a transient mechanism for electrocatalytic reduction of IO_3^- is coupled to reduction of OHPt and PtO. However, results for an oxide-free Pt surface indicate that IO_3^- reduction requires a more intimate involvement of IO_3^- with the surface than previously thought.

EXPERIMENTAL

Reagents

All solutions were prepared from reagent grade chemicals. Sulfuric acid was Ultrex grade (J. T. Baker). Water was distilled, demineralized and passed through a Nanopure II purification system (Barnstead). The supporting electrolyte was 0.50 M H₂SO₄. Dissolved O₂ was removed from all solutions by saturation with dispersed N₂. Nitrogen was filtered through active carbon.

Apparatus

All data were obtained at a Pt, Model AFMD19, rotated disk electrode (RDE, 0.196 cm²) or a Pt-Pt, Model AFMT28 rotated ring-disk electrode (RRDE, disk diameter: 0.180 inch, ring I.D.: 0.194 inch, ring O.D.: 0.212 inch; Pine Instrument Co.). Rotation speed was controlled by a Model MSRX rotator (Pine Instrument Co.). Cyclic voltammetry was achieved by a Model AFRDE-4 potentiostat (Pine Instrument Co.) and i-E curves were recorded on a Model 7035B X-Y recorder (Hewlett Packard). All potential values were measured and are reported as volts (V) vs. the saturated calomel electrode (SCE).

Data in Figures 1, 2 and 6 were obtained by computer control of the potentiostat. A program (see Appendix) written in QuickBASIC (Microsoft Corp.) generated a staircase waveform and i-E data were collected using a

Standard 286/10 microcomputer equipped with a DT 2801/5716 input-output board and associated software (Data Translation, Inc.).

Procedures

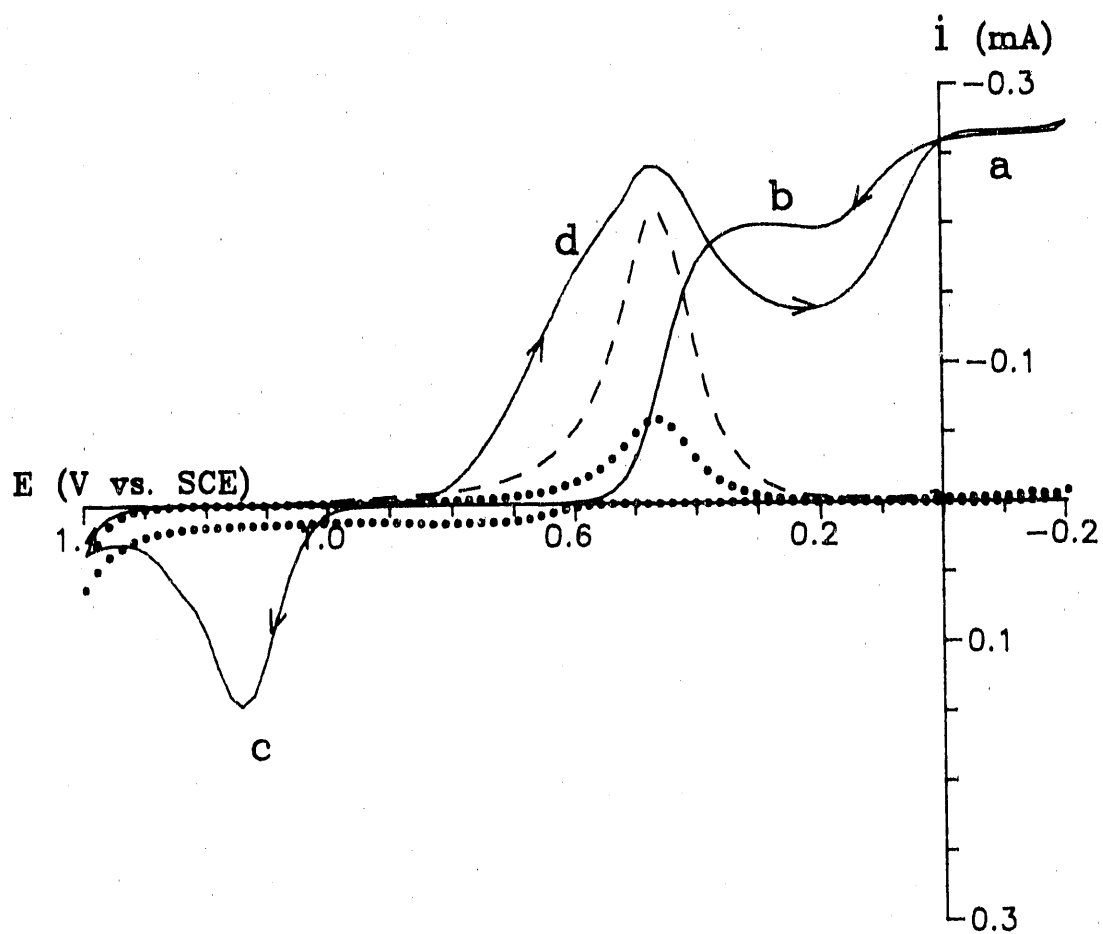
The electrode surface was polished prior to each use with 0.05- μm alumina (Buehler) on microcloth followed by thorough rinsing with deionized water. To ensure removal of all alumina residue, the electrode surface was then wiped with either a cotton swab, a Kimwipe tissue, or microcloth wetted with deionized water. Electrodes were electropolished by cyclic scans of the potential between 1.45 and -0.25 V vs. SCE until i-E curves were reproducible. The number of scans required to reach reproducible response varied from 20 to 200 scans depending on the type of material used to clean the alumina from the electrode. Unless specified to the contrary, voltammetric data shown correspond to the reproducible i-E curves.

RESULTS AND DISCUSSION

Cyclic voltammetry

Current-potential (i - E) curves are shown in Fig. I-1 obtained by cyclic voltammetry at the Pt RDE in 0.50 M H_2SO_4 before (...) and after (—) addition of 5.0×10^{-4} M IO_3^- . In the absence of IO_3^- , the small anodic current observed during the positive potential scan in the region $E_d = 0.1$ to 0.55 V resulted from double-layer charging. At $E_d > 0.55$ V on the positive scan, surface oxide was formed: PtOH and OHPt in the region $0.55V \leq E_d \leq 1.0$ V and PtO at $E_d > 1.0$ V (1). Because appreciable evolution of O_2 occurred for $E_d >$ ca. 1.45 V, the potential scan was reversed at that value. During the subsequent negative scan, reduction of the surface oxide produced the large cathodic peak in the region 0.8 V $\geq E_d \geq 0.2$ V with a peak potential (E_p) of ca. 0.50 V. The cathodic and anodic formation and dissolution, respectively, of adsorbed atomic hydrogen (H_{ads}) occurred on the negative and positive scans, respectively, in the region 0.1 V $\geq E_d \geq -0.2$ V. Cathodic evolution of H_2 occurred for $E_d < -0.25$ V and, therefore, the negative scan was reversed at that potential.

Following addition of IO_3^- (—), Wave a was observed during the positive scan for $-0.25 \leq E_d \leq 0.15$ V. Wave a corresponded to reduction of IO_3^- to I^- at the oxide-free Pt surface. A well-defined Wave b was also obtained during the



Scan rate = 6.0 V min^{-1}

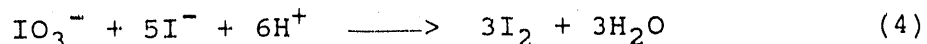
Rotation speed = $1000 \text{ rev min}^{-1}$

(...) 0.00 mM IO_3^- ; (—) 0.50 mM IO_3^- ;

(---) $7/2$ times sensitivity for (...)

Figure I-1. Current-potential curves for IO_3^- at a Pt RDE by cyclic voltammetry in $0.50 \text{ M H}_2\text{SO}_4$

positive scan in the region $0.15 \text{ V} \leq E_d \leq 0.55 \text{ V}$ which was initially concluded to correspond to the reduction of dissolved molecular iodine ($I_{2, \text{aq}}$) formed in the diffusion layer according to Equation 4. Adsorbed atomic iodine (I_{ads}°) present on the electrode surface inhibited the



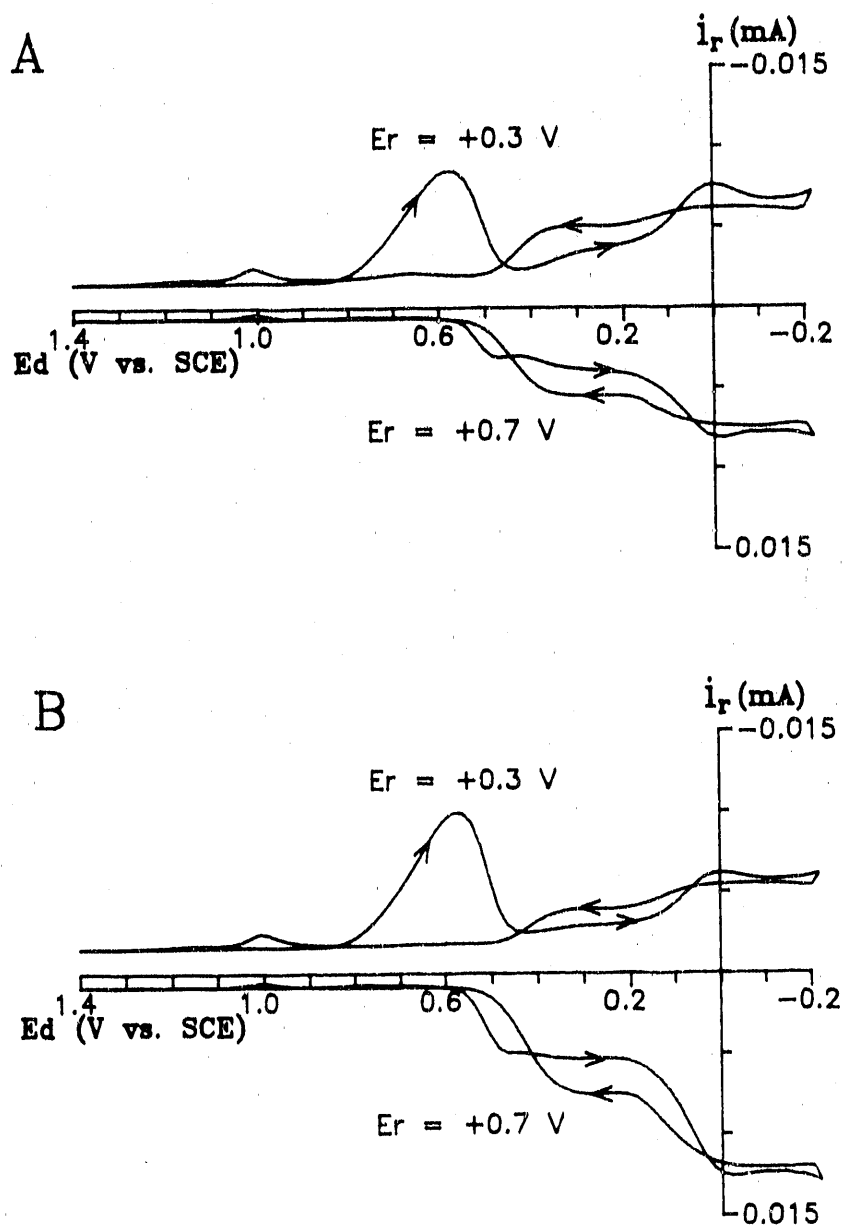
formation of PtOH during the positive scan and, therefore, only charging current was observed for $0.55 \text{ V} \leq E_d \leq 0.95 \text{ V}$. At $E_d > 0.95 \text{ V}$, the anodic current increased rapidly (Peak c) reaching a maximum value at $E_p = \text{ca. } 1.15 \text{ V}$. Peak c resulted from the concurrent anodic processes of oxidative desorption of I_{ads}° , primarily as IO_3^- , and the formation of surface oxide (9). For the negative scan (Fig. I-1), cathodic Peak d in the region $0.8 \text{ V} \geq E_d \geq 0.4 \text{ V}$, with $E_p = 0.48 \text{ V}$, corresponded to the reduction of Pt oxide in the residual i_d - E_d curve (...). However, the area under Peak d in the presence of IO_3^- was considerably greater than that for the absence of IO_3^- . Hence, IO_3^- is confirmed to be reduced concurrently with the oxide film. It was speculated initially that reduction of IO_3^- simultaneously with PtO reduction might be promoted by adsorption of a reduction product, e.g., I° . However, reduction of IO_3^- to I_{ads}° at every Pt site would have produced an area under Peak d $7/2$ times larger than the peak for reduction of PtO. The dashed line in Fig. I-1 represents that hypothetical i_d - E_d response which is considerably smaller than the curve

observed in the presence of IO_3^- . Hence, the turnover of IO_3^- at PtO sites was greater than 1.0 mol mol^{-1} . Based on the area measured for Peak d and assuming a 5-electron process, it was estimated that ca. three IO_3^- ions were reduced per Pt site. Anson has reported the reduction of as much as 1000 equivalents of IO_3^- per equivalent of PtO (17).

Considerable hysteresis was observed in the region of Wave b for IO_3^- (—) on the positive and negative scans (see Fig. I-1). This seemed inconsistent with prior conclusions that the cathodic signal in this region originated from reduction of $\text{I}_{2,\text{aq}}$ generated by the reaction of IO_3^- and I^- within the diffusion layer. Such a mechanism would not be expected to depend on scan direction for the low scan rates applied in this study. Therefore, further mechanistic study was considered necessary.

Rotated ring-disk studies

Collection experiments were performed at a Pt-Pt rotated ring-disk electrode (RRDE) to obtain information about the product(s) of the disk reaction in the region $0.5 \text{ V} \geq E_d \geq 0.1 \text{ V}$. The ring current response was recorded as a function of disk potential for two values of E_r . The resulting i_r - E_d curves are shown in Fig. I-2A. For $E_r = 0.3 \text{ V}$, very little cathodic response was obtained for IO_3^- . This is suspected to be a consequence of the combination of slow electrode kinetics for the reaction and the higher flux

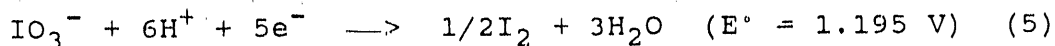


Scan rate = 6.0 V min^{-1}

Figure I-2. Current-potential curves for 0.50 mM IO_3^- at a Pt RRDE by cyclic voltammetry in $0.50 \text{ M H}_2\text{SO}_4$

- A) Ring response, $1000 \text{ rev min}^{-1}$;
 B) Ring response, $2000 \text{ rev min}^{-1}$

density at the ring electrode. Conversely, reduction of $I_{2, aq}$ to I^- proceeded readily at the ring electrode ($E_r = 0.3$ V) and, therefore, the i_r-E_d curve in Fig. I-2A gave direct evidence for $I_{2, aq}$ production at the disk electrode corresponding to Waves a, b and d (compare Figs. I-1 and I-2A). It is especially noteworthy that $I_{2, aq}$ was produced at the disk electrode during the negative E_d scan in the region of Wave d, as predicted in Equation 5.



The peak shape for detection of $I_{2, aq}$ at the ring electrode simultaneously with Peak d at the disk was virtually symmetric with the cathodic peak for PtO reduction at the disk shown in Fig. I-1 (...). This is consistent with the conclusion that IO_3^- is reduced to $I_{2, aq}$ by a mechanism coupled to the reduction of PtO (Equation 5).

Very little $I_{2, aq}$ was detected at the ring electrode during the negative scan in the region $0.35 \text{ V} \geq E_d \geq 0.25 \text{ V}$ when the disk surface was virtually free of oxide. Because $I_{2, aq}$ is reduced to I^- for $E < 0.55 \text{ V}$, the cathodic ring current obtained at $E_r = 0.3 \text{ V}$ for $E_d < 0.55 \text{ V}$ resulted from detection of only that portion of $I_{2, aq}$ produced by reaction of IO_3^- and I^- in the diffusion-layer region of the RRDE (Eqn. 4) which escaped reduction at the disk electrode. As discussed previously, some of that $I_{2, aq}$ returned to the disk electrode for reduction to I^- .

Iodide (I^-) was detected anodically at the ring electrode for $E_r = 0.7$ V (Fig. I-2A). Hence, the peak in the i_r - E_d curve observed during the negative scan of E_d ($E_p = 0.48$ V) corresponded to the cathodic maximum observed for Wave d at the disk electrode (see Fig. I-1). This peak is attributed to direct reduction of IO_3^- to I^- by a process catalyzed by PtO reduction. In the region $0.55 < E_d < -0.2$ V, the anodic waves for I^- detection ($E_r = 0.7$ V) were approximately symmetric to the cathodic waves for I_2 detection ($E_r = 0.3$ V). A small anodic signal appeared in the region 1.4 V $> E_d > 0.6$ V. However, no process occurs in that region and the signal is the result of an offset produced by the computer-controlled data acquisition device.

It was expected that increases of rotation speed (ω) for the RRDE would result in an increased ratio of I^-/I_2 detected at the ring in the region 0.5 V $\geq E_d \geq 0.1$ V. This was verified by comparison of the i_r - E_d response obtained at 2000 rev min $^{-1}$ (Fig. I-2B) with data for 1000 rev min $^{-1}$ (Fig. I-2A). The anodic value of i_r at $E_r = 0.7$ V increased and the cathodic value of i_r at $E_r = 0.3$ V was decreased, as predicted.

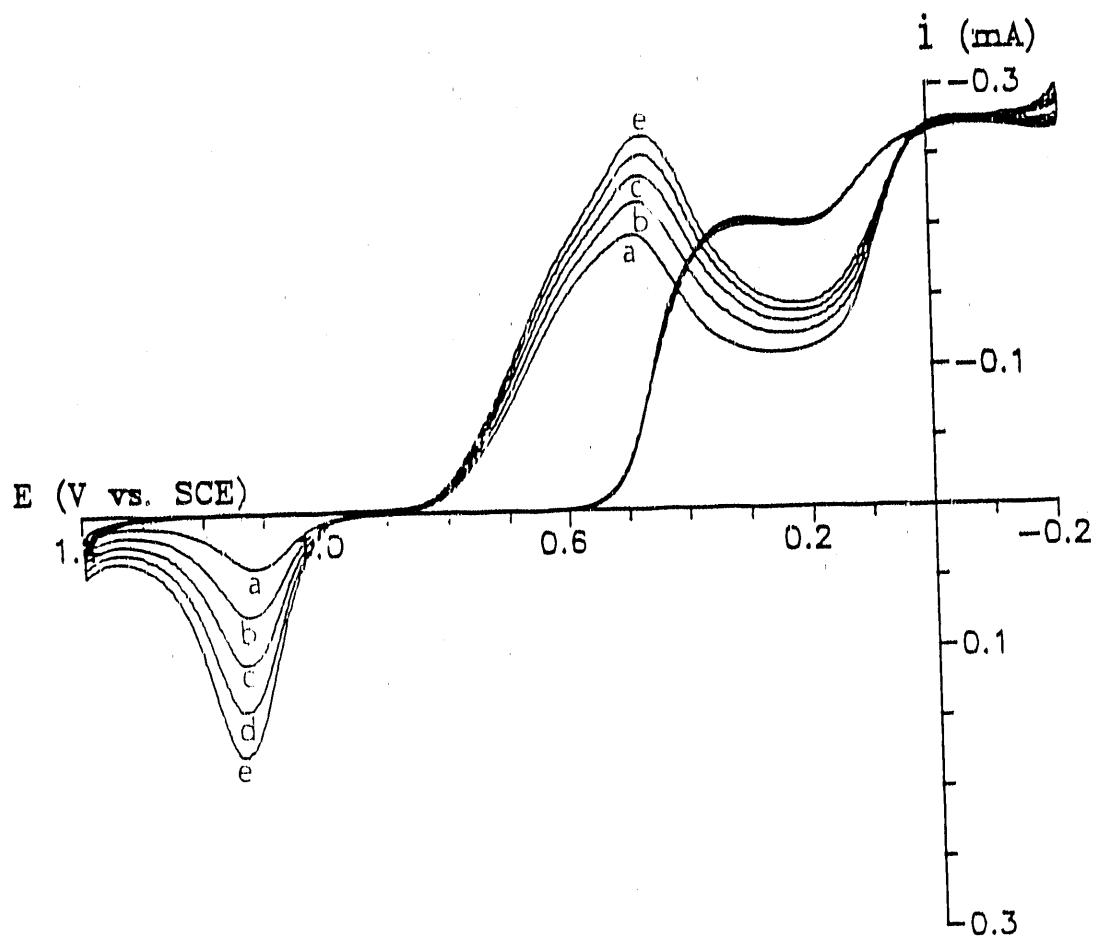
A peak in the i_r - E_d response for $E_r = 0.3$ V was observed during the negative scan at $E_d = \underline{ca.}$ 0.0 V in the region of Wave a in the i_d - E_d response (Fig. I-2A-B). This is speculated to correspond to I_2 generated by reaction of IO_3^- with I^- from cathodic desorption of I_{ads}^- at the disk

electrode by the formation of some H_{ads} or $\text{H}_{2,\text{ads}}$ as E_d approached the potential for onset of rapid H_2 evolution at the Pt disk (9).

A cathodic ring current peak was observed at $E_d = 1.0$ V for both $E_r = 0.3$ V and $E_r = 0.7$ V. It was speculated that this current maximum resulted from reduction of intermediate products formed at the onset of the oxidative desorption of I_{ads} at the disk (e.g., IO^- and IO_2^-). That anodic desorption process yields predominantly IO_3^- .

Variation of scan rate

Variation of potential scan rate (ϕ) in voltammetric studies can be useful for discriminating between surface-controlled and transport-controlled faradaic processes. Current-potential curves recorded at the RDE as a function of ϕ are shown in Fig. I-3. The height of Peak c observed during the positive scan, caused by simultaneous oxidations of I_{ads} and the Pt surface, varied nearly as a linear function of ϕ , which is expected for surface-controlled reactions. The height of Peak d on the negative scan varied in a nonlinear manner with ϕ . This is indicative of mixed control by surface- and transport-controlled processes. The plateau current for 0.0 V $>$ E_d -0.2 V (Wave a) was virtually independent of scan rate, which is representative of a purely transport-controlled process. For 0.4 V $>$ E_d $>$ 0.1 V, i.e., the region of Wave b, the variation of current with



Rotation speed = 1000 rev min⁻¹

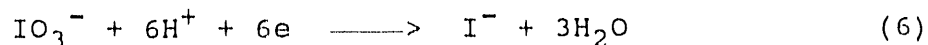
Scan rate (V min⁻¹): a) 1.0, b) 2.0, c) 3.0,
d) 4.0, e) 5.0

Figure I-3. Current-potential curves for IO_3^- at a Pt RDE by cyclic voltammetry in 0.50 M H_2SO_4

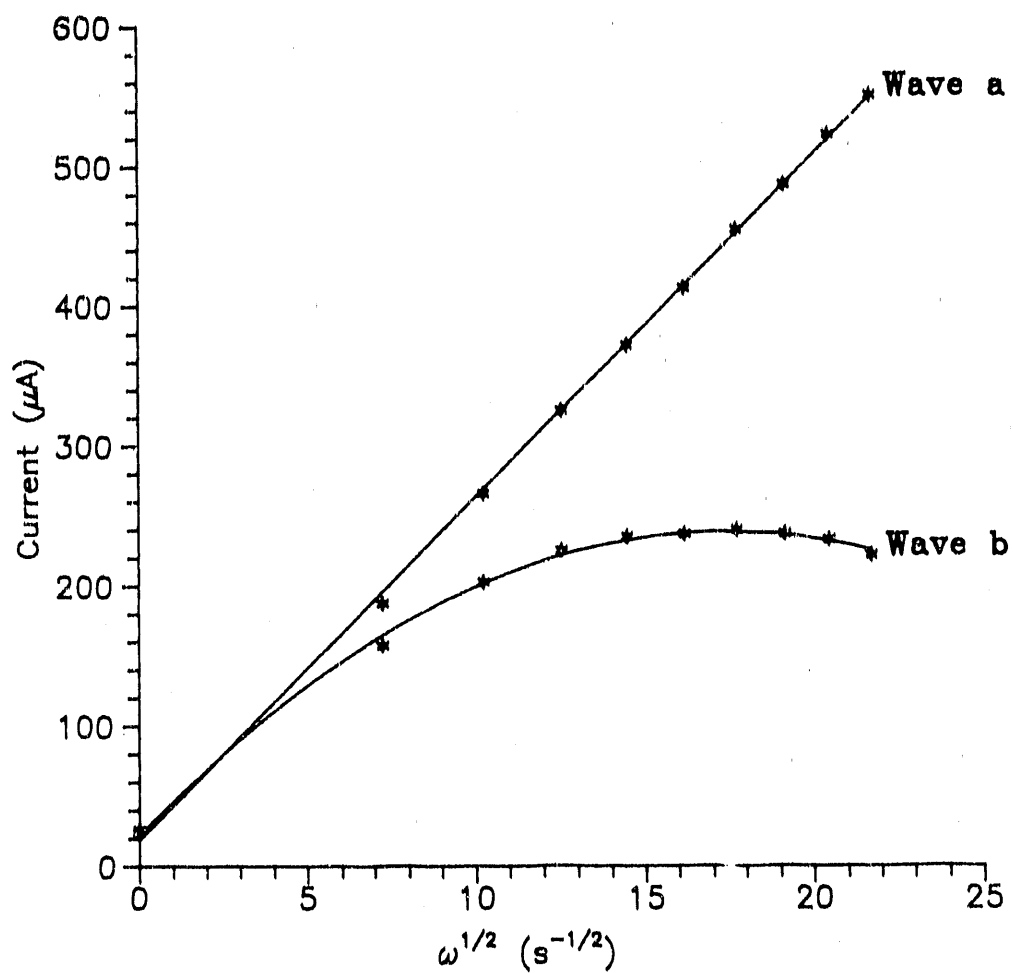
changing ϕ was more pronounced for the negative scan than the positive scan. This is indicative of a greater influence by the surface-controlled component of total current during the negative scan.

Variation of rotation speed

Voltammetric results were recorded at the RDE as a function of rotation speed (ω) for a constant ϕ and the results are summarized in Fig. I-4. The value of i_d at $E_d = -0.05$ V on the positive scan (Wave a) increased as a linear function of $\omega^{1/2}$ ($r = 0.9997$), which is indicative of a transport-controlled reaction at the RDE. The slope of the i - $\omega^{1/2}$ plot for Wave a (Fig. 4) corresponded to a 4-electron process, as estimated from the Levich equation (25) using $D = 1.09 \times 10^{-5}$ cm² s⁻¹ for IO₃⁻ (26). This is lower than expected for the 6-electron reduction of IO₃⁻ to I⁻ (Equation 6) and might have resulted, at least in part,



because some I₂ produced by the coupled homogeneous reaction of IO₃⁻ from the bulk solution with I⁻ coming from the disk (Eqn. 4) can be lost from the diffusion layer without undergoing reduction to I⁻. The pseudo-limiting value of i_d in Wave b reached a maximum at ca. 3000 rev min⁻¹ and then decreased at higher rotation speeds. The distinct negative slope for Wave b at high rotation speeds is considered



E_d (vs. SCE): Wave a) -0.05 V, Wave b) 0.25 V

Figure I-4. Current vs. $\omega^{1/2}$ data obtained from i-E curves recorded at 6.0 V min^{-1} scan rate

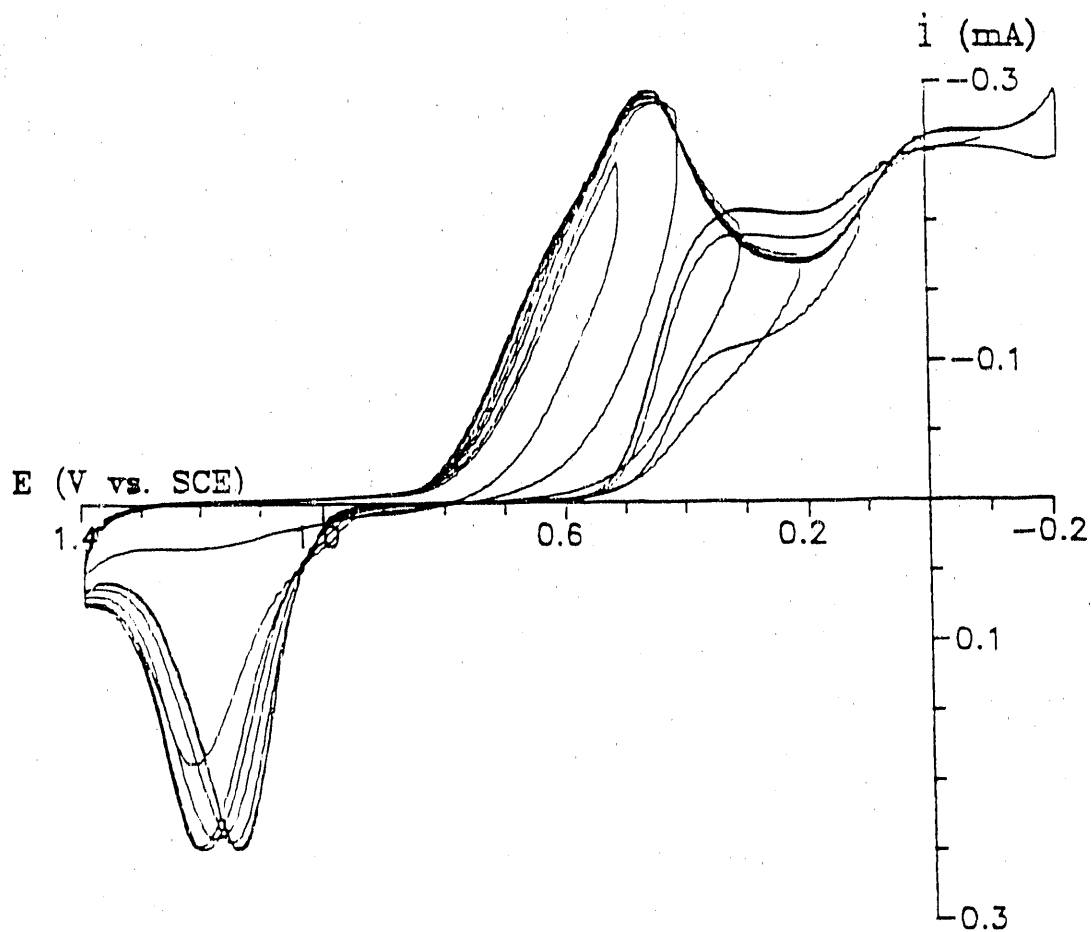
indicative of loss of other intermediate reaction products, in addition to $I_{2,aq}$, from the electrode surface in the mechanism producing Wave b.

Peak c, corresponding to the simultaneous processes of surface oxide formation and oxidative desorption of I_{ads} , was determined to be independent of w , as expected for purely surface-controlled processes. The plot of i_p vs. $w^{1/2}$ for Peak d was virtually linear for low values of w , but with a nonzero intercept. This is consistent with the simultaneous occurrence of the surface-controlled reduction of PtO and transport-controlled reduction of IO_3^- by the surface-catalyzed mechanism.

Variation of scan limits

Current-potential curves were recorded at the RDE as a function of the negative scan limit (E_-) for a positive scan limit (E_+) of 1.4 V and the data is shown in Fig. I-5. Peak c (positive scan) in the region $0.95 \text{ V} \leq E_d \leq 1.3 \text{ V}$ was only a small fraction of its limiting area for $E_- = 0.45 \text{ V}$. Hence, a relatively small amount of I_{ads}^o was formed at the disk electrode during the negative scan in the region $0.8 \text{ V} > E_d \geq 0.5 \text{ V}$ in spite of the observation that a large amount of $I_{2,aq}$ was generated in this region (see Fig. I-2A). Peak c reached its limiting area for $E_- \leq 0.3 \text{ V}$.

For $E_- < 0.4 \text{ V}$, Peak c shifted slightly to more negative values as E_- was made more negative, as is also



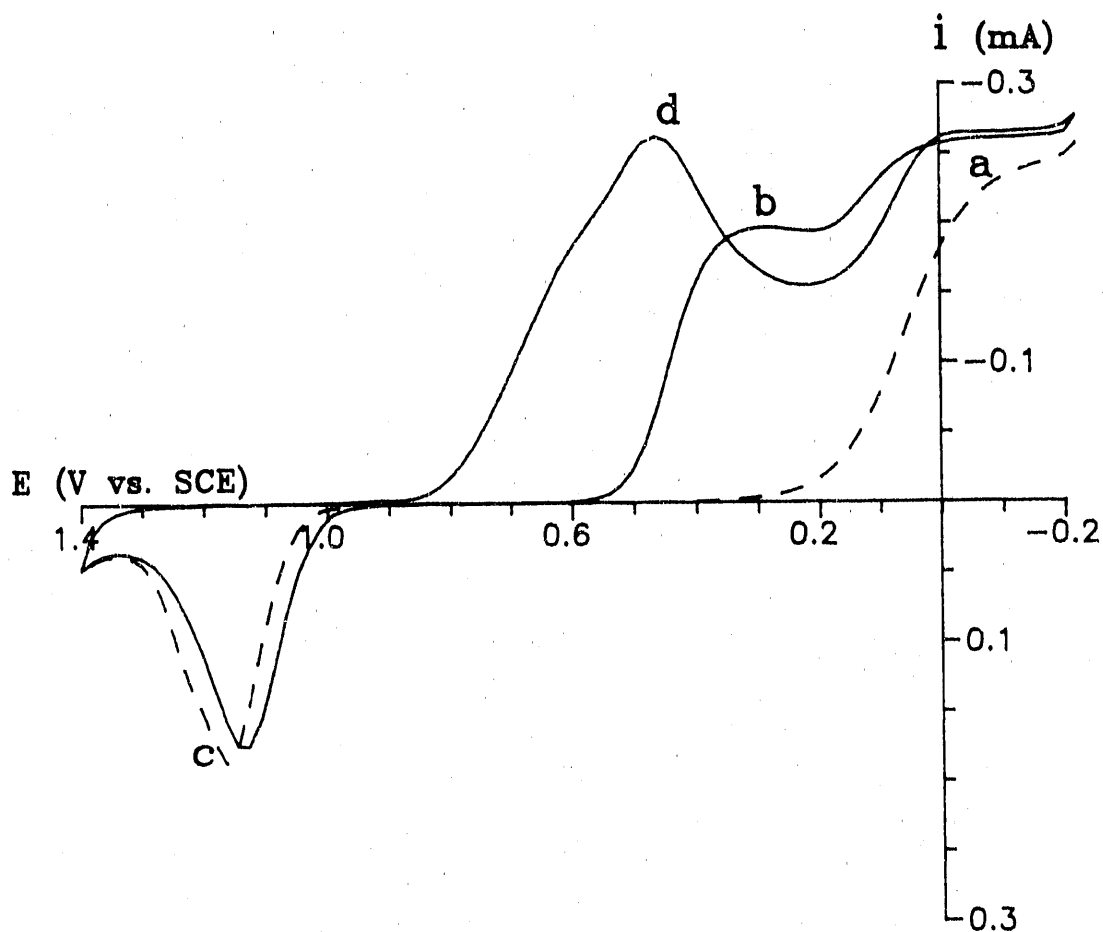
Scan rate: 6.0 V min^{-1}

Rotation speed: $1000 \text{ rev min}^{-1}$

Figure I-5. Effect on i - E curves of changing the cathodic scan limit (E_-) for 0.50 mM IO_3^- at a Pt RDE in $0.50 \text{ M H}_2\text{SO}_4$

shown in Fig. I-5. Because the peak potential for an oxidative desorption reaction is indicative, in part, of the energy required to desorb I_{ads}° during the anodic process, the data indicate a decrease in adsorption stability as E_- was made more negative. It was also observed that Wave b (positive scan) decreased dramatically for $E_- > 0.05$ V. The co-dependence of Waves b and c on E_- suggests a mechanistic link between the stability of I_{ads}° and faradaic mechanism producing Wave b. In a separate experiment, i_d-E_d curves were recorded as a function of E_+ for $E_- = -0.2$ V. For $E_+ \leq 1.0$ V, only Waves a and b were observed during the negative scan. Peak d was absent because the presence of I_{ads}° on the Pt surface inhibited anodic formation of PtO during the positive scan to $E_+ \leq 1.0$ V. The height and area of Peak d (negative scan) were observed to be increased linearly with increasing values of $E_+ > 1.0$ V. This increase was a direct consequence of the increasing quantity of oxide which formed for increasing values of E_+ .

For any value of $E_+ < 1.0$ V, Waves a and b gradually decreased with successive scans. Figure I-6 contains $i-E$ curves for $E_+ = 1.4$ V and $E_- = -0.2$ V that were recorded prior to the start and at the conclusion of a 4-hr period during which E_d was cycled repetitively between $E_+ = 1.0$ V and $E_- = -0.2$ V using $\phi = 6.0$ V min⁻¹. The i_d-E_d response recorded prior to the start of this period represents the reproducible voltammetric response for IO_3^- at the Pt



Scan rate: 6.0 V min^{-1}

Rotation speed: $1000 \text{ rev min}^{-1}$

(—) Anodic scan limit of 1.40 V

(---) Positive scan after repeated cycling for
4 hr within the range 1.00 V to -0.22 V

Figure I-6. Effect of changing anodic scan limit on current-potential curves for 0.50 mM IO_3^- at a Pt RDE in $0.50 \text{ M H}_2\text{SO}_4$

electrode. During the 4-hr period, Wave b disappeared completely and the height of Wave a decreased by approximately 15-20%. One possible cause of this effect is the accumulation of adsorbed impurities (e.g., trace organic compounds) from the solution onto the Pt electrode. For cyclic voltammetry with $E_+ = \text{ca. } 1.3 \text{ V}$, the Pt surface is maintained relatively free of excessive quantities of adsorbed impurities because of the benefit of oxidative desorption simultaneously with PtO formation (Peak c). This is supported by the observation that substitution of reagent grade H_2SO_4 for the Ultrex grade and the use of unfiltered N_2 resulted in the disappearance of Wave b in ca. 30 min.

It is readily apparent from Fig. I-6, that there was a slight change in the shape of Peak c but virtually no change in peak area during the 4-hr period. Hence, the supposed accumulation of adsorbed impurity had no effect on the surface coverage by I_{ads}° . On the basis of this supposition, the data are consistent with adsorption of the impurity onto the I_{ads}° . Furthermore, the disappearance of Wave b under these circumstances possibly indicates a reduction mechanism for IO_3^- requiring weak adsorption of IO_3^- to I_{ads}° sites. Hence, a more strongly adsorbed impurity would prevent adsorption of IO_3^- and, thereby, suppress Wave b.

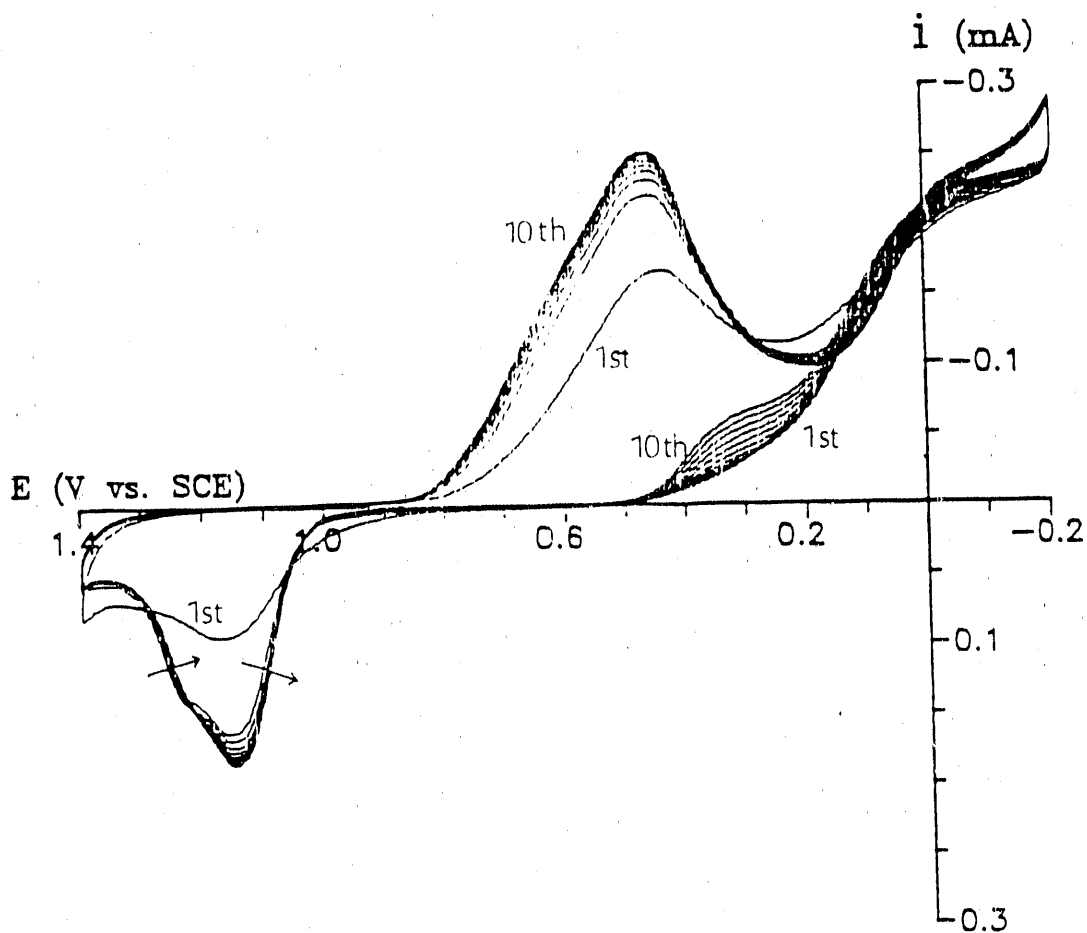
The slight positive shift in E_p for Peak c could have resulted from adsorbed impurities. The shift could also indicate a slightly greater stability of I_{ads}° resulting from

atomic rearrangements at the Pt surface during the prolonged period of cathodic polarization.

Surface pretreatment

The height of Wave b ($0.5 \text{ V} \geq E_d \geq 0.2 \text{ V}$) was determined to be highly sensitive to alterations in the procedure for surface pretreatment. Prior to the start of experiments described above, the electrode was polished with 0.05- μm alumina on microcloth wetted with deionized water. To ensure removal of residual adherent alumina, the surface was rinsed with deionized water, wiped with cotton swabs which had been profusely wetted with deionized water, and again rinsed with deionized water. The applied potential was then cycled repeatedly within the designated potential limits until the i_d - E_d response was reproducible.

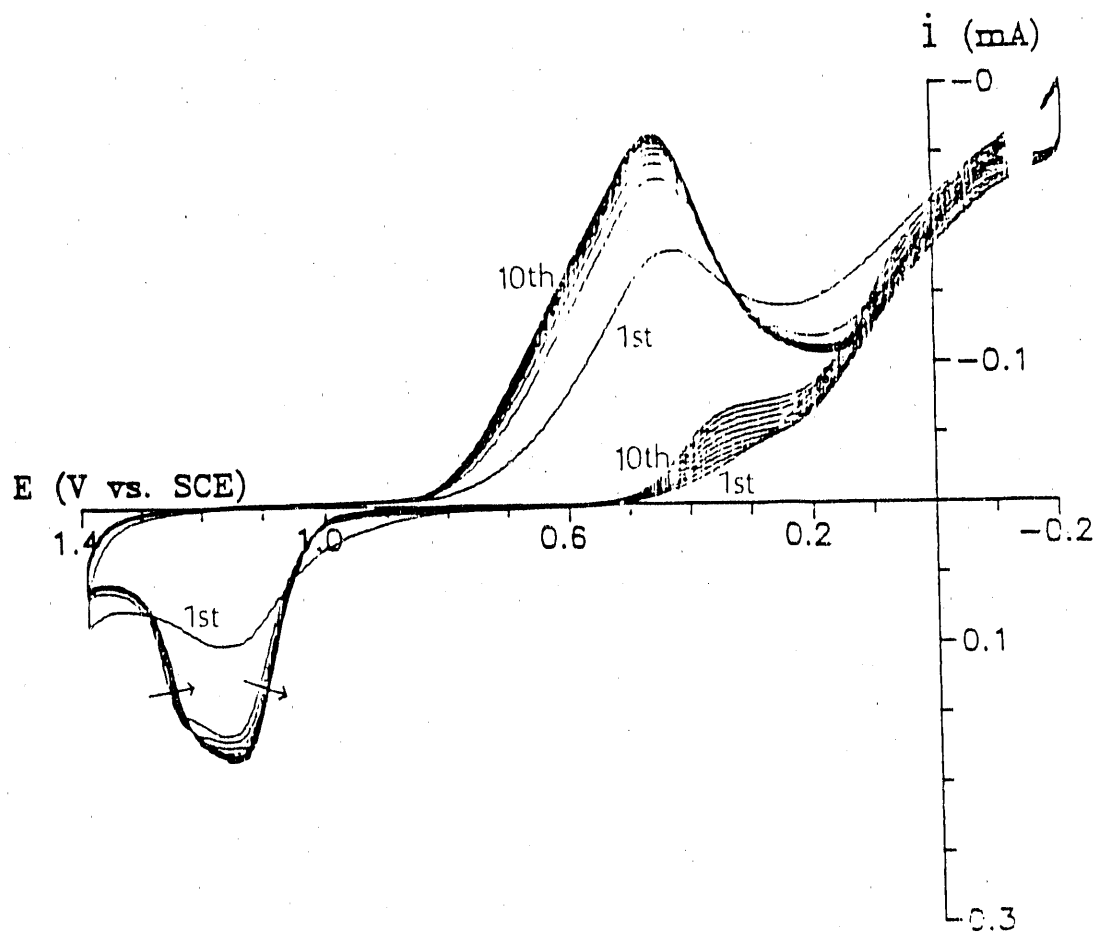
In separate experiments, the i_d - E_d response for IO_3^- was compared for use of three different absorbent materials to remove residual alumina: cotton swabs, Kimwipe tissues, and microcloth. Alternatively, the electrode was merely rinsed after polishing without wiping. The evolution of the i_d - E_d curves during repeated cycles of E_d after each treatment is shown in Fig. I-7A-D. Waves a and b and Peaks c and d were initially suppressed in all cases. However, the rate of recovery of Wave b was especially sensitive to surface treatment. The most severe effect was observed when cellulosic materials (*i.e.*, cotton swabs and Kimwipe



Scan rate: 6.0 V min^{-1}

Rotation speed: $1000 \text{ rev min}^{-1}$

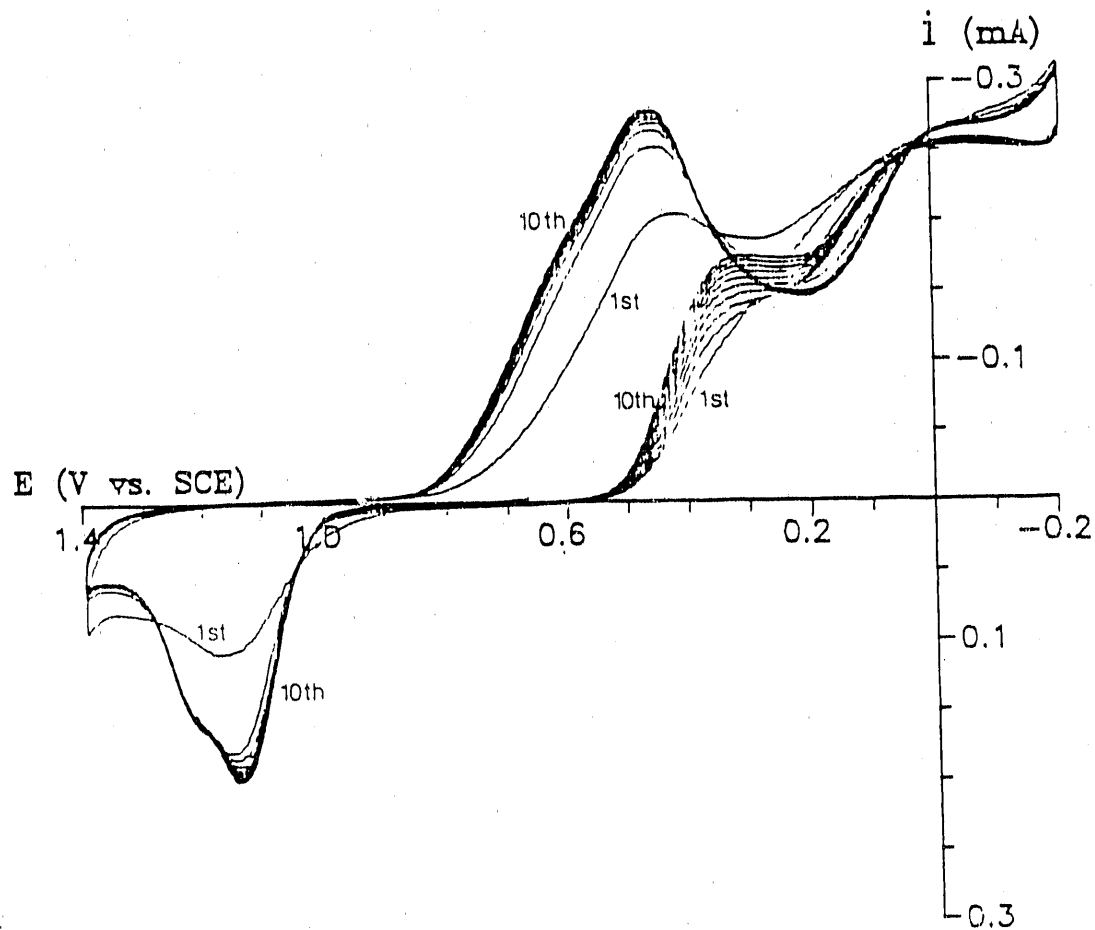
Figure I-7A. Effect of surface treatment on current-potential curves for 0.50 mM IO_3^- at a Pt RDE in $0.50 \text{ M H}_2\text{SO}_4$. Electrode was polished with $0.05\text{-}\mu\text{m}$ alumina prior to treatment with H_2O and a cotton swab. Arrows indicate scan direction



Scan rate: 6.0 V min^{-1}

Rotation speed: $1000 \text{ rev min}^{-1}$

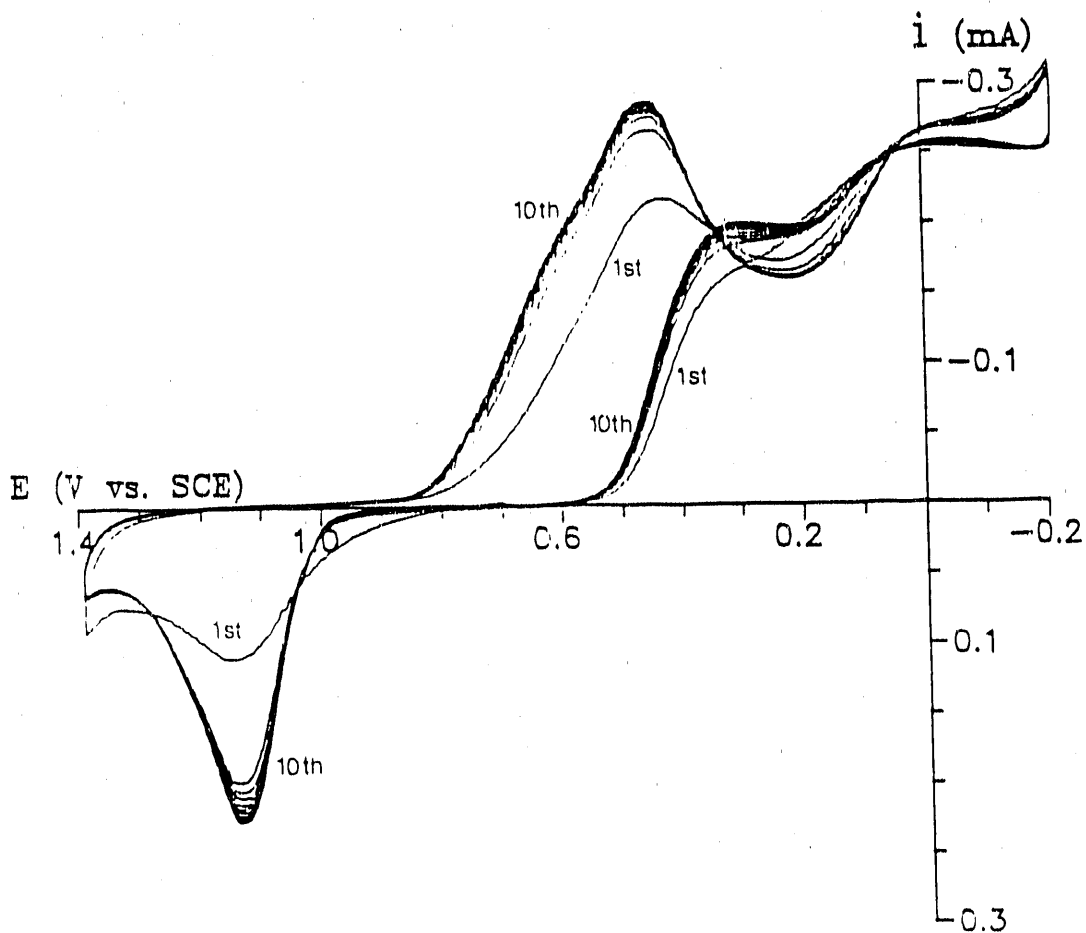
Figure I-7B. Effect of surface treatment on current-potential curves for 0.50 mM IO_3^- at a Pt RDE in $0.50 \text{ M H}_2\text{SO}_4$. Electrode was polished with $0.05\text{-}\mu\text{m}$ alumina prior to treatment with H_2O and a Kimwipe. Arrows indicate scan direction



Scan rate: 6.0 V min^{-1}

Rotation speed: $1000 \text{ rev min}^{-1}$

Figure I-7C. Effect of surface treatment on current-potential curves for 0.50 mM IO_3^- at a Pt RDE in $0.50 \text{ M H}_2\text{SO}_4$. Electrode was polished with $0.05\text{-}\mu\text{m}$ alumina prior to treatment with H_2O and a microcloth



Scan rate: 6.0 V min^{-1}

Rotation speed: $1000 \text{ rev min}^{-1}$

Figure I-7D. Effect of surface treatment on current-potential curves for 0.50 mM IO_3^- at a Pt RDE in $0.50 \text{ M H}_2\text{SO}_4$. Electrode was polished with $0.05\text{-}\mu\text{m}$ alumina prior to rinsing with H_2O

tissues) were used (Figs. I-7A & I-7B, respectively). Simple rinsing without use of an absorbent material produced the least suppression of Wave b and allowed the fastest recovery to its reproducible response (Fig. I-7D).

Examination of the residual i_d - E_d response in 0.5 M H_2SO_4 in the absence of IO_3^- also revealed effects from variation of the pretreatment conditions. Use of the cellulosic materials resulted in large initial suppressions of the waves for PtO formation, PtO reduction, and H-adsorption and desorption. Continued potential cycling eventually (ca. 20 min) restored these voltammetric features to the shape and areas normally expected for pure Pt electrodes. The i_d - E_d response obtained immediately following subsequent addition of IO_3^- corresponded to the reproducible curve shown in Fig. I-1 (—).

In other experiments it was determined that the cathodic wave for reduction of $I_{2,aq}$ in the same potential region as Wave b was not decreased below the transport-limited value by alteration of the various pretreatment procedures. Furthermore, a Pt electrode for which Wave b was absent in the presence of IO_3^- was rinsed in water and transferred to a solution of $I_{2,aq}$ in 0.5 M H_2SO_4 . The wave for $I_{2,aq}$ was present in the i_d - E_d curve obtained for the first cyclic E_d scan. The electrode then was rinsed and returned to the IO_3^- solution. Still, Wave b was absent from the i_d - E_d curve. These results demonstrate: i) the

mechanism producing Wave b is more complex than previously thought (19), and probably involves weak adsorption of IO_3^- to $\text{I}_{\text{ads}}^\circ$ sites on the Pt surface, and ii) impurities can be transferred from absorbent materials used in electrode pretreatment to electrode surfaces with dire consequence for some faradaic reactions.

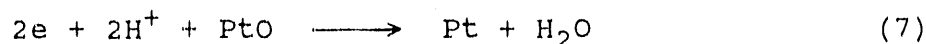
CONCLUSIONS

The original goal of this research was satisfied and evidence obtained indicates an electrocatalytic link between reduction of surface oxide and reduction of IO_3^- during the negative scan at an oxide-covered Pt electrode. Furthermore, the quantity of IO_3^- reduced is larger than calculated on the basis of a mechanism in which the process is promoted by the adsorption of a reduction product (e.g., I°). The possibility still exists, therefore, that the IO_3^- reduction process is coupled with the oxide reduction mechanism via adsorbed hydroxyl radicals ($\cdot\text{OH}_{\text{ads}}$) assumed to be involved in both processes. However, a stronger statement supporting this conjecture must await the results of further investigations demonstrating that the cathodic oxygen-transfer process on Pt is not unique to IO_3^- . The ultimate failure of the suggested mechanism to produce a persistent cathodic signal for IO_3^- on the oxide-free surface is thought to result from the eventual coverage of the Pt surface by $\text{I}_{\text{ads}}^\circ$. This is discussed in more detail below.

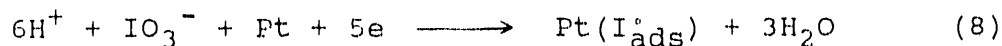
Desideri (19,20) observed that the cathodic wave for IO_3^- reduction on oxide-free Pt decreased with time. In one study (19), the decrease in wave height after prolonged use of a Pt electrode was concluded to be caused by adsorption of I_2 . In another (20), the cathodic wave height was

observed generally to be lower on a pre-reduced electrode than on a pre-oxidized electrode. Addition of $I_{2, aq}$ was reported to eliminate differences in voltammetric response that were estimated to be caused by electrode pretreatment. Desideri concluded that the first stage of IO_3^- reduction is electrochemical and the second stage is chemical in nature, involving reduction of $I_{2, aq}$ produced in the diffusion layer by reaction of IO_3^- with I^- .

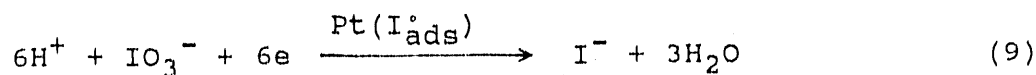
The conclusions of Desideri are shown to be incorrect by the observation that the reduction of IO_3^- on oxide-free Pt (Wave b) can be blocked even when reduction of $I_{2, aq}$ persists. The results are consistent with the general description given by Equations 14-17. For a pre-anodized electrode, PtO is reduced to Pt during the negative scan in the region $0.8 > E_d > \text{ca. } 0.4 \text{ V}$ (Equation 7).



The reduction of IO_3^- during the negative scan at the oxide-free Pt can yield I_2 ($0.8 > E_d > 0.45 \text{ V}$) and I^- ($E_d < 0.45 \text{ V}$) with the immediate result that iodine (I°) is adsorbed at the Pt surface (Equation 8).

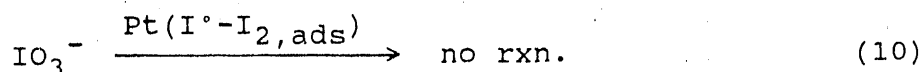


In the region $0.5 > E_d > 0.2 \text{ V}$ (neg./pos. scans), the direct reduction of IO_3^- to I^- can occur at $Pt(I_{ads}^\circ)$ sites (Equation 9).



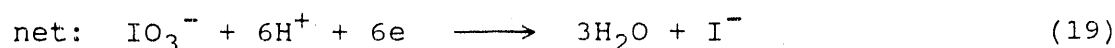
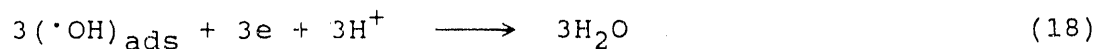
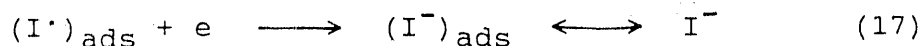
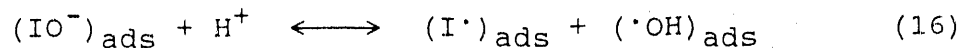
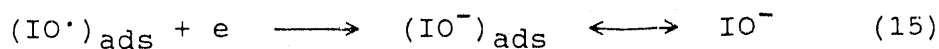
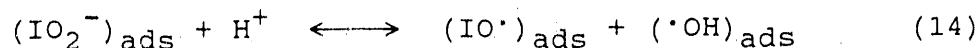
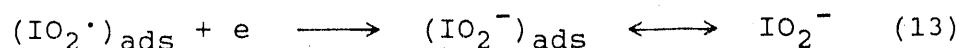
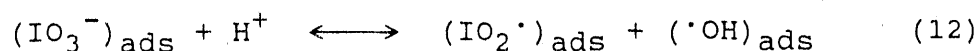
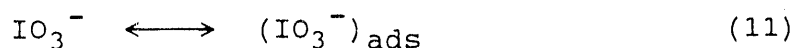
That mechanism is not fast and, consequently, the surface concentration of IO_3^- at the electrode surface is not zero. Hence, an appreciable quantity of IO_3^- reacts with I^- in the diffusion layer to produce $\text{I}_{2,\text{aq}}$, a portion of which reacts at the electrode to yield I^- and the remainder escapes the region of the disk electrode by convective-diffusional processes. The consequence is that the plateau current for Wave b is below the transport-limited value for the 6-electron reduction of IO_3^- . It is apparent that the reduction mechanism changes for $E_d < \text{ca. } 0.15 \text{ V}$ with the result that the concentration of IO_3^- is zero at the electrode surface and the amount of $\text{I}_{2,\text{aq}}$ generated by homogeneous reaction in the diffusion layer is substantially decreased. Hence, the plateau current for Wave a adheres more closely to the Levich response predicted for a transport-limited process.

Of greatest interest is the mechanistic reason that the $E_{1/2}$ for Wave b is virtually the same as that for $\text{I}_{2,\text{aq}}$. It is proposed that the mechanism for direct reduction of IO_3^- in the region of Wave b requires the adsorptive association of IO_3^- with $\text{Pt}(\text{I}_{\text{ads}}^\circ)$ sites. For $E_d > 0.5 \text{ V}$, $\text{I}_{2,\text{aq}}$ is not reduced and can be adsorbed at $\text{Pt}(\text{I}_{\text{ads}}^\circ)$ sites to produce the equivalent of $\text{Pt}(\text{I}^- - \text{I}_{2,\text{ads}})$ (9). The adsorbed I_2 thereby blocks the direct reduction mechanism for IO_3^- (Equation 10).



Furthermore, the component of Wave b from reduction of $\text{I}_{2,\text{aq}}$ does not persist because $E_d > E_{1/2}$ for the $\text{I}_{2,\text{aq}}\text{-I}^-$ half reaction.

Any step-wise mechanism proposed for direct reduction of adsorbed IO_3^- is tenuous at best. However, the mechanism given by Equations 11-17 appears to be consistent with the observations presented here. Possible adsorption-desorption equilibria for the intermediate products, e.g., IO_2^- and IO^- (Equations 12-15), could explain the effect of rotation speed on Wave b (see Fig. I-4). Alternatively, the disproportionation of iodite ($3\text{IO}_2^- \longrightarrow 2\text{IO}_3^- + \text{I}^-$) could be substituted for Equations 14-17.



The dependence of Wave b on the negative scan limit (E_-)

mentioned above indicates that not all forms of I_{ads}° sites on Pt are suitable for the direct reduction of IO_3^- . The possibility that a distribution of adsorption energies for I_{ads}° exists is supported by the observation that the potential of Peak c shifted to less positive values as E_- was made more negative in the range 0.4 - 0.0 V (see Fig. I-5). It is interesting to note that a well-formed Wave b was developed only for values of E_- approaching ca. 0.05 V which corresponds to the onset of cathodic adsorption of hydrogen (H_{ads}°). Surface rearrangement of I_{ads}° is suspected to result and Johnson (9), using a ring-disk electrode, observed a portion of the I_{ads}° undergo cathodic desorption with subsequent collection of the I^- at the ring electrode during the negative scan. There was no evidence for the reverse process occurring during the following positive scan (9). It is speculated, then, that the process producing Wave b involves association of IO_3^- with both H_{ads}° and I_{ads}° on the Pt surface, perhaps as illustrated below.

It is speculated that for the positive scan, following a negative scan to $E_- < 0.0$ V, the electrode surface does not undergo change in the region $E_d = 0.0 - 0.4$ V. Hence, it is significant to note that Waves a and b are quite distinct for values of rotation speed used to obtain the data shown (see Fig. I-4). However, the values of limiting current for Waves a and b were virtually identical for Waves a and b at low rotation speeds (*i.e.*, < 400 rev min^{-1}). Because a severe negative deviation from linearity occurs for the plateau current of Wave b as a function of increasing $w^{1/2}$, it is concluded that intermediate products of the reduction reaction are soluble and, therefore, can escape the disk surface at high rotation velocities. However, the plot of i_{lim} vs. $w^{1/2}$ for Wave a was linear for all values of rotational velocity. Therefore, it is speculated that a different mechanism exists for Wave a for which the overall rate of electron transfer is sufficiently larger than for Wave b so that negligible quantities of soluble intermediate products are formed. However, the cause of the difference in mechanisms for IO_3^- reduction in the regions of Waves a and b during the negative scan is unknown at this time.

REFERENCES

1. Angerstein-Kozłowska, H.; Conway, B. E.; Sharp, W. B. A. J. Electroanal. Chem. 1973, 43, 9.
2. Austin, D. S.; Polta, J. A.; Polta, T. Z.; Tang, A. P.-C.; Cabelka, T. D.; Johnson, D. C. J. Electroanal. Chem. 1984, 168, 227.
3. Damjanovic, A.; Jovanovic, B. J. Electrochem. Soc. 1976, 123, 374.
4. Cabelka, T. D.; Austin, D. S.; Johnson, D. C. J. Electrochem. Soc. 1984, 131, 1595.
5. Austin, D. S.; Johnson, D. C.; Hines, T. G.; Berti, E. T. Anal. Chem. 1983, 155, 2222.
6. Zakharov, V. A.; Songina, O. A. Russ. J. Phys. Chem. 1964, 38, 412.
7. Lown, J. A.; Johnson, D. C. Anal. Chim. Acta 1980, 116, 41.
8. Hubbard, A. T.; Osteryoung, R. A.; Anson, F. C. Anal. Chem. 1966, 38, 692.
9. Johnson, D. C. J. Electrochem. Soc. 1972, 119, 331.
10. Zakharov, V. A.; Songina, O. A.; Kal'nitskaya, L. P. Elektrokhimiia 1971, 7, 1702.
11. Erlich, Yu. I.; Anni, K. L.; Palm, U. V. Elektrokhimiia 1978, 14, 1066.
12. Erlich Yu. I.; Anni, K. Elektrokhimiia 1979, 15, 1573.
13. Watanabe, M.; Motoo, S. J. Electroanal. Chem. 1975, 60, 267.
14. Tilak, B. V.; Conway, B. E.; Angerstein-Kozłowska, H. J. Electroanal. Chem. 1973, 48, 1.
15. Feldberg, S. W.; Enke, C. G.; Bricker, C. E. J. Electrochem. Soc. 1963, 110, 826.
16. Gossner, K.; Mizera, E. J. Electroanal. Chem. 1981, 125, 347.
17. Anson, F. C. J. Am. Chem. Soc. 1959, 81, 1554.

18. Davis, D. G. Talanta 1960, 3, 335.
19. Desideri, P. G. J. Electroanal. Chem. 1965, 9, 218.
20. Desideri, P. G. J. Electroanal. Chem. 1965, 9, 229.
21. Beran, P.; Bruckenstein, S. Anal. Chem. 1968, 40, 1044.
22. Beran, P.; Bruckenstein, S. J. Phys. Chem. 1968, 72, 3630.
23. Vallat, A.; Person, M.; Laviron, E. Electrochim. Acta 1982, 27, 657.

62a

PART II. ELECTROCATALYTIC OXIDATION OF CYANIDE

INTRODUCTION

The oxidative degradation of cyanide wastes can be important in industrial waste management and for wastewater treatment. Electrolytic methods of waste treatment can minimize the need for chemical additives and sludge disposal while offering the possibility of economic recovery of metals by simultaneous deposition at the cathode. Commonly used anodes (e.g., graphite and stainless steels) exhibit low current efficiency for CN^- oxidation and are slowly degraded during electrolysis. Electrodeposited PbO_2 has been demonstrated to be superior to graphite and stainless steels for CN^- oxidation; however, poor current efficiency was observed for dilute solutions of CN^- ($< 0.2 \text{ M}$) (1).

Lead dioxide electrodes are easily obtained by electrodeposition from solutions of lead salts (2-5) or by anodization of lead (2,3,6-8). Of the two crystallographic forms of lead dioxide, $\beta\text{-PbO}_2$ (rutile) is more common. β -Lead dioxide is deposited from Pb^{II} solutions of low pH. Anodization of lead electrodes in H_2SO_4 also yields $\beta\text{-PbO}_2$. α -Lead dioxide (orthorhombic) is deposited from neutral or alkaline solutions of Pb^{II} . Likewise, anodization of lead in alkaline media yields $\alpha\text{-PbO}_2$.

Lead dioxide is a good conductor having a resistance measured as 2×10^{-4} ohm cm (9). α -Lead dioxide is slightly more conductive than the β -form. It has been suggested that

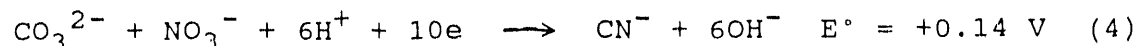
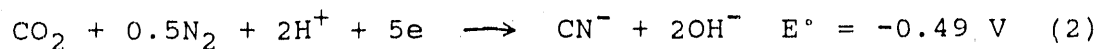
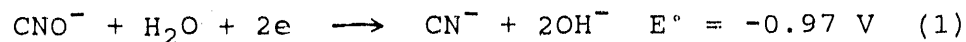
the conductivity of PbO_2 is associated with a deficiency of oxygen (10). This is supported by the observation that, in many cases, the oxygen content of α - PbO_2 is less than for β - PbO_2 . According to several workers (11,12), the stoichiometry of lead dioxide approaches $\text{PbO}_{1.98}$.

Perhaps the most important commercial use of PbO_2 is as the anode in lead-acid batteries (13). An examination of the literature reveals that PbO_2 is also widely used in electroorganic synthesis (14,15). Lead dioxide anodes have been used in preparative chemistry to produce periodic acid (HIO_4) (16) and iodoform (CHI_3) (17). Lead dioxide electrodes have been described as inert, having no specific catalytic activity (2). The presence of other metal oxides in the PbO_2 matrix has been observed to improve the reactivity and the stability of the electrode (13,18).

Recently, Johnson *et al.* (19) took advantage of this effect in order to enhance the electrocatalysis of many oxygen-transfer reactions on PbO_2 . By analogy with n-type electronic semiconductors, doping PbO_2 with Group V elements was concluded to produce an oxygen-rich mixed oxide of the general formula $\text{PbO}_2 \cdot \text{MO}_{2.5}$ (20). The rate of oxidation of Mn^{II} , phenol, hydroquinone, and several sulfur-containing organic compounds was determined to be increased at these mixed oxide electrodes (19). Although the oxidizing power of Bi^{V} and As^{V} differ substantially, the enhanced electrocatalytic activities for $\text{PbO}_2 \cdot \text{BiO}_{2.5}$ and $\text{PbO}_2 \cdot \text{AsO}_{2.5}$

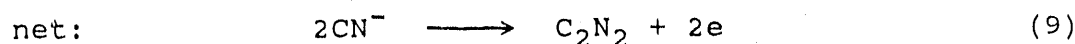
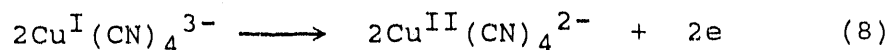
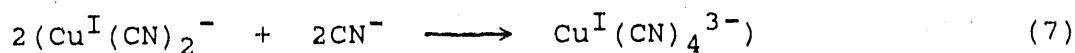
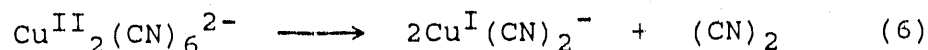
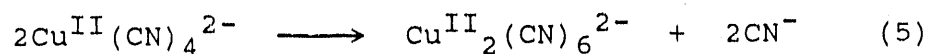
were similar. The observed $E_{1/2}$ values for Mn^{II} and As^{III} were virtually the same at $\text{PbO}_2 \cdot \text{BiO}_{2.5}$, even though the reversible potentials for $\text{As}^{\text{V}}/\text{As}^{\text{III}}$ (0.31 V) and $\text{Mn}^{\text{VII}}/\text{Mn}^{\text{II}}$ (1.51 V) are quite different. The observed $E_{1/2}$ was concluded to be characteristic of the discharge of H_2O to produce the active adsorbed oxygen at the electrode surface. Although the electrocatalytic benefit of doping PbO_2 with $\text{BiO}_{2.5}$ was concluded to be general, exceptions do exist. For example, the anodic oxidation of cyanide occurs slowly at PbO_2 electrodes, and the rate of oxidation is not increased by doping with bismuth.

A consideration of possible cyanide oxidation products in alkaline media, based on standard reduction potentials given below, indicates that cyanate (CNO^-) is thermodynamically preferred at low values of applied potential. However, oxidations to CO_2 and N_2 , as well as CO_3^{2-} and NO_3^- , are allowed at positive potential values easily achieved at common anodes in alkaline media.



The addition of small quantities of Cu^{II} to alkaline solutions was demonstrated by Katagiri *et al.* (21) to enhance the anodic oxidation of CN^- at Pt electrodes. This

observation, plus the common knowledge that Cu^{II} rapidly oxidizes CN^- to cyanogen (C_2N_2) led Katagiri *et al.* (21) to suggest the mechanism given in Equations 5-9 for the anodic response of CN^- . Accordingly, the cyclic interconversion of the $\text{Cu}^{\text{II}}\text{-Cu}^{\text{I}}$ redox couple functions for electron-transfer mediation in the oxidation reaction. This mechanism predicts no pH dependency for the half-wave potential ($E_{1/2}$) and a value of unity for n (eq mol^{-1}).



The availability of catalytically active anode materials for CN^- oxidation at transport-limited rates could have importance for fabrication of amperometric sensors (22) as well as for waste management. Whereas copper, copper oxide, and copper-modified electrodes have been studied for the oxidation of amines (23,24), amino acids (25), and carbohydrates (26), little work has been devoted to oxidation of CN^- . In this research, an improved oxide electrode is sought for the anodic oxidation of cyanide.

EXPERIMENTAL

Chemicals and apparatus

Chemicals used were reagent grade and water was deionized in a NANOpure-II system (Barnstead). A rotated disk electrode (RDE; 0.196 cm²) and a rotated Pt-Pt ring-disk electrode (RRDE; disk diameter: 0.180 inch, ring I.D.: 0.194 inch, ring O.D.: 0.212 inch) were obtained from Pine Instrument Co. An MSRX speed controller and RDE4 potentiostat (Pine) were under the control of a STANDARD 286/10 microcomputer. A DT2801/5716A input/output board and accompanying software (Data Translation) were used in data acquisition. Current-potential (i-E) curves were recorded on a Model 7035B X-Y recorder (Hewlett Packard). Electrode potentials were controlled and are reported in volts (V) vs. a saturated calomel electrode (SCE; Fisher Scientific). Micrographs were obtained using a JSM-840A scanning electron microscope (JEOL). X-ray diffraction was performed on a model D-500 diffractometer (Siemens). Elemental analysis was performed using a Model 5000 atomic absorption spectrometer (Perkin-Elmer) with a HGA-5000 graphite furnace.

Procedures

β-Lead dioxide A solution containing 10mM Pb^{II} and 0.1 M HClO₄ was used for electrodeposition of β-PbO₂ films on rotated disk electrodes (RDE). Electrodeposition was

performed under conditions of constant anodic current (5.0 mA cm⁻²) for 5.0 min. Electrode rotation speed during deposition was 1000 rev min⁻¹.

Bi-doped PbO₂ Solutions used for the electrodeposition of Bi-doped PbO₂ films contained 0.1 M HClO₄, 1.0 mM Pb^{II} and the indicated quantity of Bi^{III}. For example, an electrode designated "30 mole %" would have been prepared from a 0.1 M HClO₄ solution containing 1.0 mM Pb^{II} and 0.3 mM Bi^{III}. Electrodeposition was performed at 1.6 mA cm⁻² for 15 min. Electrodes were rotated at 1000 rev min⁻¹ during deposition.

alpha-Lead dioxide A stock solution of Pb^{II} was prepared by equilibrating 2.0 M NaOH with solid PbO. Ten ml of this stock solution was diluted with 0.1 M NaClO₄ to 100 ml for deposition. Electrodeposition was performed at a constant potential of 0.65 V for 5 min after scanning the potential from 0.0 V to 0.60 V at 1.8 V min⁻¹. Electrodes were rotated at 400 rev min⁻¹.

Cu-doped PbO₂ The procedure for the preparation of Cu-doped PbO₂ films was identical to the procedure for a-PbO₂ films with the exception that the stock solution contained solid CuO, as well as PbO.

Lead dioxide films were removed from substrates by immersion in a cleaning solution containing equal volumes of H₂O₂ (30%) and glacial acetic acid. Following removal of the films, the electrodes were rinsed with deionized water.

New films could be deposited without further treatment of the substrate.

The voltammetric behavior of these films was observed to be affected by deviation from the above deposition procedures.

Copper oxide electrodes A 0.10 M stock solution of $\text{Na}_3\text{Cu}(\text{CN})_4$ was prepared by mixing one part CuCN with three parts NaCN in water which had been previously purged with N_2 to prevent oxidation of Cu^{I} by dissolved O_2 . Unless stated to the contrary, electrodeposition of copper oxide films was achieved at the rotated disk electrode (RDE) using a constant anodic current of 5.0 mA cm^{-2} applied for 20 min in an alkaline solution (pH 12) containing $3.0 \text{ mM Na}_3\text{Cu}(\text{CN})_4$. Alternately, $\text{Na}_3\text{Cu}(\text{CN})_4$ was substituted by a 1:4 mixture of a Cu^{II} salt (CuSO_4) and excess NaCN . The concentration of $\text{Na}_3\text{Cu}(\text{CN})_4$ was not critical for satisfactory film deposition. Use of excessively high CN^- concentration (i.e., $\text{CN}^-/\text{Cu}^{\text{I}} > \text{ca. } 8:1$) and high alkalinity (e.g., 1 M NaOH) inhibited film formation. Prior to deposition, disk electrodes were rinsed in $1 \text{ M H}_2\text{SO}_4$ and deionized water. Electrode rotation speed during deposition was 100 rev min^{-1} . Speeds above 200 rev min^{-1} resulted in the deposition of copper oxide around the edge of the disk substrate, leaving the center of the disk bare. The diameter of the bare spot was observed to increase as rotation speed was increased.

The films were not strongly adherent to the Pt/SS

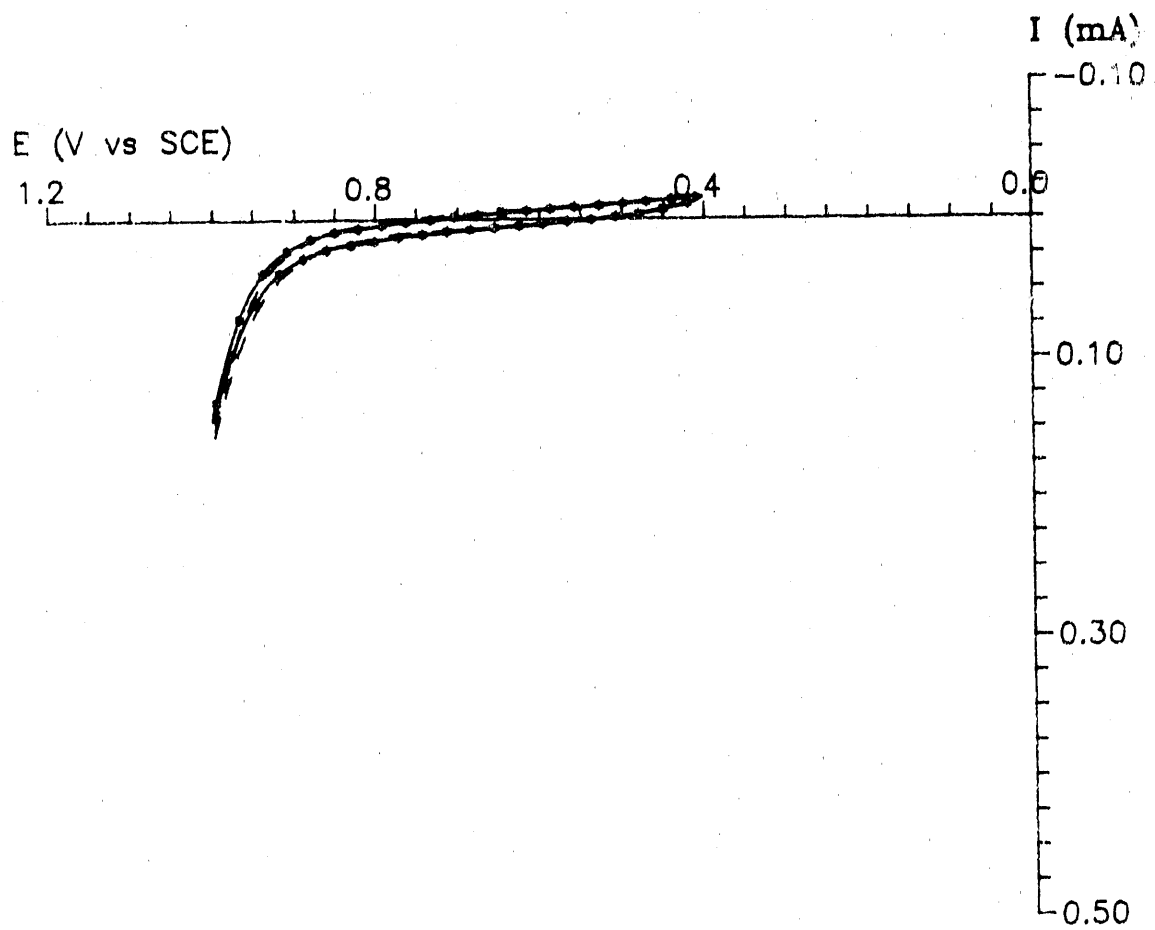
substrate. The use of Cu^{II} (ethylenediamine) $_2$ also produced a film (27), but without a distinct electrocatalytic advantage. Use of other ligands (NH_3 , EDTA) was not successful in producing films. Platinum interlayers were prepared by vapor deposition and electrodeposition. Voltammetric results were independent of the interlayer thickness and were virtually the same as for thick Pt substrates. Prior to use, freshly deposited copper oxide films were preconditioned in the electrolyte solution by potential cycles (1.0 V min^{-1}) between the values 0.0 V and 0.75 V vs. SCE for 10 min.

Minimum values of the thickness of copper oxide films were estimated from deposition current, deposition time, electrode area, the density of CuO (6.3 g cm^{-3}), and the mass-to-charge ratio for the deposition (0.10 mg C^{-1}) obtained with an electrochemical quartz crystal microbalance (EQCM). For a 20-min deposition at 5.0 mA , the calculated thickness was $5 \text{ }\mu\text{m}$. The films were believed to be porous and, hence, the actual film thickness undoubtedly was greater than this minimal value. All values of thickness given here are the minimal calculated values because the extent of porosity was not known. All experiments were performed at ambient laboratory temperature ($26\text{-}28 \text{ }^\circ\text{C}$).

RESULTS AND DISCUSSION

Doped PbO₂ electrodes

Voltammetric response The voltammetric response of CN⁻ at a β-PbO₂ electrode is shown in Figure II-1 for three values of the bulk concentration of CN⁻ (C_{CN}^b). Oxygen evolution commenced at ca. 0.90 V. It can be seen from Figure II-1 that the electrode response was virtually independent of C_{CN}^b . The voltammetric response of CN⁻ at a 30 mole% Bi-doped PbO₂ electrode is shown in Figure II-2 for three values of C_{CN}^b . The large cathodic and anodic peaks observed in the region 0.4 V < E < 0.7 V were concluded to result from redox processes of Bi ions in the PbO₂ matrix. This conclusion is supported by the observation that peak heights were affected by bismuth doping levels. A slight increase in the anodic response was observed in the region of oxygen evolution (E > 0.75 V) as C_{CN}^b increased. The voltammetric response of CN⁻ at an α-PbO₂ electrode is shown in Figure II-3 for three values of C_{CN}^b . The anodic and cathodic charging currents were noticeably larger than for β-PbO₂ (Figure II-1). This is likely to be the result of a more porous film. A small, anodic current was observed in the presence of cyanide, but this current was independent of rotation speed. These results indicate the occurrence of slow oxidation of cyanide controlled by electron-transfer kinetics. The voltammetric response of CN⁻ at a Cu-doped

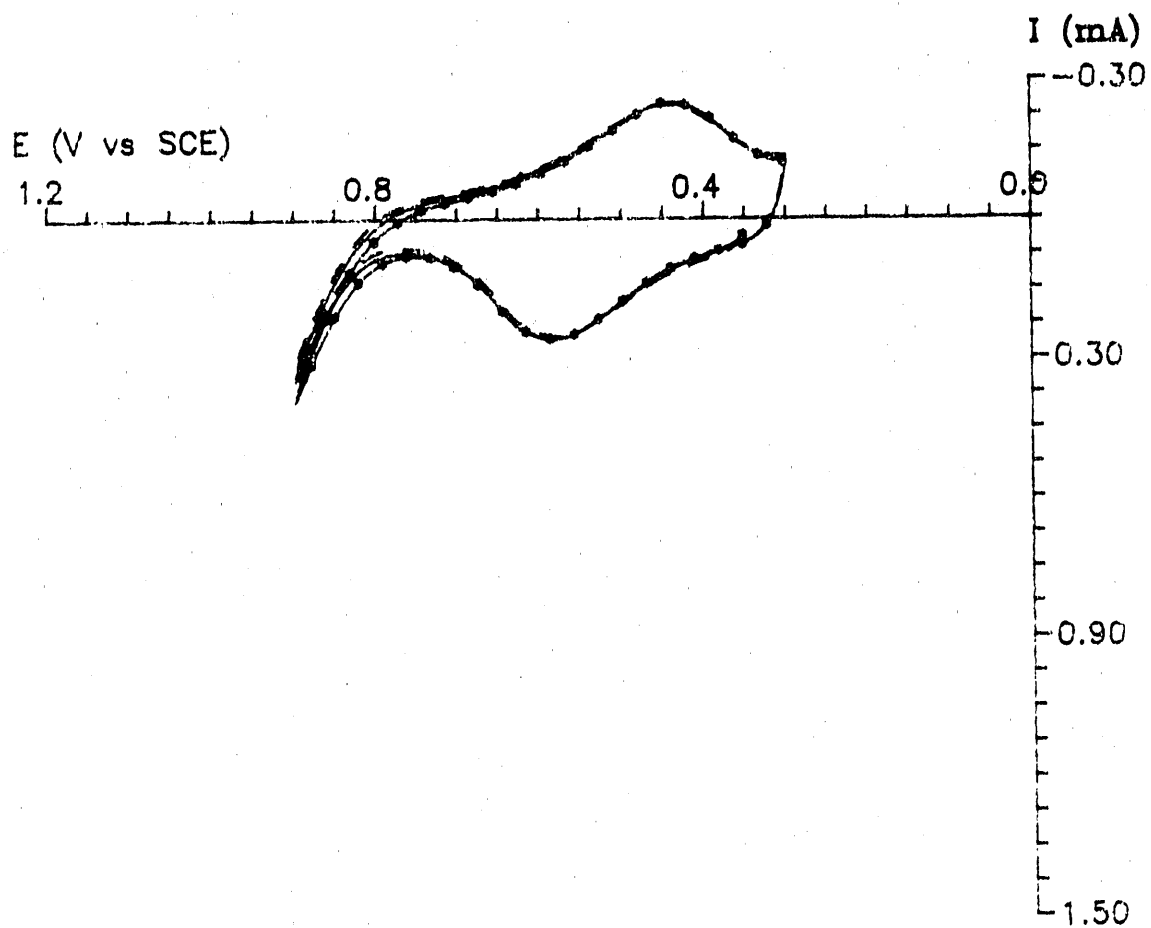


Scan rate = 3.0 V min^{-1}

Rotation speed = $1000 \text{ rev min}^{-1}$

NaCN concentration (mM): (---) 0.0,
(—) 1.0,
(-*-) 5.0.

Figure II-1. Current-potential curves for CN^- at a $\beta\text{-PbO}_2$ RDE in 0.1 M NaClO_4 , 10 mM NaOH

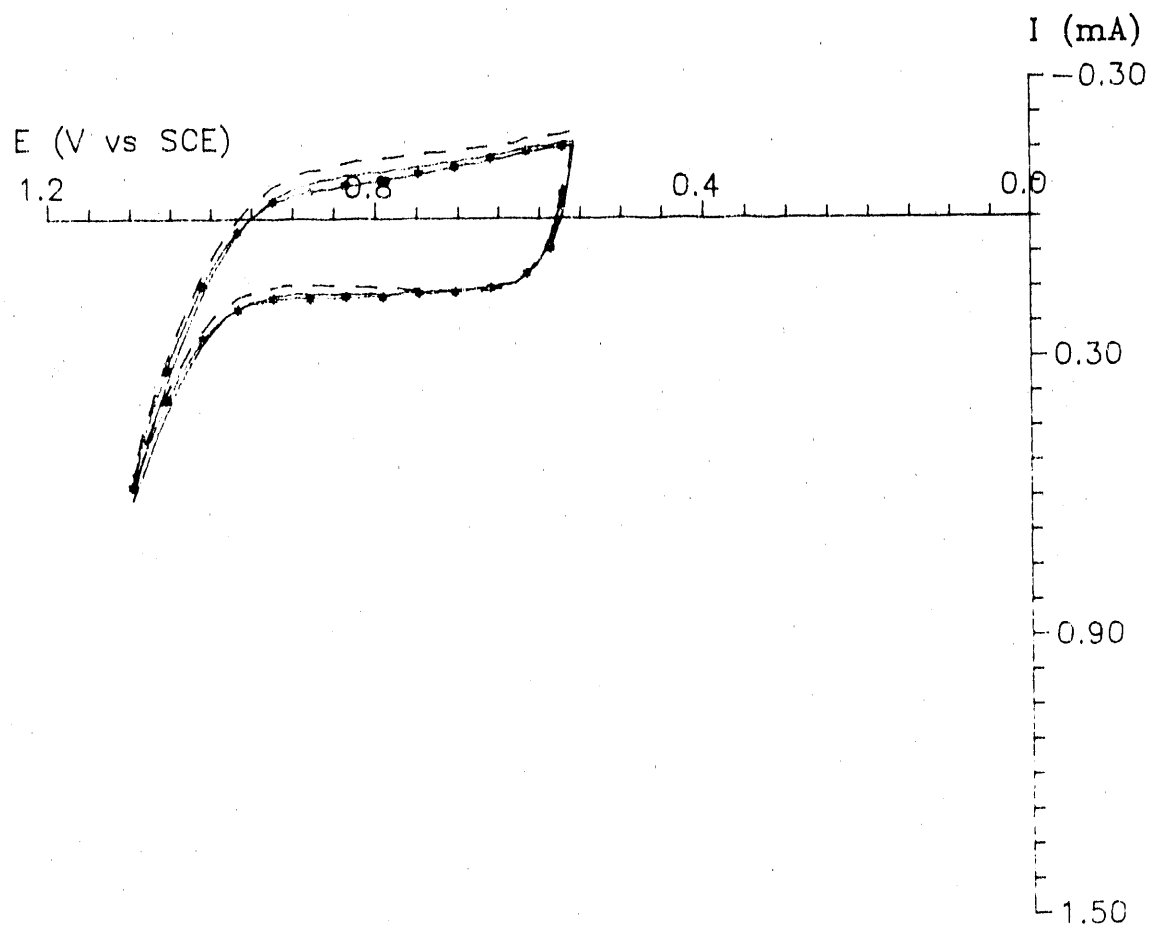


Scan rate = 3.0 V min^{-1}

Rotation speed = $1000 \text{ rev min}^{-1}$

NaCN concentration (mM): (---) 0.0,
 (—) 1.0,
 (-*-) 5.0.

Figure II-2. Current-potential curves for CN^- at a Bi-doped (30 mole % Bi) PbO_2 RDE in 0.1 M NaClO_4 , 10mM NaOH



Scan rate = 3.0 V min^{-1}

Rotation speed = $1000 \text{ rev min}^{-1}$

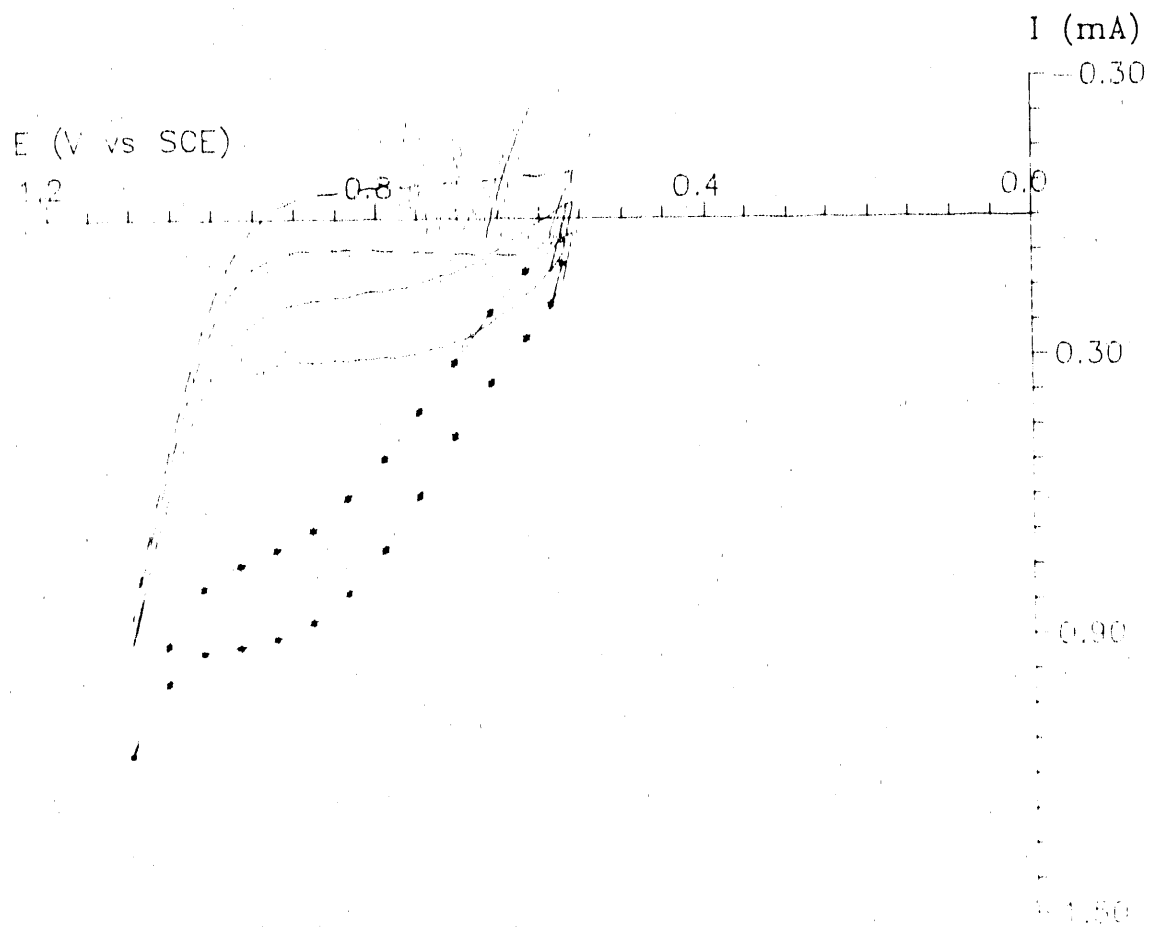
NaCN concentration (mM): (---) 0.0,
 (—) 1.0,
 (-*-) 5.0.

Figure II-3. Current-potential curves for CN^- at an $\alpha\text{-PbO}_2$ RDE in 0.1 M NaClO_4 , 10 mM NaOH

PbO₂ electrode is shown in Figure II-4 for three values of $C_{CN^-}^b$. A well-defined anodic wave was observed in the presence of CN⁻ at $E > 0.55$ V. The plateau current was a function of $C_{CN^-}^b$. The half-wave potential ($E_{1/2}$) was observed to shift more positive at higher values of $C_{CN^-}^b$. This positive shift of $E_{1/2}$ indicates that the electrode process is occurring under mixed control by electron-transfer and mass-transport kinetics.

Film characterization The mole ratio of Cu:Pb in the Cu-doped PbO₂ films was determined to be 8×10^{-3} by elemental analysis.

The X-ray diffraction data shown in Figure II-5 were obtained from a Cu-doped PbO₂ film deposited on a stainless steel RDE. The film was identified as α -PbO₂ by comparison to a PbO₂ standard (JCPDS #11-0549). Spectral lines from the steel substrate were also identified (JCPDS #33-0397). The extremely small quantity of Cu in the film resulted in only weak spectral lines in Figure II-5 which could be associated with CuO. Nevertheless, a computerized library search identified CuO (JCPDS #5-0661) based on residual intensities in the spectrum. The existence of CuO crystallites is indicated by these data rather than a mixed oxide of specific stoichiometry. The sharpness of the spectral lines suggests large crystallite size in the film. Increasing the concentration of Cu^{II} in the deposition solution resulted in broadening of the spectral lines. No



Scan rate = 3.0 V min^{-1}

Rotation speed = $1000 \text{ rev min}^{-1}$

NaCN concentration (mM): (---) 0.0,
 (—) 1.0,
 (-*-) 5.0.

Figure II-4. Current-potential curves for CN^- at a Cu-doped PbO_2 RDE in 0.1 M NaClO_4 , 10 mM NaOH .

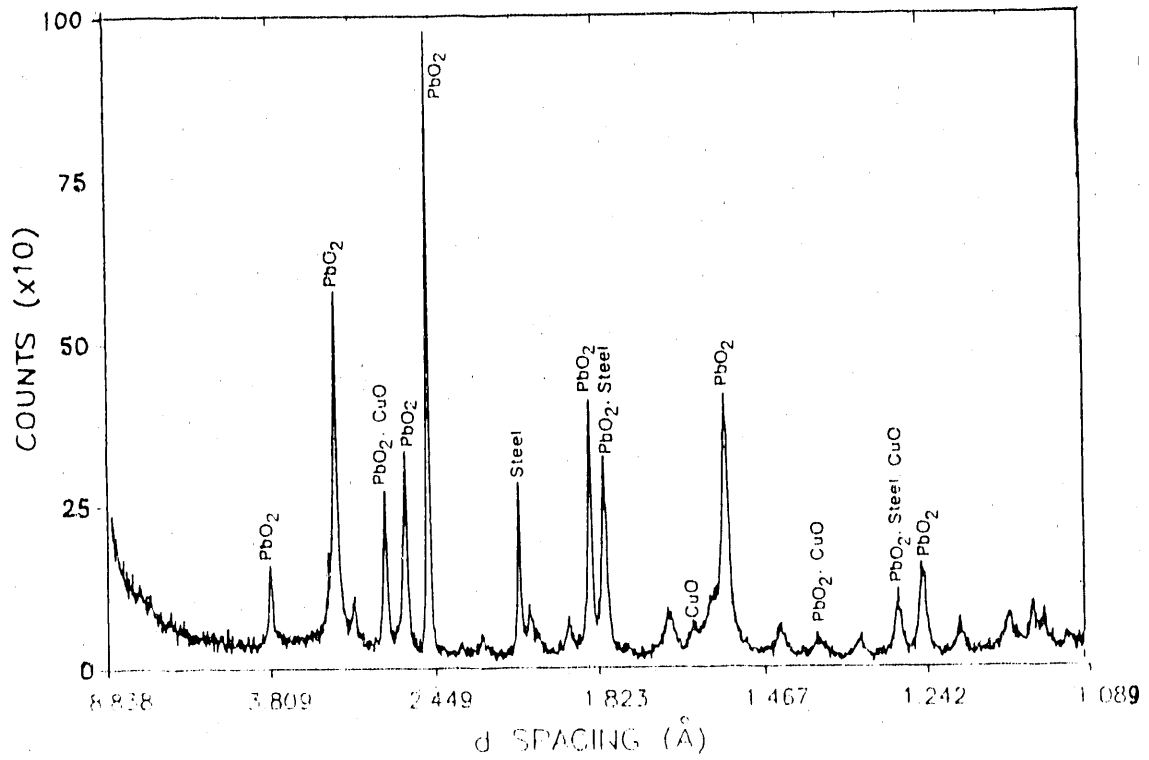


Figure II-5. X-ray diffraction spectra of Cu-doped PbO₂

increase in the CuO content of the film was indicated.

The response of CN^- at Cu-doped PbO_2 electrodes shown in Figure II-4 was observed to decrease with subsequent scans. A likely explanation for this decrease in signal is that the CuO crystallites are slowly dissolved by CN^- . In order to obtain a response of longer duration for scientific study, a higher concentration of CuO in the electrode would be required. For this reason, CuO-film electrodes were prepared.

Copper oxide electrodes

Film characterization A scanning electron micrograph is shown in Figure II-6A for a copper oxide film deposited on a thin (ca. 1 μm) Pt interlayer at a stainless steel (SS) substrate. The film was prepared with a constant anodic current of 4 mA cm^{-2} applied for 80 min with a rotation speed of 200 rev min^{-1} in 0.10 M Na_2SO_4 containing 0.010 M NaOH and 4 mM $\text{Na}_3\text{Cu}(\text{CN})_4$. This film had a fine-grain appearance with cracks that, presumably, were formed during the air-drying process. Figure II-6B shows the micrograph of a film deposited at 1000 rev min^{-1} using multiple cyclic potential scans (5 V min^{-1}) for 20 min within the potential limits 0.1 V and 0.8 V in 0.10 M Na_2SO_4 containing 0.01 M NaOH and 2 mM $\text{Na}_3\text{Cu}(\text{CN})_4$. This micrograph clearly shows a surface composed of closely packed spheres. The films appeared to be porous.

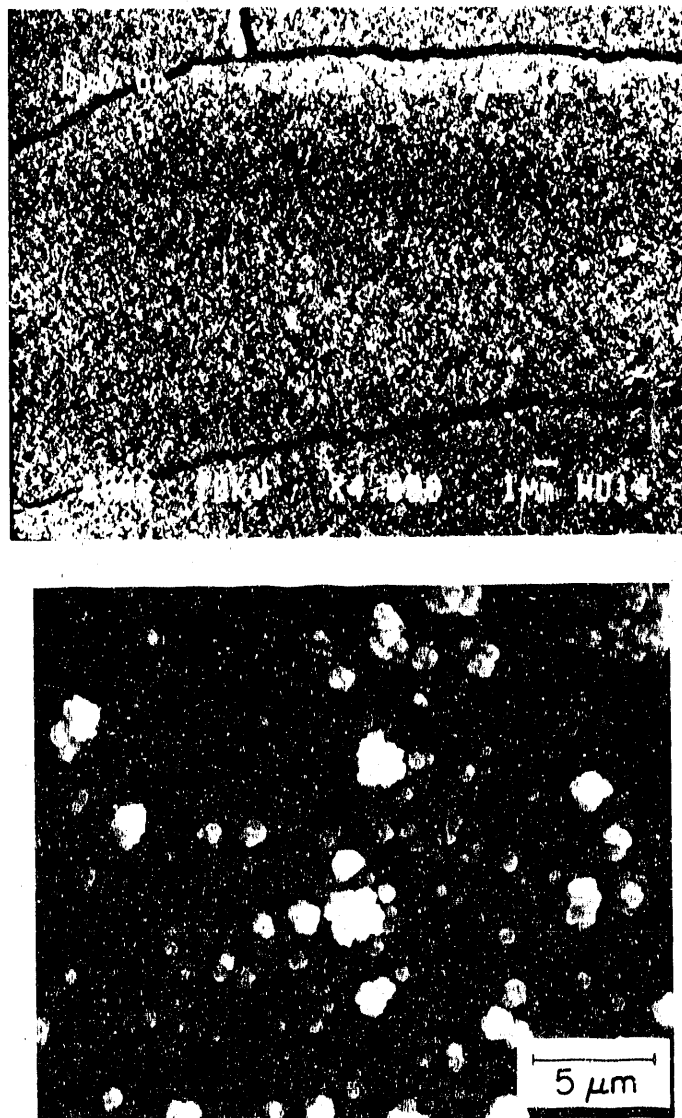


Figure II-6. Scanning electron micrographs of copper oxide films

- (A) Stainless steel substrate with Pt interlayer. Constant current deposition (4 mA cm^{-1}) for 80 min from $4 \text{ mM Na}_3\text{Cu}(\text{CN})_4$ at 200 rev min^{-1} .
- (B) Stainless steel substrate without Pt interlayer. Controlled potential deposition with cyclic scan (0.1 to 0.8 V ; 5 V min^{-1}) for 20 min from $2 \text{ mM Na}_3\text{Cu}(\text{CN})_4$ at $1000 \text{ rev min}^{-1}$.

The deposited films were identified as copper(II) oxide (CuO) on the basis of X-ray diffraction data shown in Figure II-7 and compared to a CuO standard (JCPDS #5-0661). Because of the thinness of both the CuO film (ca. 5 μm) and Pt interlayer (ca. 1 μm), the diffraction pattern was dominated by strong reflections from the SS substrate (Fe, Cr, Ni). Peaks A-C were not present in the diffraction pattern of the substrate with the interlayer and were, therefore, concluded to be representative of the copper oxide film. Peaks A and B correspond to the (-1,1,1) plane and the (1,1,1) plane of CuO, respectively. Peak C was tentatively concluded to correspond to the (-1,1,3) plane of CuO.

Voltammetric response of cyanide The voltammetric response of CN^- at a thin (5 μm) CuO-film electrode is shown in Figure II-8 for four values of the bulk concentration of CN^- ($C_{\text{CN}^-}^b$). Oxidation of CN^- occurred for $E > \text{ca. } 0.25 \text{ V}$ with a half-wave potential ($E_{1/2}$) of 0.35 V for 1.0 mM CN^- and a current plateau in the region 0.45 V to 0.65 V. The $E_{1/2}$ value increased slightly as $C_{\text{CN}^-}^b$ was increased (ca. +30 mV mM^{-1}). A current maximum was obtained near the onset of the current plateau during the positive scan for 1.0 mM NaCN (Fig. II-8, Curve b), but decreased in prominence at higher concentrations. The current at 0.6 V was a linear function of $C_{\text{CN}^-}^b$ to ca. 5 mM; plots are shown in Figure II-9 for $C_{\text{CN}^-}^b$ to 1 mM at three rotation speeds.

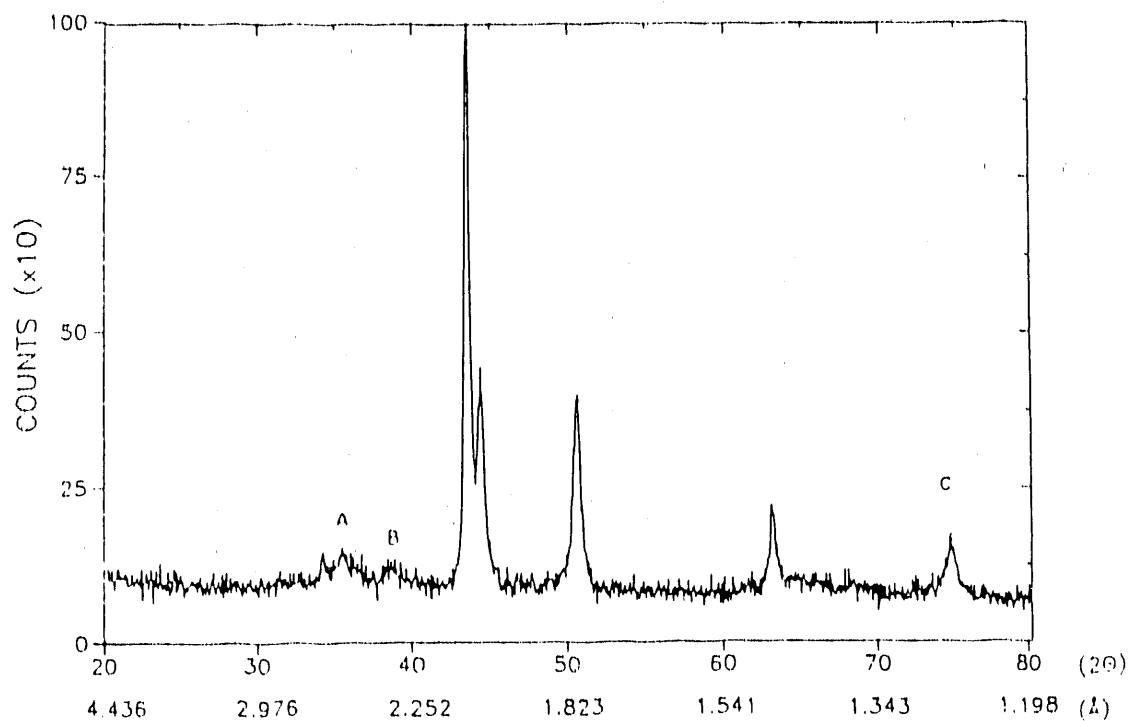
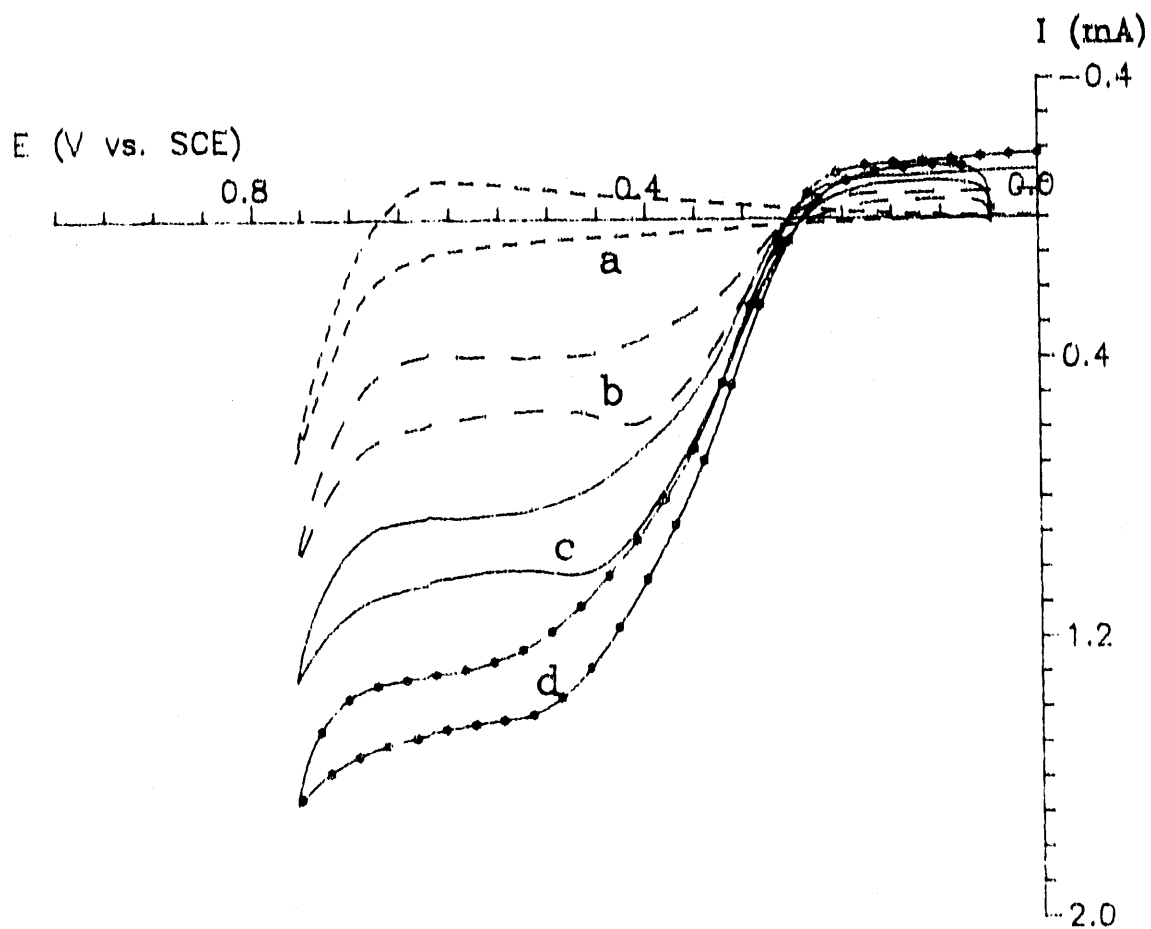


Figure II-7. X-ray diffraction spectra of copper oxide films from Figure II-6A

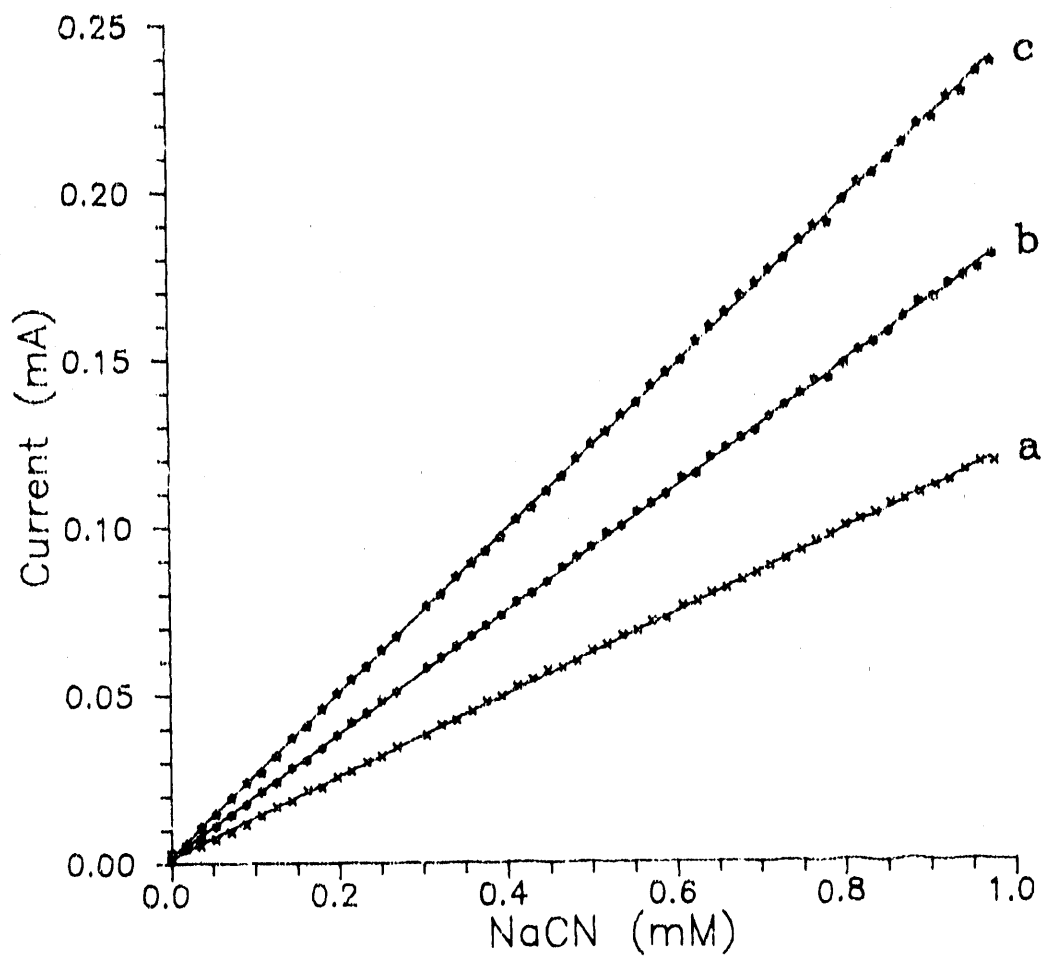
Diffraction peaks (Å): (A) 2.51, (B) 2.32,
(C) 1.47.



Conditions: $1600 \text{ rev min}^{-1}$ rotation speed,
 1.0 V min^{-1} scan rate.

C_{NaCN}^b (mM): (a) 0, (b) 1.0, (c) 2.0, (d) 3.0.

Figure II-8. Voltammetric response of NaCN at a rotated, CuO-film, disk electrode as a function of concentration in $0.10 \text{ M Na}_2\text{SO}_4$ with 0.010 M NaOH



Conditions: +0.60 V vs. SCE applied potential.

Rotation speed (rev min⁻¹): (a) 100, (b) 225,
(c) 400.

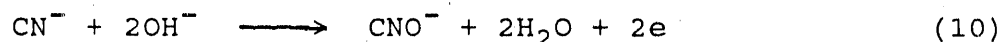
Figure II-9. Amperometric response for NaCN at a rotated, CuO-film, disk electrode as a function of concentration in 0.10 M Na₂SO₄ with 0.010 M NaOH

A soluble, electroactive product of the disk reaction at $E_{\text{disk}} > \text{ca. } 0.65 \text{ V}$ was detected using the Pt-Pt RRDE with a CuO-plated disk. The voltammetric response of the product detected at the ring was identical to that of dissolved O_2 .

A study was made of the origin of the small anodic current maximum at ca. 0.35 V (see Fig. II-8, Curve b). The peak current (i_p), measured with respect to the plateau current, increased for larger values of potential scan rate (ϕ). This is indicative of a surface-controlled faradaic process tentatively concluded to be the oxidation of CN^- that was weakly adsorbed on the CuO surface. For increasing values of $C_{\text{CN}^-}^b$ above 1.0 mM , the maximum was not evident because the $E_{1/2}$ of the wave was shifted to more positive values with the result that the current maximum from oxidation of adsorbed CN^- contributed to the rising portion of the wave (Fig. II-8, Curve d). Increased rotation speeds above $1600 \text{ rev min}^{-1}$ also caused the $E_{1/2}$ to shift slightly more positive and the current maximum was not evident. The positive shift of $E_{1/2}$ for increased values of $C_{\text{CN}^-}^b$ and rotation speed is diagnostic evidence for a faradaic process under mixed control by electron-transfer and mass-transport kinetics.

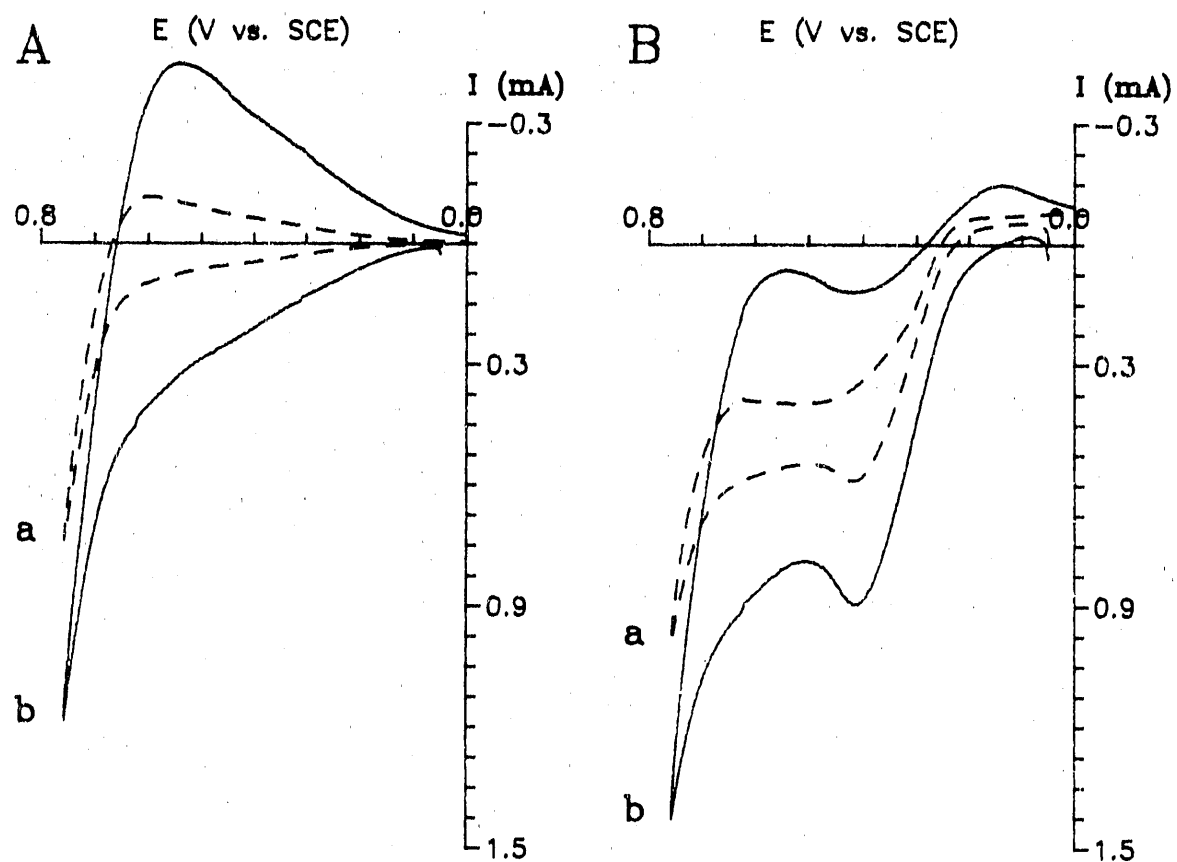
Reaction stoichiometry Exhaustive electrolyses were performed in a stirred solution of $0.10 \text{ M Na}_2\text{SO}_4$ containing 0.010 M NaOH (pH 12) for a constant potential of 0.60 V at a CuO-film deposited on a Pt-gauze electrode. The

concentration of CN^- was 2.5 mM and electrolyses were completed in ca. 15 min. The background charge determined in the absence of CN^- was subtracted from the total current in the presence of CN^- to give the net charge for CN^- oxidation. From data for nine consecutive electrolyses, the value of n for the reaction was calculated to be 1.9 ± 0.1 eq mol^{-1} (90% confidence interval). This value is consistent with production of CNO^- according to Equation 10.



Residual response The voltammetric curves in Figure II-8 revealed a rather large hysteresis between the anodic and cathodic currents obtained for the positive and negative scans, respectively, with a maximum hysteresis at ca. 0.6 V. Since the CuO films were suspected as being very porous, double-layer charging was expected to contribute to the hysteresis. Charging currents are proportional to the true surface area, rather than the geometric area, and it was expected that the hysteresis would be significantly larger for a thicker CuO -film electrode.

The residual voltammetric response is shown in Figure II-10A for two films having significantly different thicknesses. The film thicknesses were estimated on the basis of the applied current (5.0 mA cm^{-2}) and deposition times of 5 min and 20 min to be ca. 1.2 μm (Curve a) and 5 μm (Curve b), respectively. As predicted, hysteresis in the



Conditions: $1600 \text{ rev min}^{-1}$ rotation speed,
 1.0 V min^{-1} scan rate.

Minimum estimated
 film thickness (μm): (a) 1.2, (b) 5.

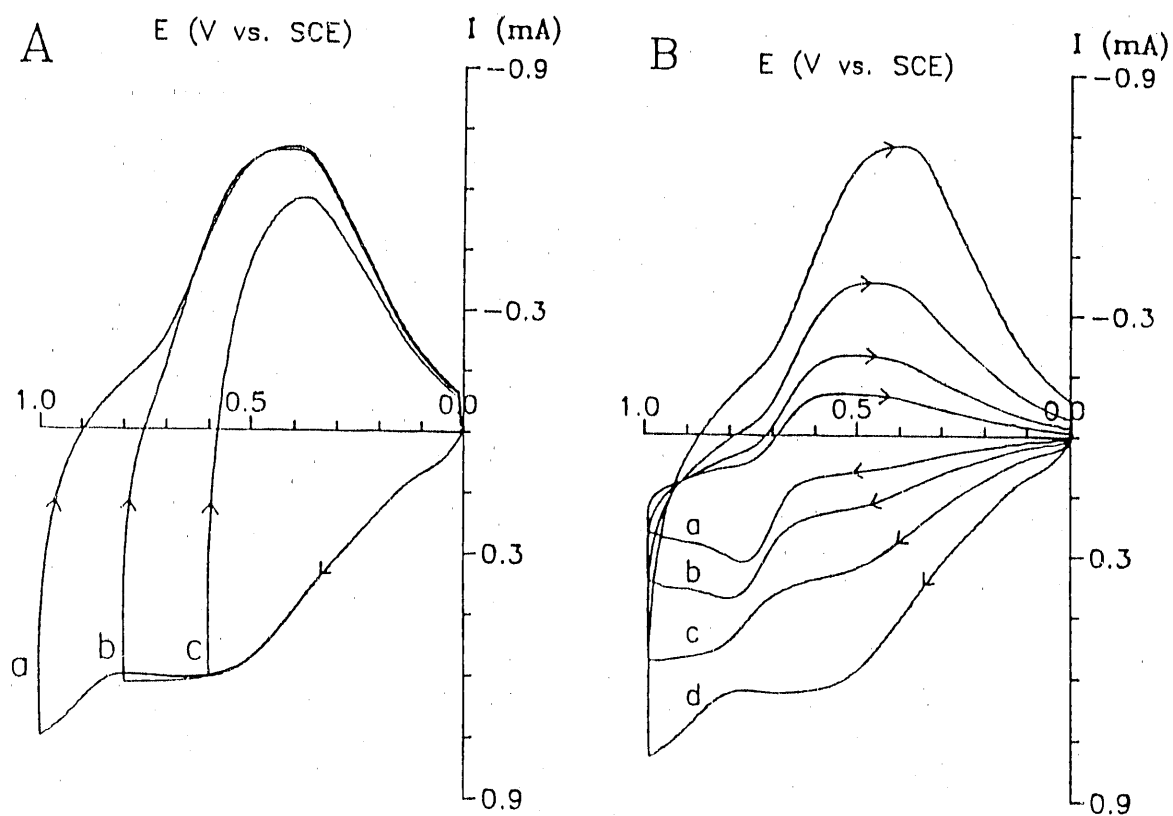
Figure II-10. Voltammetric response of a rotated, CuO-film, disk electrode as a function of film thickness in $0.10 \text{ M Na}_2\text{SO}_4$ with 0.010 M NaOH

- (A) Residual response.
 (B) Response for 1.0 mM NaCN .

residual curve was significantly greater for the thicker film (Curve b). The effect of CuO-film thickness on the i-E response of CN^- is illustrated in Figure II-10B for the two films that produced the data in Figure II-10A. Again, hysteresis was greatest for the thickest film (Curve b).

Figure II-11A contains residual i-E curves obtained as a function of variations in the positive scan limit. As the limit increased from ca. 0.6 V to 0.8 V, the cathodic charge increased dramatically for the subsequent negative scan. We attribute the increase in cathodic charge to the reduction of a product of an anodic reaction occurring at $E > \text{ca. } 0.5 \text{ V}$. We tentatively conclude the oxidation product to be a Cu^{III} -oxide, perhaps CuO(OH) . The anodic evolution of O_2 was concluded above to occur for $E > \text{ca. } 0.7 \text{ V}$ and the increase of positive scan limit from 0.8 V to 1.0 V produced a relatively small increase in the subsequent cathodic charge (Fig. II-11A). From the cathodic charge for a scan limit of 0.8 V, the quantity of CuO(OH) formed was estimated to be ca. 60 μmol . This corresponds to an anodic conversion of less than 1% of the original CuO film. Considering the probability that double-layer charging contributes to the total charge observed, the percent of the film converted is even less than this estimate. We suspect that only the surface layer of CuO contacting the electrolyte solution is converted to CuO(OH) during the positive scan.

Figure II-11B contains residual i-E curves as a



Conditions: 1600 rev min⁻¹ rotation speed.

Figure II-11. Residual voltammetric response of a rotated, CuO-film, disk electrode in 0.10 M Na₂SO₄ with 0.010 M NaOH

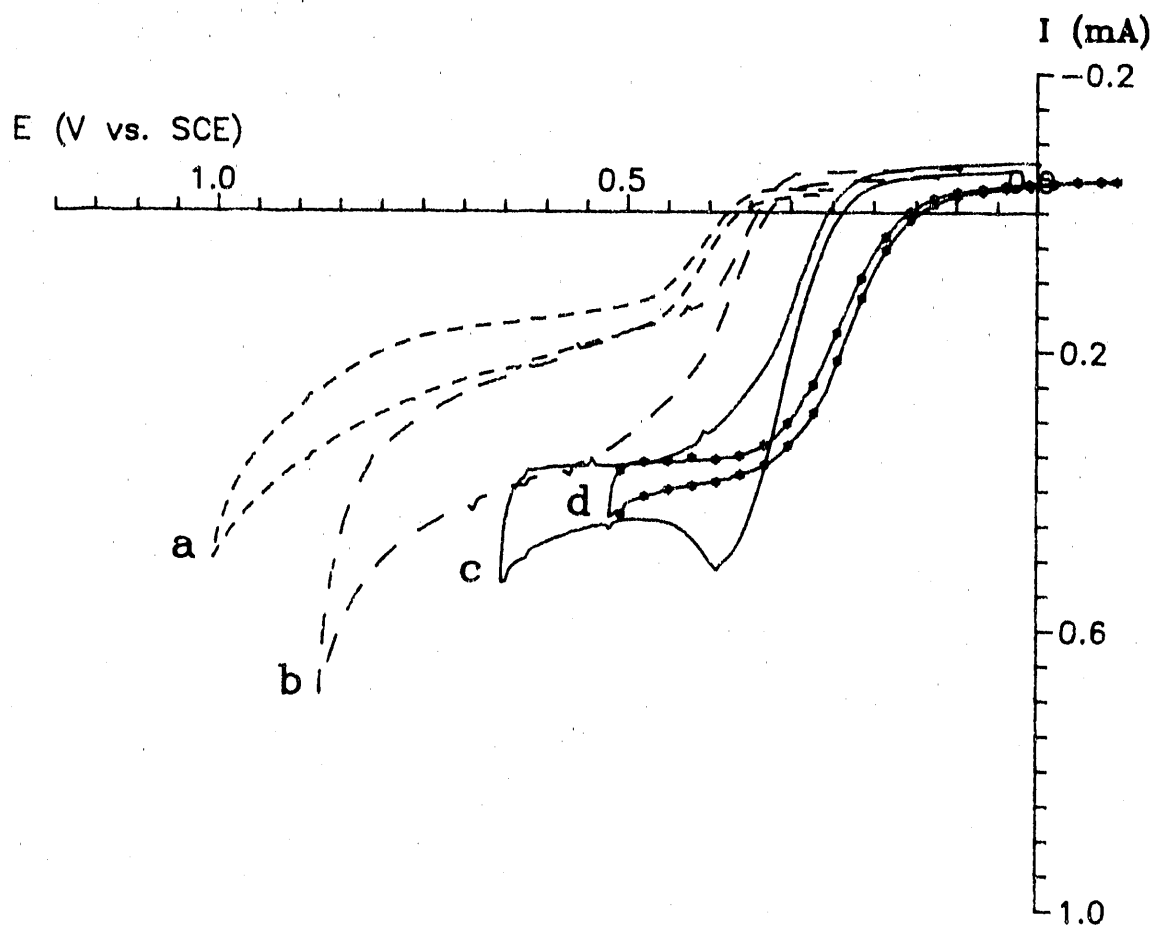
(A) Variation of positive scan limit.
 Scan rate (V min⁻¹): 4.0.
 Scan limit (V vs. SCE): (a) 0.60,
 (b) 0.80,
 (c) 1.00.

(B) Variation of potential scan rate.
 Scan rate (V min⁻¹): (a) 0.5, (b) 1.0,
 (c) 2.0, (d) 4.0.

function of scan rate (ϕ) for a constant positive scan limit. The potential for the cathodic peak current shifted slightly to more negative values as ϕ was increased. This is evidence of a slow faradaic process and is consistent with the estimation that a product of the anodic reaction during the positive scan was subsequently reduced during the subsequent negative scan.

pH effects The i - E curves shown in Figure II-12 were obtained with identically prepared CuO films (5 μm) as a function of pH. The ionic strength of the test solutions was maintained at 1.0 M using Na_2SO_4 . Because of the similarity of film thickness used to obtain the curves, the differences observed in the i - E curves are attributed to pH effects. The $E_{1/2}$ value of the CN^- wave shifted to more negative values as pH was increased (ca. -40 mV pH^{-1}), indicating involvement of OH^- in the reaction mechanism. The apparent reversibility of the anodic waves was a maximum at pH 12, as estimated from the slope of the i - E curve at $E_{1/2}$. The anodic current plateau also had a maximum value at pH 12.

The current maximum at ca. 0.35 V on the positive scan was observed only at pH 12 (Fig. II-12, Curve c); however, this maximum was not observed for a 0.1 M phosphate buffer at pH 12. It is apparent that the extent of adsorption of CN^- , believed to be the source of the maximum, is a sensitive function of pH as well as other anionic components



Conditions: $1600 \text{ rev min}^{-1}$ rotation speed,
 1.0 V min^{-1} scan rate.

Electrolytes: (a) 0.10 M borate with 0.30 M
 Na_2SO_4 (pH 8.0);
 (b) 0.10 M borate with 0.30 M
 Na_2SO_4 (pH 10.0);
 (c) 0.33 M Na_2SO_4 with 0.010 M
 NaOH (pH 12.0);
 (d) 1.0 M NaOH (pH 14).

Figure II-12. Effect of pH on the voltammetric response for 1.0 mM NaCN at a rotated, CuO-film electrode at constant ionic strength

in the solution which can compete for adsorption sites. The hysteresis between the i - E curves for the positive and negative scans was at a maximum for pH 10, indicating a strong pH effect on double-layer properties which contributed to the hysteresis. The addition of phosphate also decreased the hysteresis.

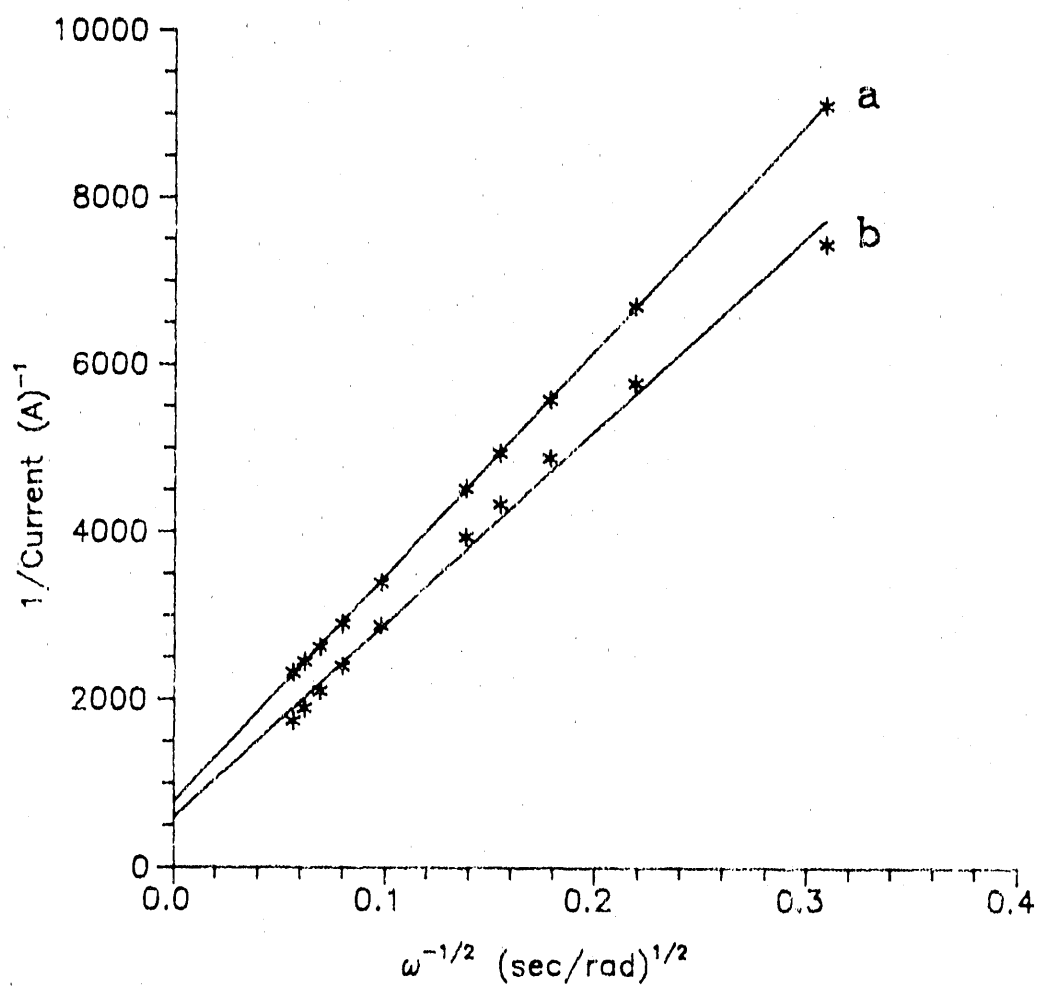
Heterogeneous rate constant The apparent heterogeneous rate constant (k_{app}) for the anodic reaction of CN^- was estimated on the basis of so-called Koutecky-Levich plots (28) of $1/i$ vs. $\nu^{-1/2}$, as illustrated in Figure II-13 for data obtained at constant potential values of 0.35 V (Curve a) and 0.60 V (Curve b). The slope and intercept of these plots are predicted by Equations 11 and 12, where F , A , and D have their usual electrochemical significance, ν is kinematic viscosity of the solution ($0.010 \text{ cm}^2 \text{ sec}^{-1}$), and $n = 2 \text{ eq mol}^{-1}$.

$$\text{slope} = (0.62nFAD^{2/3}\nu^{-1/6}C^b)^{-1} \quad (11)$$

$$\text{intercept} = (nFAk_{app}C^b)^{-1} \quad (12)$$

The potential-independent rate constant (k_0) was assumed to be related to k_{app} by Equation 13, where a_a is the asymmetry constant for the 2-electron process. The a_a term was eliminated by use of k_{app} values measured at the two potentials (0.35 V and 0.60 V). The k_0 values are given in Table II-1 for 1.0 mM NaCN vs. pH.

$$k_{app} = k_0 \exp\{(a_a/0.059)(E-E^{\circ'})\} \quad (13)$$



Potential (V vs. SCE): (a) +0.35, (b) +0.60.

Figure II-13. Koutecky-Levich plot for 1.0 mM NaCN at a rotated, CuO-film, disk electrode in 0.10 M Na₂SO₄ with 0.010 M NaOH

The maximum value of k_0 , $8.0 \times 10^{-3} \text{ cm s}^{-1}$, was obtained at pH 12 with Na_2SO_4 present to maintain constant ionic strength. This value for CN^- oxidation at the catalytic CuO electrode is ca. 4×10^5 times larger than the value of 2.1×10^{-8} reported by Sawyer and Day (29) for a Pt electrode. The value of k_0 at pH 12 was determined to be depressed significantly by addition of phosphate (see Table II-1). This is concluded to result from changes in double-layer structure resulting from adsorption of phosphate anions and competition by phosphate for adsorption sites needed by CN^- in the catalytic oxidation. The presence of carbonate also slightly decreased k_0 (see Table II-1).

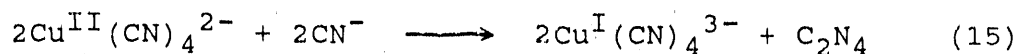
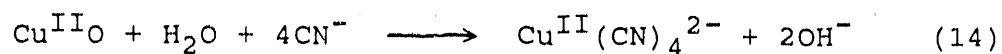
The large value of k_0 obtained for pH 12 corresponds nearly to a reaction rate controlled by convective-diffusional mass transport. Accordingly, a Levich plot of i_{lim} vs. $1/2$ was nearly linear for small values of rotation speed. The value of D was calculated from the slope to be $1.4 \times 10^{-5} \text{ cm}^2 \text{ sec}^{-1}$.

Film stability The CuO-film electrodes (ca. 5 μm) were observed to dissolve slowly over a period of ca. 30 min during voltammetric experiments in the presence of high concentrations of CN^- (i.e., $\gg 1 \text{ mM}$). The rate of dissolution increased as values of $C_{\text{CN}^-}^b$ and rotation speed were increased. The dissolution is suspected to occur by Equations 14 and 15.

Table II-1. Kinetic data for oxidation of 1.0 mM NaCN at the rotated, CuO-film, disk electrode

pH ^a	electrolyte	k_0 (cm s ⁻¹)
8.0	0.1 M borate	1.4×10^{-6}
10.0	0.1 M borate	2.4×10^{-4}
10.0	0.1 M carbonate	2.0×10^{-6}
12.0	10 mM NaOH/ 0.1 M Na ₂ SO ₄	8.0×10^{-3}
12.0	0.1 M phosphate	3.0×10^{-8}
14	1.0 M NaOH	4.9×10^{-9}

^apH adjusted by addition of NaOH, H₂SO₄, or H₃PO₄.



Application of a constant large positive potential in the region of the current plateau decreased the rate of film dissolution, undoubtedly because the anodic reaction of CN^- resulted in a surface concentration ($C_{\text{CN}^-}^{\text{S}}$) substantially lower than $C_{\text{CN}^-}^{\text{b}}$. Furthermore, visual inspection of CuO-film electrodes after ca. 1 hr of electrolysis in NaCN, showed less deterioration when the potential was controlled at 0.6 V rather than at 0.35 V. Slow film dissolution can occur even for $E \gg E_{1/2}$ because $C_{\text{CN}^-}^{\text{S}}$ always has a finite value, even in the potential region of the current plateau. These results indicate that CuO-film electrodes as prepared in this research would be unsuitable for treatment of industrial wastes containing large amounts of CN^- . The CuO-film electrodes withstood gentle rinsing by a stream of water. However, the slightest mechanical abrasion removed portions of the films from the Pt/SS substrates. Furthermore, occasional peeling of the CuO-films occurred during air-drying unless the films had been pretreated after deposition by application of repetitive cyclic scans.

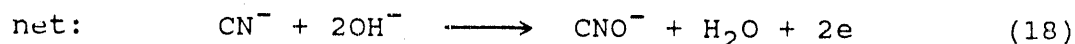
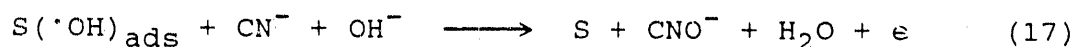
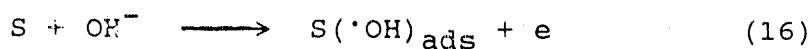
CONCLUSIONS

Several amines have been reported to undergo oxidation at CuO electrodes and the anodic reaction has been attributed to the oxidizing power of a Cu^{III} species in the oxide film, perhaps $\text{CuO}(\text{OH})$, generated at increasingly positive potential values (23,27). The formal reduction potential for the $\text{CuO}(\text{OH})$ -CuO couple was estimated as 0.65 V vs. the Hg/HgO (i.e., 0.51 V vs. SCE) at pH 14 (23). Some $\text{CuO}(\text{OH})$ is expected to be formed at $E < 0.5$ V and the observation that $E_{1/2} = \text{ca. } 0.3$ V for CN^- oxidation to CNO^- in 1 M NaOH is consistent with a mechanism in which the Cu^{III} - Cu^{II} redox couple functions an electron-transfer mediator.

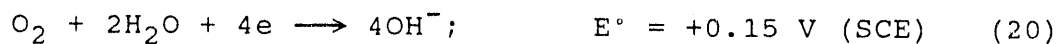
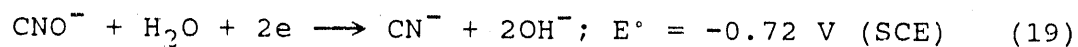
It does not seem reasonable to ascribe the electrocatalytic activity of CuO-film electrodes merely to chemical oxidation at the electrode-solution interface. The applied potential for $E > E_{1/2}$ is more than sufficient to bring about charge transfer. Hence, the faradaic transformation of redox state for surface sites located within the applied electric field hardly seems sufficient for promoting the anodic process unless there is a dramatic change in the associated chemical steps available for the reaction mechanism.

It is proposed that anodic conversion of Cu^{II} to Cu^{III} starting at $E > \text{ca. } 0.2$ V provides a favorable mechanism for

the oxygen-transfer step which must occur concomitantly with electron transfer in the oxidation of CN^- to CNO^- . We propose that the appropriate activated state of oxygen at Cu^{III} sites is the adsorbed hydroxyl radical $(\cdot\text{OH})_{\text{ads}}$ generated by anodic discharge of H_2O . Such an O-transfer mediated mechanism is described by Equations 16-18, where $\underline{\text{S}}$ represents an active surface sites.



Adsorbed $\cdot\text{OH}$ has been proposed as an intermediate product in the anodic evolution of O_2 (30). Based on the standard reduction potentials for the half reactions in Equations 19 and 20, the oxidation of CN^- is predicted to be much more favorable than anodic evolution of O_2 .



Nevertheless, $E_{1/2}$ for the anodic conversion of CN^- to CNO^- was ca. 0.3 V vs. SCE in 1 M NaOH. This large overpotential for CN^- oxidation is consistent with the concept that $\cdot\text{OH}_{\text{ads}}$ generated at Cu^{III} sites as an intermediate product in O_2 evolution can participate in the oxidation of CN^- . As the applied potential is increased to values approaching the

region for onset of rapid O_2 evolution, the surface activity of $(\cdot OH)_{ads}$ is increased substantially by adsorption at Cu^{III} sites and, hence, the mechanism described by Equations 16-18 is enabled.

Electrocatalytic electrodes described previously for anodic O-transfer reactions have made use of mixed oxide films deposited from solutions of Pb^{2+} and various metal cations (20). Most notable is the case of Bi^V -doped PbO_2 -film electrodes. However, CN^- was observed not to be reactive at $Bi-PbO_2$ electrodes, and the mere creation of catalytic sites for adsorption of $\cdot OH$ is apparently not sufficient to catalyze oxidation of CN^- . It is proposed that an oxygen tunneling mechanism comparable to electron tunneling does not occur at the electrode-solution interface. Therefore, successful electrocatalysis of all anodic O-transfer reactions also requires that surface sites exist for adsorption of the reactant with the consequence that reaction sites on reactants are fully desolvated. Hence, metallic candidates for the doping of PbO_2 electrodes to achieve oxidation of CN^- have been chosen on the basis of the existence of a strong coordination bond between CN^- and the metal ion in homogeneous aqueous solutions. The logic is that trends observed in solution-phase d-orbital (coordination) chemistry are reflected by trends in chemisorption of ligands on metal and metal oxide electrodes which are a consequence of interaction with surface d-orbitals. Based

on the knowledge of the high stability of $\text{Fe}(\text{CN})_6^{3-}$ and $\text{Fe}(\text{CN})_6^{4-}$, Feng and Johnson (31) tested the activity of Fe^{III} -doped PbO_2 electrodes and discovered that oxidation of CN^- proceeded at a mass transport-controlled rate in alkaline media.

Following similar logic, it is expected that CN^- can be adsorbed at oxygen-deficient defect sites in the surface lattice with adsorption of $\cdot\text{OH}$ at other sites. Hence, the electrocatalytic oxidation of CN^- might proceed by a synergistic cooperation of surface sites in dissimilar states. It is possible that Cu^{III} sites might function both for adsorption of $\cdot\text{OH}$ and the reactant. We note that the formation constant for $\text{Pt}(\text{CN})_4^{2-}$ (10^{+40} M^{-4}) is much larger than that for $\text{Cu}(\text{CN})_4^{2-}$ ($10^{+26.7} \text{ M}^{-4}$) (32). Nevertheless, CN^- is not electroactive at Pt electrodes under conditions of constant applied potential (33). This can be explained from the observation that oxidative desorption of the strongly adsorbed CN^- on Pt occurs at sufficiently large positive potentials so that the electrode surface is virtually instantaneously converted to the corresponding inert oxide (34).

The interpretation of the pH dependency of k_0 values shown in Table I is even more speculative. If the preferred oxidation mechanism occurs with pre-adsorption of CN^- , $\text{pH} \leq \text{ca. } \text{p}K_{\text{a,HCN}}$ (i.e., ca. 9) would be expected to interfere because of the protonation of CN^- . Furthermore, extremely

high values of pH would be expected to interfere because of the competitive adsorption by OH^- .

The CuO-film electrodes were stable when used in alkaline solutions of CN^- at concentrations of ca. 1 mM and lower. Whereas application of the electrodes for industrial treatment of cyanide wastes appears not to be feasible, the electrodes can have significance as analytical transducers for detection of CN^- at low concentrations. Preliminary results have shown a 6-fold improvement in the response at a Au electrode following the deposition of a thin CuO film.

SUMMARY

In Part I, it was learned that the reduction of IO_3^- at Pt electrodes was catalyzed by the reduction of surface oxide (PtO). The turnover number per PtO site was determined to be greater than one, virtually eliminating the possibility of an adsorbed reactant or reduction product. The involvement of $\cdot\text{OH}_{\text{ads}}$, which is an intermediate product in the reduction of PtO, was suggested.

On oxide-free Pt electrodes, the reduction of IO_3^- was found to be strongly influenced by surface treatment. Previous investigations have relied on a chemical reduction step to explain the electrochemical reduction of IO_3^- on oxide-free Pt electrodes. Data presented here are consistent with the conclusion that IO_3^- reduction occurs by a mechanism which involves adsorption of IO_3^- to the electrode surface. The adsorption of zero-valent iodine (I^0) on oxide-free Pt is well-known. Thus, the adsorption sites for IO_3^- were proposed to be $\text{Pt}(\text{I}^0_{\text{ads}})$.

In Part II, data were presented that indicates the electrocatalytic oxidation of CN^- requires the existence of adsorption sites for CN^- . Anodic currents attributable to the oxidation of CN^- were not observed at PbO_2 or Bi-doped PbO_2 electrodes. However, an anodic wave for the oxidation of CN^- was obtained at Cu-doped PbO_2 and CuO film electrodes. The half-wave potential and the heterogeneous

rate constant (k_0) were determined to be a function of pH. In addition, k_0 was strongly influenced by addition of anions.

While electron tunneling has been used to explain some electrocatalytic phenomena, the possibility of tunneling oxygen atoms cannot be considered as likely to occur. The adsorption of CN^- at Cu sites was proposed as the necessary prerequisite for this anodic oxygen-transfer. Likewise, adsorption of IO_3^- was concluded necessary for direct reduction of that species on Pt electrodes.

Adsorption of reactants to the electrode surface was concluded to be an important requirement for electrocatalysis in both Part I and Part II of this dissertation. Whereas it was not the original intention of this research to draw such a parallel, it was a serendipitous discovery that has far-reaching implications for development of new electrocatalytic materials.

SUGGESTIONS FOR FUTURE RESEARCH

The study of oxygen-transfer reactions should not be limited to PbO_2 electrodes. The numerous oxygen evolution catalysts currently being investigated should be studied for their suitability as oxygen-transfer electrocatalysts.

Use of fabrication techniques other than electrodeposition will permit investigation of a wider variety of electrodes. For example, it can be postulated that improved catalytic activity will be observed if adsorption sites for CN^- (i.e., Cu) and $\cdot\text{OH}_{\text{ads}}$ (i.e., Bi) were introduced into the same PbO_2 electrode. This is not possible using electrodeposition since incorporation of Cu and Bi into PbO_2 require widely different pH conditions.

The possible application of electrocatalytic electrodes as chemical sensors should be investigated. Electrolytic treatment of hazardous chemical waste was alluded to in this research. The practicality of such an application needs to be tested further by constructing a bench-scale reactor.

REFERENCES

1. Hine, F.; Yasuda, M.; Iida, T.; Ogata, Y. Electrochim. Acta 1986, 31, 1389.
2. Carr, J. P.; Hampson, N. A. Chem. Rev. 1972, 72, 679.
3. Sharpe, T. F. in Encyclopedia of Electrochemistry of the Elements; Bard, A. J., Ed.; Marcel Dekker: New York, 1973; Vol. 1, Chapter 5.
4. Ruetschi, P.; Angstadt, R. T.; Cahan, B. D. J. Electrochem. Soc. 1959, 106, 547.
5. Mindt, W. J. Electrochem. Soc. 1969, 116, 1076.
6. Baker, R. A. J. Electrochem. Soc. 1962, 109, 337.
7. Ruetschi, P.; Cahan, B. D. J. Electrochem. Soc. 1957, 104, 406.
8. Ruetschi, P.; Cahan, B. D. J. Electrochem. Soc. 1958, 105, 369.
9. Thomas, U. B. Trans. Electrochem. Soc. 1948, 94, 42.
10. Frey, D. A.; Weaver, H. E. J. Electrochem. Soc. 1960, 107, 930.
11. Collat, J. W.; Lingane, J. J. J. Am. Chem. Soc. 1954, 76, 4214.
12. Duisman, J. A.; Giaque, W. F. J. Phys. Chem. 1968, 72, 562.
13. Vinal, G. W. Storage Batteries; John Wiley: New York, 1965.
14. Organic Electrochemistry; Baizer, M. M., Ed.; Marcel Dekker: New York, 1973.
15. Weinberg, N. L.; Weinberg, H. P. Chem. Rev. 1968, 68, 449.
16. Willard, H.; Ralston, R. R. Trans. Electrochem. Soc. 1932, 62, 239.
17. Ramaswamy, R.; Venkatachalapathy, M. S.; Udupa, H. V. K. J. Electrochem. Soc. 1963, 110, 294.

18. Sinfelt, J. H. Catal. Rev. 1974, 9, 147.
19. Johnson, D. C.; Polta, J. A.; Polta, T. Z.; Neuburger, G. G.; Johnson, J.; Tang, A. P-C.; Yeo, I-H.; Baur, J. J. Chem. Soc. Faraday Trans. 1 1986, 82, 1081.
20. Yeo, I-H.; Johnson, D. C. J. Electrochem. Soc. 1987, 134, 1973.
21. Katagiri, A.; Yoshimura, S.; Deguchi Y.; Yoshizawa, S. Proceedings of the Symposium on Electrocatalysis; O'Grady, W. E.; Ross, P. N.; Will, F. G., Eds.; The Electrochemical Society: Pennington, NJ, 1982; pp. 336-346.
22. Rocklin, R. D.; Johnson, E. L. Anal. Chem. 1933, 55, 4.
23. Fleischmann, M.; Korinek, K.; Pletcher, D. J. Chem. Soc., Perkin Trans. II, 1972, 10, 1396.
24. Stulik, K.; Pacakova, V.; Le, K.; Hennissen, B. Talanta 1988, 35, 455.
25. Kok, W. Th.; Hanekamp, H. B.; Bos, P.; Frei, R. W. Anal. Chim. Acta 1982, 142, 31.
26. Prabhu, S. V.; Baldwin, R. P. Anal. Chem. 1989, 61, 852.
27. Meyerstein, D.; Hawkrige, F. M.; Kuwana, T. J. Electroanal. Chem. 1972, 40, 377.
28. Bard, A. J.; Faulkner, L. R. Electrochemical Methods; John Wiley & Sons: New York, 1980; pp. 286-292.
29. Sawyer, D. T.; Day, R.J. J. Electroanal. Chem. 1963, 5, 195.
30. Hoare, J. P. The Electrochemistry of Oxygen; Interscience Publishers: New York, 1968; pp. 86-112.
31. Feng, J.; Johnson, D. C. J. Electrochem. Soc. 1987, 137, 507.
32. Sharpe, A. G. The Chemistry of Cyano Complexes of the Transition Metals; Academic Press: New York, 1976.
33. Austin, D. S.; Polta, J. A.; Polta, T. Z.; Tang, A. P-C.; Cabelka, T. D.; Johnson, D. C. J. Electroanal. Chem. 1984, 168, 227.
34. Polta, J. A.; Johnson, D. C. Anal. Chem. 1985, 57, 1373.

ACKNOWLEDGMENTS

I would like to express my appreciation to Professor Dennis Johnson for his guidance and enthusiastic support during my years of graduate study at Iowa State University. I would like to thank Dr. William LaCourse as well as other members of the electrochemistry group for their friendship and support. I especially wish to thank my mother and brother for their encouragement and interest in my education.

I gratefully acknowledge the assistance of Jerry Amenson and Scott Schlorholtz in obtaining scanning electron micrographs and X-ray diffraction data. I am indebted to James Gordon for his assistance in obtaining the ratio of mass:charge for deposition of CuO films.

This work was performed at Ames Laboratory under contract no. W-7405-eng-82 with the U. S. Department of Energy. The United States government has assigned the DOE Report number IS-T 1450 to this thesis.

APPENDIX

This appendix contains the printout of the computer program used for the collection of voltammetric data. It is written in QuickBASIC, version 3.0. Documentation has been inserted for the reader's clarification. A glossary of variable names used in the program has been included at the end of the printout.

Description

Subroutines supplied by Data Translation, Inc. perform digital-to-analog (D/A) conversions using analog data values (ADV) as input arguments. The ADV and the desired output voltage are related by the expression given below.

$$\text{ADV} = (\text{voltage} - \text{low}) \times \frac{\text{NC}}{(\text{high} - \text{low})}$$

"High" and "low" refer to the high and low voltage values of the analog range. For this system, these values are +10 V and -10 V, respectively. The number of codes (NC) is determined by raising the number 2 to the power "n" where n is the resolution of the converter. A 12-bit D/A converter was supplied with this system, therefore $\text{NC} = 2^{12} = 4096$.

The voltage analog of the electrode current is measured at the potentiostat using an analog-to-digital (A/D) converter. Analog data values are returned by the A/D subroutine. These ADVs are converted to voltages by a separate subroutine supplied by Data Translation, Inc.

This program calculates the ADVs corresponding to each applied potential comprising the voltammogram and stores them in an array. A series of electrode current measurements is at a preselected frequency following a time delay which is also preselected by the user. Analog data values returned by the A/D subroutine are also stored in the array before being converted to current values for use in preparing data plots.

```

DIM raw%(11,1500), buf%(960)      'Dimension data arrays,
common shared i, k$, y%          'identify variables shared
zero%=2048 : schan%=0            'with subprograms, and
dac0%=0      : echan%=0         'assign values to constants
dac1%=1      : ts%=0            'and variables.
nov%=11      : gain%=2
freq!=100    : dry$="C:\DATA\"
vlmsg$(0)="Import file of experimental parameters from _
disk."
vlmsg$(1)="Save experimental parameters to disk file."
vlmsg$(3)="Modify present experimental parameters."
v2msg$(0)="Data from prescans are not saved."
v2msg$(1)="Enter rotation speed (0-10000 rpm)."
v2msg$(2)="Enter potential step (Multiple of 5 mV)."
v2msg$(3)="Length of delay (ms) following potential step."
v2msg$(4)="Anodic potential limit in mV."
v2msg$(5)="Cathodic potential limit in mV."
v2msg$(6)="Choose starting potential (mV) in low current _
region."
slmsg$(0)="Change file directory."
slmsg$(1)="Change frequency with which current is sampled."
slmsg$(2)="(1,2,4,8) Maximum current (mA) = 10/GAIN"
slmsg$(3)="0=soft trig/int clock 1=soft/ext 2=ext/int _
3=ext/ext"
slmsg$(4)="0-8 Requires hardware change."

'Setup screen for menu...

SCREEN 9,,1,1
COLOR 7,1
PRINT spc(26);"ELECTROCHEMISTRY SOFTWARE"
PRINT spc(26);"Support for the Rotated Disc"

```



```

COLOR 9,1
For x=2 to 79
  LOCATE 4,x
  PRINT chr$(205)
  LOCATE 11,x
  PRINT chr$(205)

```

```

Next x
LOCATE 3,5 : COLOR 12,1
PRINT "VOLTAMMETRY"
COLOR 7,1
LOCATE 5,28
PRINT"CURRENT EXPT: "

```

'Assign more variables...

```

DATA Import experiment, Save experiment, Run experiment
DATA Change parameters, Configure system, Prescans, RPM
DATA Step, Delay, Anodic limit, Cathodic limit,
DATA Start potential, Directory, Clock frequency
DATA Gain, Timing source, ADC channel
DATA 6,10,6,50,7,10,7,50,8,10,8,50,9,10,9,50,10,10,10,50

```

```

For x=0 to 4
  READ vm1$(x)
Next x
For x=0 to 6
  READ vm2$(x)
Next x
For x=0 to 4
  READ sm1$(x)
Next x
For x=0 to 9
  READ row(x),col(x)
Next x

```

```

CALL set.clock.frequency(freq!)           'Transfers control to
CALL dac.value(dac0%,zero%)              'Data Translation
CALL dac.value(dac1%,zero%)              'subroutines.
CALL setup.adc(ts%,schan%,echan%,gain%)

```

'Install menu...

```

WHILE kuit=0
  CALL menu(vm1$(), row(), col(), 4, vlmsg$())
  If asc(k$)=27 then
    LOCATE 13,5 : Print spc(65)
    LOCATE 13,5 : Input"Exit to DOS";x$
    If x$="y" then kuit=1
    LOCATE 13,5
    Print spc(15)

```

```

Else
  If i=0 then Gosub IMPORT
  If i=1 then Gosub STASH
  If i=2 then Gosub VRUN
  If i=3 then Gosub CHANGE
  If i=4 then Gosub CONSYS
End if
WEND
CLS : END

```

'Menu subroutine...

```

SUB menu (label$(1), row(1), col(1), last%, mess$(1)) static
  COLOR 15,1
  FOR x=0 to 9
    LOCATE row(x),col(x)
    Print spc(25)
    LOCATE row(x),col(x)
    Print label$(x)
    If x=0 then COLOR 7,1
  NEXT x
  locate 13,5 : print mess$(0)
  i=0 : oldi=0 : k$=""
  WHILE k$=""
    WHILE k$=""
      k$=inkey$
    WEND
    IF len(k$)=2 then
      kval=asc(right$(k$,1))
      if kval=72 then i=i-2
      if kval=80 then i=i+2
      if kval=75 then i=i-1
      if kval=77 then i=i+1
      if i<0 then i=last%
      if i>last% then i=0
      locate row(oldi),col(oldi) : print label$(oldi)
      color 15,1
      locate row(i),col(i) : print label$(i)
      color 7,1
      locate 13,5 : print spc(70)
      locate 13,5 : print mess$(i)
      oldi=i : k$=""
    END IF
  WEND
END SUB

```

```

IMPORT:
  locate 15,5
  input "Name of file to import: ",name$
  open dry$name$.vex" for input as #2
  input#2, pscan%, rpm%
  input#2, t3%, alim%, clim%
  input#2, start%, vstep%
  close #2
  locate 5,42 : print name$
  locate 15,5 : print spc(32)
RETURN

STASH:
  locate 15,5
  input "Name of file to save: ",name$
  open dry$name$.vex" for output as #2
  for x=0 to 4
    print#2, pscan%; rpm%
    print#2, t3%; alim%; clim%
    print#2, start%; vstep%
  next x
  close #2
  locate 5,42 : print name$
  locate 15,5 : print spc(32)
RETURN

VRUN:
  DIM proc(1,1500)
  LOCATE 13,5
  INPUT "Current converter setting on RDE4 (mA/V): ";etoi
  LOCATE 13,5 : PRINT spc(55)

  nop%=2.048*(alim%-clim%)/vstep%
  If nop%>1500 then
    PRINT "ARRAY OVERFLOW!"
    RETURN
  End if

  raw%(0,0)=.2048*(start%+10000)
  low%=.2048*(clim%+10000)
  hi%=.2048*(alim%+10000)
  incr%=.2048*vstep%

  FOR z=1 to nop%
    raw%(0,z)=raw%(0,z-1)+incr%
    If raw%(0,z)+incr%<low% then incr%=-incr%
    If raw%(0,z)+incr%>hi% then incr%=-incr%
  NEXT z

```

'Previously
'saved exper-
'imental param-
'eters are
'loaded...

'Experimental
'parameters
'are saved to
'a data file

'Calculate number
'of points in
'voltammogram...

'Calculate analog
'data values for
'start potential,
'potential limits,
'and potential step

'Fill array with
'analog data vlues

```

'Remove overlap
'from number of
'points in voltam-
'mogram.
n=z-1
WHILE ABS(raw%(0,n)-raw%(0,0))>ABS(incr%)
  nop%=nop%-1
  n=n-1
WEND

rot%=.2048*rpm%+2048          'Calculate analog data
CALL dac.value(dac0%,rot%)    'value for rotation
CALL dac.value(dac1%,raw%(0,0)) 'speed and execute...
x=0
DO
  clk(3)=TIMER                'Check time of day...
  FOR z=0 to nop%
    CALL dac.value(dac1%,raw%(0,z)) 'Step potential
    clk(0)=TIMER
    DO
      clk(1)=TIMER              'Monitor time-of-
      clk(2)=clk(1)-clk(0)      'day clock during
                                'delay...
      LOOP WHILE clk(2)<t3%/1000
      CALL begin.adc.dma(nov%,raw%(1,z)) 'Fill data
      CALL wait.adc.dma(raw%(11,z))    'array with
      CALL stop.adc.dma              'current values
    NEXT z
    clk(4)=TIMER                'Check time of day...
    x=x+1
  LOOP UNTIL x>pscan%
  sr%=2.048*(alim%-clim%)/(clk(4)-clk(3)) 'Calculate scan
                                          'rate...
  CALL dac.value(dac0%,zero%)        'Stop rotator

                                          'Calculate analog data values
                                          'into voltages, currents...
FOR z=0 to nop%
  proc(0,z)=(raw%(0,z)-2048)*(625/128)
  FOR n=1 to 10
    CALL analog.to.volts(raw%(n,z),gain%,pot)
    proc(1,z)=proc(1,z)+pot
  NEXT n
  proc(1,z)=proc(1,z)*etoi/10
NEXT z

'Plot data on screen...
SCREEN 9,,0,0
CLS : t$=time$
INPUT"Title of graph= ";title$

```

```

DO
  INPUT "Name of data file= ";filnam$
  IF len(filnam$)>7 then PRINT "7 characters only!"
LOOP UNTIL len(filnam$)<8
CLS : d$=date$
COLOR 7,0
PRINT "Current expt: ";name$;tab(30);t$;tab(45);d$
PRINT "RPM: ";rpm$;tab(30);"Scan rate: ";sr$;"mV/s"
PRINT "Title: ";title$
PRINT spc(62);"+/-      Zoom"
PRINT spc(62);"<enter> Save"
PRINT spc(62);"<esc>   Exit"
PRINT:PRINT
ic=-1 : ec=-clim%
ia=1  : ea=-alim%
COLOR 7,0
VIEW (5,45)-(470,330),,7
DO
  WINDOW SCREEN (ea,ic)-(ec,ia)
  LOCATE 15,62 : PRINT "mV RANGE:"
  LOCATE 16,63 : PRINT -ea;"to";-ec
  LOCATE 18,62 : PRINT "ma RANGE:"
  LOCATE 19,63 : PRINT ia;tab(78)
  LOCATE 20,63 : PRINT " to"
  LOCATE 21,63 : PRINT ic;tab(78)
  FOR z=1 to nop%
    LINE (-proc(0,z-1),proc(1,z-1))-(-proc(0,z), _
      proc(1,z)),14
  NEXT z

  k$=inkey$
  WHILE k$=""
    k$=inkey$
  WEND
  kval=asc(k$)
  IF kval=43 then
    CLS
    ic=ic/1.5
    ia=ia/1.5
  Elseif kval=45 then
    CLS
    ic=ic*1.5
    ia=ia*1.5
  Elseif kval=13 then
    GOSUB DUMP
    CLS

    'Save data on disk...

    OPEN dry$+filnam$+".dat" for output as #1

```

```

FOR z=0 to nop%
  PRINT#1, proc(0,z)/1000;proc(1,z)
NEXT z
CLOSE #1

LPRINT chr$(27);"x";"1"
LPRINT "Data filename: ";filnam$;tab(40); _
      "Prescans: ";pscan%
LPRINT
LPRINT "Gain: ";gain%;tab(40);"Current _
      converter: ";etoi
LPRINT "Delay: ";t3%;tab(40);"Step: ";vstep%
VIEW
ERASE proc
SCREEN 9,,1,1
RETURN
Elseif kval=27 then
  VIEW
  ERASE proc
  SCREEN 9,,1,1
  RETURN
End if
LOOP

```

CHANGE:

'Change experimental
'parameters...

```

FOR x=16 to 22
  LOCATE x,2
  PRINT vm2$(x-16)
NEXT x
LOCATE 16,19 : PRINT pscan%
LOCATE 17,19 : PRINT rpm%
LOCATE 18,19 : PRINT vstep%
LOCATE 19,19 : PRINT t3%
LOCATE 20,19 : PRINT alim%
LOCATE 21,19 : PRINT clim%
LOCATE 22,19 : PRINT start%
y%=0
DO
  If y%=0 then CALL param(vm2$(), pscan%, v2msg$())
  If y%=1 then CALL param(vm2$(), rpm%, v2msg$())
  If y%=2 then CALL param(vm2$(), vstep%, v2msg$())
  If y%=3 then CALL param(vm2$(), t3%, v2msg$())
  If y%=4 then CALL param(vm2$(), alim%, v2msg$())
  If y%=5 then CALL param(vm2$(), clim%, v2msg$())
  If y%=6 then CALL param(vm2$(), start%, v2msg$())
LOOP UNTIL len(k$)=1
LOCATE 13,5 : PRINT spc(65)

```

```

For x=15 to 22
  LOCATE x,2
  PRINT spc(35)
NEXT x
RETURN

```

'Subroutine for changing
'parameters...

```

SUB param (label$(1), value%, msg$(1)) static
  LOCATE 13,5 : PRINT msg$(y%);tab(70)
  COLOR 15,1
  LOCATE y%+16,2 : PRINT label$(y%)
  COLOR 12,1
  LOCATE y%+16,19
  PRINT value%
  DO
    k$=""
    WHILE k$=""
      k$=inkey$
    WEND
    If len(k$)=2 then kval=asc(right$(k$,1)) _
      else kval=asc(k$)
    SELECT CASE kval
      CASE 48 to 57, 45
        LOCATE y%+16,19 : PRINT spc(6)
        LOCATE y%+16,19
        For z%=1 to 5
          WHILE k$=""
            k$=inkey$
          WEND
          If len(k$)=2 or asc(k$)<45 then Exit For
          ent$=ent$+k$
          PRINT k$;
          k$=""
        Next z%
        value%=val(ent$)
        LOCATE y%+16,19
        PRINT value%
        ent$=""
      CASE 72
        oldy%=y%
        y%=y%-1
        If y%<0 then y%=6
        kval=0
      CASE 80
        oldy%=y%
        y%=y%+1
        If y%>6 then y%=0
        kval=0
    END SELECT
  LOOP

```

```

CASE 27
    kval=0
CASE ELSE
    BEEP
END SELECT
LOOP UNTIL kval=0
COLOR 7,1
LOCATE oldy%+16,2 : PRINT label$(oldy%)
LOCATE oldy%+16,19
PRINT value%
END SUB

```

```

CONSYS:                                'Setup menu for changing
DO                                       'system parameters...
CALL menu(sm1$(), row(), col(), 4, sm1msg$())
If asc(k$)=27 then
    LOCATE 13,5 : Print spc(65)
    RETURN
Else
    If i=0 then Gosub DIRECT
    If i=1 then Gosub FREQ
    If i=2 then Gosub GAIN
    If i=3 then Gosub TIMSRC
    If i=4 then Gosub ADCHAN
End if
LOCATE 14,5
PRINT spc(65)
PRINT spc(65)
LOOP

```

```

DIRECT:                                'Change directory...
LOCATE 14,5 : PRINT"Directory: ";dry$
Gosub ENTER
If sent$="" then RETURN
dry$=sent$
RETURN

```

```

FREQ:                                    'Change frequency of analog to
LOCATE 14,5 : PRINT"Clock frequency: ";freq!
Gosub ENTER
If sent$="" then RETURN
freq!=val(sent$)
CALL set.clock.frequency(freq!)
RETURN

```


'Change gain...

```
GAIN:
  LOCATE 14,5 : PRINT"Gain: ";gain%
  Gosub ENTER
  If sent$="" then RETURN
  gain%=val(sent$)
  CALL setup.adc(ts%,schan%,echan%,gain%)
RETURN
```

'Change timing source...

```
TIMSRC:
  LOCATE 14,5 : PRINT"Timing source: ";ts%
  Gosub ENTER
  If sent$="" then RETURN
  ts%=val(sent$)
  CALL setup.adc(ts%,schan%,echan%,gain%)
RETURN
```

'Change analog to digital
'channel...

```
ADCHAN:
  LOCATE 14,5 : PRINT"Starting channel: ";schan%
  Gosub ENTER
  If sent$="" then
    LOCATE 14,5 : PRINT"Ending channel: ";echan%
    Gosub ENTER
    If sent$="" then RETURN
    echan%=val(sent$)
    CALL setup.adc(ts%,schan%,echan%,gain%)
    RETURN
  Else
    schan%=val(sent$)
  End if
  LOCATE 14,5 : PRINT"Ending channel: ";echan%
  Gosub ENTER
  If sent$<>"" then echan%=val(sent$)
  CALL setup.adc(ts%,schan%,echan%,gain%)
RETURN
```

'Subroutine for inputing data...

```
ENTER:
  ent$="" : sent$=""
  DO
    k$=""
    WHILE k$=""
      k$=inkey$
    WEND
```

```

    If asc(k$)=27 then RETURN
    If asc(k$)=13 then sent$=ent$
    ent$=ent$+k$
    PRINT k$;
  LOOP UNTIL asc(k$)=13
RETURN

```

```

DUMP:                                     'Subroutine for printing screen
                                         'display of data plot...
width "lpt1:", 255
lprint chr$(27); "3"; chr$(24);
For col%=0 to 75
  DEF SEG = &HA000
  i=699
  For j=0 to 349
    out &H3CE, 4
    out &H3CF, 0
    sbyte=PEEK(j*80+col%)
    out &H3CE, 4
    out &H3CF, 2
    sbyte=sbyte or peek(j*80+col%)
    out &H3CE, 4
    out &H3CF, 3
    sbyte=sbyte or peek(j*80+col%)
    buf%(i)=sbyte
    i=i-1
    buf%(i)=sbyte
    i=i-1
  next j
  lprint chr$(27);"L"; chr$(188); chr$(2);
  for i=0 to 699
    lprint chr$(buf%(i));
  next i
  lprint
next col%
DEF SEG
lprint chr$(27);"@"
RETURN

```

Glossary

alim% - anodic scan limit (mV).
 buf%() - screen display image bits for printer output.
 clim% - cathodic scan limit (mV).
 col() - x-coordinate for menu selections.
 d\$ - today's date.
 dac0% - D/A channel number 0.
 dac1% - D/A channel number 1.
 dry\$ - directory name for storage retrieval of data files.

ea - anodic potential limit for displayed plot of data.
 ec - cathodic potential limit for displayed plot of data.
 echan% - ending channel number for A/D converter.
 ent\$ - sum of keyboard input.
 etoi - current converter setting on potentiostat (mA/V).
 filnam\$ - name of file to hold data.
 freq! - frequency (Hz) at which A/D conversions are made.
 gain% - gain of A/D converter.
 hi% - ADV corresponding to anodic limit.
 i - marker for menu subprogram.
 ia - anodic current limit for displayed plot of data.
 ic - cathodic current limit for displayed plot of data.
 incr% - ADV corresponding to potential step.
 k\$ - keyboard input characters.
 kval - ASCII code of keyboard input.
 label\$() - used in menu subprogram for menu selections.
 low% - ADV corresponding to cathodic limit.
 mess\$() - used in menu subprogram for selection messages.
 msg%() - selection messages in parameter subprogram.
 name\$ - name of file holding list of experimental parameters.
 nop% - number of points in voltammogram.
 nov% - number of values of current measured per potential step.
 oldi - marker for menu subprogram.
 oldy% - marker for parameter subprogram.
 pot - voltage analog of measured current.
 proc() - processed ADV's from raw%().
 pscan% - number of prescans executed before data is processed.
 raw%() - ADV's for voltammetric data.
 rot% - ADV corresponding to rotation speed.
 row() - y-coordinate for menu selections.

 rpm% - rotation speed (rev min⁻¹).
 slmsg\$() - messages for "Configure system" menu selections.
 sbyte - screen image bit for printer output.
 schan% - starting channel number for A/D converter.
 sent\$ - sum of keyboard input.
 sm1\$() - "Configure system" menu selections.
 sr% - scan rate (mV/s).
 start% - initial potential (mV) of voltammogram.
 t\$ - time of day.
 t3% - time delay (ms) following potential step and before current is measured.
 title\$ - title for plot of data.
 ts% - timing source.
 value% - parameter values in parameter subprogram.
 v1msg\$() - messages for main menu selections.
 v2msg\$() - messages for "Change parameters" menu selections.
 vm1\$() - main menu selections.
 vm2\$() - parameters menu selections.

vstep% - size of potential step (mV).
y% - marker for parameter subprogram
zero% - ADV corresponding to 0.0V output.

END

DATE FILMED

11 / 14 / 90

